Repositioning FDA-approved drugs to identify potential mycobacterial FadD23 inhibitors

By

Chitra Dipika Pillay

220023954

A dissertation submitted in partial fulfilment of the requirements for the degree of Master of Medical Science

College of Health Sciences

School of Laboratory Medicine & Medical Sciences

Department of Medical Biochemistry

University of KwaZulu-Natal, Durban 4000, South Africa

Preface

This thesis is divided into four chapters:

Chapter 1: In this chapter, the background, aims and objectives, relevance as well as general outline and structure of the thesis are addressed.

Chapter 2: The background of the study is provided in this chapter. Updated statistics on TB infections and deaths worldwide, as well as pathogenesis, are covered. This chapter also provides an overview of computational chemistry molecular modelling and molecular simulation techniques and their applications. Theoretical explanations for the computational methods have been provided. A discussion of the various computational tools used in TB research is provided, with a particular emphasis on molecular dynamics simulations and trajectory analysis.

Chapter 3: Manuscript by the title; ‘’ Repositioning FDA approved drugs to identify potential mycobacterial FadD23 inhibitors’’

Chapter 4: Conclusions and Future Prospects.

Declaration

I, Chitra Dipika Pillay, declare as follows:

1. This dissertation contains original work conducted by the author and has not been submitted to UKZN or any other tertiary institution to obtain an academic qualification, whether by myself or any other party. The use of other people's work has been duly acknowledged in the text.
2. The research work presented in this study was carried out in the Department of Medical Biochemistry, School of Laboratory Medicine and Medical Science, Faculty of Health Sciences, University of KwaZulu-Natal, Durban, under the supervision of Dr N.N Mhlongo.

3. Author Contributions were as follows:

- Miss Chitra Dipika Pillay: Manuscript writing and data analysis, conducted MD simulations and trajectory analysis calculations.
- Dr Ndumiso N. Mhlongo.: Supervisor, manuscript proofreading, assisted with MD calculations.

Chitra Dipika Pillay Signature_[redacted] Date:06-05-2025

Dr Ndumiso N. Mhlongo Signature___[redacted] Date: 06-05-2025

Dedication

This dissertation is dedicated to:
Sri Krsna who has guided me from beginning to end.

Acknowledgements

- I want to thank my parents Ms Dhamaynthree Pillay and the late Balakrishna Kisten Pillay for all the sacrifices they made to enable me to become the person I am today.
- I want to thank my supervisor Dr Ndumiso Mhlongo for his support and guidance provided through my postgraduate journey.
- I want to thank my brother Yogesh, who supports me and encourages me through my academic life.
- I want to thank my friends Shweta Rajkumar, Krislyn Govender, Alisha Naidoo and Joshua Govender for always believing in me and encouraging me when I wanted to give up.
- I also want to express gratitude to my colleagues in the Department of Medical Biochemistry for their support and insight.
- To Centre of High-Performance Computing, Cape Town, South Africa for their resources.
- UKZN College of Health Sciences department for the financial support during the course of my Master's degree.

Table of Contents

List of figures

List of tables

List of Abbreviations

Tuberculosis	TB
Palmitic Acid	PLM
Phosphoaminophosphonic acid-adenylate	ANP
Mycobacterium tuberculosis	*M.tuberculosis*
Extreme Drug resistance	XDR
Multi-Drug Resistance	MDR
Sulfolipid-1	SL-1
Phthiocerol dimycocerosate	PDIM
Fatty acid adenylating enzyme	FadD
Fatty acyl-coenzyme A ligase	FACL
Fatty acyl AMP ligases	FAAL
Adenosine triphosphate	ATP
Polyketide synthase	Pks
Molecular Dynamics	MD
Arabinogalactan	AG
Mycolic Acid	MA
Phenolic glycolipids	PGL
Lipoarabinomannan	LAM
Trehalose dimycolate	TDM
World Health Organisation	WHO
Isoniazid	INH
Ethambutol	EMB
Rifampicin	RIF
Pyrazinamide	PZA
Bedaquiline	BDQ
Nicotinamide adenine dinucleotide	NAD

Genomic island	GI
Sulfotransferases	ST
Adenosine monophosphate	AMP
Trehalose-2-sulfate	T2S
Directly observed treatment	DOT
Root mean square deviation	RMSD
Root mean square fluctuation	RMSF
Secondary structure elements	SSE

Abstract

Tuberculosis (TB) is a respiratory disease caused by *Mycobacterium tuberculosis (M. tuberculosis)*. The high transmission and mortality rates show that the medical and scientific community need new strategies to combat the TB burden. One strategy would be repurposing drugs which have already been Food and Drug Administration (FDA)-approved to aid in discovery of potential inhibitors against novel TB drug targets. This project aimed to identify a potential inhibitor of FadD23 through *in silico* screening of FDA-approved drugs against the FadD23 protein structure. Ligand structures were retrieved from the ZINC database and docked into FadD23 using AutoDock Vina. Simeprevir had the highest docking score (-10.5 kcal/mol), and was further subjected to 600 ns molecular dynamics (MD) simulations using Amber 18, with Phosphoaminophosphonic acid-adenylate (ANP) used as a control ligand. Post-MD analysis namely root mean square deviation (RMSD), root mean square fluctuations (RMSF), hydrogen bond (Hbond), radius of gyration (Rg), dynamic secondary structure elements (SSE), and distances were calculated using a CPPTRAJ module. Binding affinities of ligands were calculated using MM/GBSA module. The results of RMSD showed that Simeprevir (2.23 Å) was stable during simulations, where its bulky hydrophobic conformation governed complex stability. This was also supported by the compact conformation of FadD23 structure induced by Simeprevir. Simeprevir also had a higher binding affinity (-33.87 kcal/mol) compared to ANP (-17.95 kcal/mol), where its binding affinity was driven by electrostatic and van der Waals forces. Energy contributions from Thr177, Thr176, Arg555, Ala179, Lys553, and Arg460 notably influenced Simeprevir's binding affinity. RMSF suggested that Simeprevir made contact with both the N- and C-terminal domains of FadD23, where it suppressed residue displacement in the N-terminal domain and induced notable residue displacement in the C-terminal domain. SSE analysis showed that Simeprevir potentially arrests FadD23 function by altering native secondary structure elements. At present, there's no reported drug that has been approved by the FDA against FadD23, nor existence of records showing clinical studies of potential inhibitors of FadD23. Compound 5'-O-[N-(11-phenoxyundecanoyl) sulfamoyl] adenosine (Phu-Ams) was reported to be a general inhibitor of FadD enzymes; however, its interaction with FadD23 did not involve the C-terminal domain. This differs from Simeprevir, where it was noted to form interactions with residues in the C-terminal domain, a domain that is responsible for substrate catalysis. The analysis based on molecular docking, MD simulations and subsequent post-MD trajectory analysis suggest that Simeprevir may be able to serve as a potential inhibitor of FadD23, thus potentially interferes with SL-1 production in *M. tuberculosis*.

Keywords: FDA, M.tuberculosis, FadD23, drug repositioning, molecular dynamics

Chapter 1
Introduction

1.1 Background and Rationale

Tuberculosis (TB) is a respiratory disease caused by *Mycobacterium tuberculosis* (*M. tuberculosis*), which poses significant challenges to global health care. It is transmitted by emitting tiny respiratory droplets containing live, airborne *M. tuberculosis* (1, 2). TB strains that are resistant to drugs are among the most significant disease-causing agents globally, contributing to 25% of the reported mortality rates (3). Individuals with compromised immune systems, such as those afflicted with HIV or diabetes, have a higher susceptibility to infection. *M. tuberculosis* H37Rv is a micro-organism that belongs to the Mycobactericeae family that requires oxygen to survive, and it obtains energy through the electron transport chain through oxidative phosphorylation (4-8). *M. tuberculosis* is an intracellular pathogen highly adapted to infect and persist within mammalian tissue (9). Tuberculosis is managed using antimicrobial medications. Both TB infection and illness require treatment. The often-prescribed antibiotics include isoniazid, rifampin, pyrazinamide, ethambutol, and streptomycin. The emergence of extreme drug resistance (XDR) and multi-drug resistance (MDR) is a direct outcome of inadequate treatment and excessive use of antibiotics, which has led to a demand for novel targets and treatments. Although numerous pharmacological targets have been identified, more still require further characterization to understand the functionality and discover new drug targets due to antibiotic resistance and the lengthy course of treatment for TB. There is an abundance of unique glycolipids linked to tuberculosis's pathogenesis (10, 11). Sulfolipid-1 (SL-1) was found to be a component of the cell wall and was identified as being able to impede mitochondrial oxidative phosphorylation and phagosome-lysosome fusion and induce changes in phagocytic cells (12-14). SL-1 is the most abundant sulfatide, and its location allows it to interact with host cells. Surface components such as SL-1 and phthiocerol dimycocerosate (PDIM) control the modifications that occur in lysosomal systems (15). It has been found in pathogenic bacteria and the quantity has been directly related to the virulence of the strain (11, 16). The FadD enzymes are responsible for the synthesis of virulent lipids and the degradation of lipids and cholesterol (17). The fatty acyl-coenzyme A (CoA) ligases (FACL) and Fatty acyl-AMP ligase (FAAL) enzymes are responsible for the conversion of fatty acid substrates into intermediate acyl adenylates with the aid of adenosine triphosphate (ATP) (17). The enzyme FadD23 is known to play a role in the biosynthesis of SL-1 alongside polyketide synthase 2 (Pks2) (18). The structure of FadD23 was solved and noted to have a large N-terminal domain and a small C-terminal domain, which has been suggested to serve as a cover for fatty acids when binding occurs (19). Further research is necessary to gain insight into the structural and functional dynamics of this protein. *In silico* studies, while removing serendipity, have had a great impact on drug development. These include saving time and cost, as drug discovery is an expensive and time-consuming task (20). The dynamic features of protein-ligand complexes have been suggested to harbour structural fluctuations. Analysis

of these structural features may find whether proteins may be inhibited or activated (21). The information generated from these structural studies of drug targets creates the opportunity to develop new drugs and inhibitors (22). Alternate drug discovery and development methods include molecule modelling approaches utilized in the study of pharmacology (22-24). Rational drug design is facilitated by the generated interactions (25). Molecular dynamics (MD) simulations are valuable because they allow for the projection of the evolution of individual molecules over a specific period while also demonstrating the collective conformational changes within biological systems (26). Molecular modelling has demonstrated significant promise in drug discovery and drug interaction research, particularly in cardiology, cancer, neurology, and infectious diseases (20). Rational drug design is contingent upon a thorough characterization of the therapeutic target. Further structural characterization of FadD23 by its ATP activation is required to enhance our understanding of its role in SL-1 biosynthesis. There are no drugs that target FadD23 or the FadD enzyme class. The purpose of this study is to apply *in silico* techniques to identify potential inhibitors that have already been FDA-approved. This study will provide insight into how FDA drugs bind to FadD23 and impact its activity compared to ANP, an analogue of ATP (needed for activation of FadD) and palmitic acid (its natural substrate). This study may provide credibility for FadD23 as a drug target against TB transmission and the results may serve as a model after which ligands may be designed to produce an inhibitory effect against FadD23 to curb the spread of TB.

1.2 Problem Statement

TB is an ever-increasing threat, causing millions of deaths worldwide every year. With the rise of drug-resistant strains, there is a constant need to develop effective therapeutics and discover new drug targets. FadD23 presents as an attractive drug target due to its significant role in SL-1biosynthesis. The lack of information against FadD23 presents as a novel study as there have been no drugs that have been FDA-approved for FadD23. This enzyme still has areas that need to be documented in its activation by ATP and reaction with Pks2, as well as investigating potential inhibitors using FDA approved drugs which may be effective against a target that has been noted for eliciting the “coughing mechanism” often associated with the hallmark symptom of TB. Given the potential of FadD23 as a drug target, beneficial information surrounding the interactions of FadD23s interaction with an FDA-approved drug may be beneficial in providing a design basis for a new drug or reducing costs to apply an existing drug to this particular drug target.

1.3 Novelty, Significance and Implications

TB is a major cause of death worldwide, especially in developing countries such as South Africa. The evolution of drug-resistant strains has made TB treatment increasingly challenging, rendering the development of new therapeutic agents essential due to its elevated status as a lethal infection. As per the WHO guidelines, the current treatment consists of four first-line medications: isoniazid, ethambutol, rifampin, and pyrazinamide. These drugs form the foundation of the treatment and are administered for

six months. Although this treatment has shown effectiveness, the emergence of antibiotic resistance and the occurrence of various adverse effects have prompted the search for novel pharmacological targets and inhibitors with distinct modes of action (27). Additionally, traditional plants are being explored as potential therapies (28-30). Although many protein structures remain unsolved, the SL-1 biosynthetic pathway proteins have been identified as prospective targets for therapeutic development. FadD23 was solved in 2023 (19) rendering it a molecule that presents for novel studies. FadD23, in conjunction with Pks2, has been observed to have a crucial function in the synthesis of SL-1 (18). FadD23 presents as a potential drug target against tuberculosis. This target is novel compared to other well-documented drug targets, giving way to better drug design or vaccines. This study was motivated due to the lack of understanding of the SL-1 biosynthesis pathway and a lack of studies concerning inhibitors that target FadD23. SL-1 is a unique component within the bacterium's cell wall and is responsible for pathogenesis. FadD23 thus allowed an understanding of its interaction with FDA-approved drugs along with palmitic acid and ANP. The structural interaction has not been documented between FadD23 and drugs that have already been FDA-approved, which would aid in adding insight into FadD23 and its binding. The low solubility of TB proteins has made it difficult to purify and express them to yield a significant amount that allows experimental studies to occur doing protein purification is expensive and time-consuming, hence why *in silico* studies will allows us to understand protein dynamics while viable methodology can be troubleshot to increase the solubility of TB proteins to apply experimental validation. To our understanding, this is the first instalment of data from an *in-silico* drug repositioning study against FadD23. This study will hopefully provide a foundation for further experimental investigation of FadD23 and its class of proteins as a drug target for drug development for TB treatment.

1.4 Aim

To identify and reposition FDA-approved drugs as potential inhibitors for mycobacterial FadD23.

1.5 Objectives

*To generate a FadD23 + Ligand complex to characterize the structural dynamics to gain insight into the behaviour of protein and ligands ANP, PLM, and the suitable FDA-approved drug.

*To determine structural factors that contribute towards the inhibitory potential of selected ligand.

*To compare the binding affinity of selected ligand against that of ANP.

1.6 Hypothesis

An FDA-approved drug that probably possess structural properties similar to those of ANP will be identified to serve as a potential inhibitor of FadD23 by targeting the ANP binding site.

1.7 Research Questions

* Which of the selected drugs will bind to the FadD23 active site?

*What binding sites will be preferable for optimum binding affinity and potential inhibition?

* What binding affinity of the inhibitor will be exerted on the protein?

* How does the inhibitor interact with key functional N-terminal and C-terminal domains?

*What potential molecular mechanism of inhibition will be exerted on FadD23?

1.8 References

1. World Health Organization. Tuberculosis [Internet]. World Health Organization. 2023. Available from: https://www.who.int/news-room/fact-sheets/detail/tuberculosis [Accessed 18 October 2024].

2. Bussi C, Gutierrez MG. *Mycobacterium tuberculosis* infection of host cells in space and time. FEMS Microbiology Reviews. 2019 Jul 1;43(4):341–61.

3. O'Neill J. Tackling drug-resistant Infections globally: Final Report and recommendations. the Review on Antimicrobial Resistance. 2016.

4. Orcau À, Caylà JA, Martínez JA. Present epidemiology of tuberculosis. Prevention and control programs. Enfermedades Infecciosas y Microbiología Clínica. 2011 Mar;29:2–7.

5. Chitale P, Lemenze AD, Fogarty EC, Shah A, Grady C, Odom-Mabey AR, et al. A comprehensive update to the *Mycobacterium tuberculosis* H37Rv reference genome. Nature Communications. 2022 Nov 18;13(1):7068.

6. Dunn JJ, Starke JR, Revell PA. Laboratory Diagnosis of *Mycobacterium tuberculosis* Infection and Disease in Children. Kraft CS, editor. Journal of Clinical Microbiology. 2016 Mar 16;54(6):1434–41.

7. Kalia NP, Hasenoehrl EJ, Ab Rahman NB, Koh VH, Ang MLT, Sajorda DR, Hards K, Grüber G, Alonso S, Cook GM, Berney M, Pethe K. Exploiting the synthetic lethality between terminal respiratory oxidases to kill *Mycobacterium tuberculosis* and clear host infection. Proceedings of the National Academy of Sciences. 2017 Jun 26;114(28):7426–31.

8. Rao SPS, Alonso S, Rand L, Dick T, Pethe K. The protonmotive force is required for maintaining ATP homeostasis and viability of hypoxic, nonreplicating *Mycobacterium tuberculosis*. Proceedings of the National Academy of Sciences. 2008 Aug 19;105(33):11945–50.

9. Russell DG. *Mycobacterium tuberculosis*: here today, and here tomorrow. Nature reviews Molecular cell biology. 2001;2(8):569–77.

10. Brennan PJ, Nikaido H. The Envelope of Mycobacteria. Annual Review of Biochemistry. 1995 Jun;64(1):29–63.

11. Minnikin DE, Kremer L, Dover LG, Besra GS. The Methyl-Branched Fortifications of *Mycobacterium tuberculosis*. Chemistry & Biology. 2002 May;9(5):545–53.

12. Zhang L, Goren MB, Holzer TJ, Andersen BR. Effect of *Mycobacterium tuberculosis*-derived sulfolipid I on human phagocytic cells. Infection and Immunity. 1988;56(11):2876–83.

13. Goren MB, Brokl O, Das BC, Lederer E. Sulfolipid I of *Mycobacterium tuberculosis*, strain H37RV. Nature of the acyl substituents. Biochemistry. 1971 Jan;10(1):72–81.

14. Schelle MW, Bertozzi CR. Sulfate Metabolism in Mycobacteria. ChemBioChem. 2006 Aug 25;7(10):1516–24.

15. Converse SE, Mougous JD, Leavell MD, Leary JA, Bertozzi CR, Cox JS. MmpL8 is

required for sulfolipid-1 biosynthesis and *Mycobacterium tuberculosis* virulence. Proceedings of the National Academy of Sciences of the United States of America. 2003 Apr 30;100(10):6121–6.

16. Gangadharam PRJ, Cohn ML, Middlebrook G. Infectivity, pathogenicity and sulpholipid fraction of some Indian and British strains of tubercle bacilli. Tubercle. 1963 Dec;44(4):452–5.

17. Baran M, Grimes KD, Sibbald PA, Fu P, Helena I.M. Boshoff, Wilson DJ, Aldrich CC. Development of small-molecule inhibitors of fatty acyl-AMP and fatty acyl-CoA ligases in *Mycobacterium tuberculosis*. European Journal of Medicinal Chemistry. 2020 Sep 1;201:112408–8.

18. Lynett J, Stokes RW. Selection of transposon mutants of *Mycobacterium tuberculosis* with increased macrophage infectivity identifies fadD23 to be involved in sulfolipid production and association with macrophages. Microbiology. 2007 Sep 1;153(9):3133–40.

19. Yan M, Cao L, Zhao L, Zhou W, Liu X, Zhang W, Rao Z. The Key Roles of *Mycobacterium tuberculosis* FadD23 C-terminal Domain in Catalytic Mechanisms. Front Microbiol. 2023 Feb 21;14:1090534. doi: 10.3389/fmicb.2023.1090534.

20. Lin X, Li X, Lin X. A Review on Applications of Computational Methods in Drug Screening and Design. Molecules. 2020 Mar 18;25(6):1375.

21. Isa MA, Majumdhar RS, Haider S. In silico docking and molecular dynamics simulation of 3-dehydroquinate synthase (DHQS) from Mycobacterium tuberculosis. Journal of Molecular Modeling. 2018 May 11;24(6).

22. Salo-Ahen OMH, Alanko I, Bhadane R, Bonvin AMJJ, Honorato RV, Hossain S, Juffer A, Kabedev A, Lahtela-Kakkonen M, Larsen AS, Lescrinier E, Marimuthu P, Mirza MU, Mustafa G, Nunes-Alves A, Pantsur T, Saadabadi A, Singaravelu A, Vanmeert M . Molecular Dynamics Simulations in Drug Discovery and Pharmaceutical Development. Processes. 2021 Jan 1;9(1):71.

23. De Vivo M, Masetti M, Bottegoni G, Cavalli A. Role of Molecular Dynamics and Related Methods in Drug Discovery. Journal of Medicinal Chemistry. 2016 Feb 8;59(9):4035–61.

24. Liu X, Shi D, Zhou S, Liu H, Liu H, Yao X. Molecular dynamics simulations and novel drug discovery. Expert Opinion on Drug Discovery. 2017 Nov 15;13(1):23–37.

25. Kitchen DB, Decornez H, Furr JR, Bajorath J. Docking and scoring in virtual screening for drug discovery: methods and applications. Nature Reviews Drug Discovery. 2004 Nov;3(11):935–49.

26. Legge FS, Budi A, Treutlein H, Yarovsky I. Protein flexibility: Multiple molecular dynamics simulations of insulin chain B. Biophysical Chemistry. 2006 Jan;119(2):146–57.

27. Furin J, Cox H, Pai M. Tuberculosis. The Lancet. 2019 Apr;393(10181):1642–56.

28. Drewes SE, Crouch NR, M.J. Mashimbye, Leeuw BMD, Horn MM. A phytochemical basis for the potential use of Warburgia salutaris (pepper-bark tree) leaves in the place of bark. 2001 Jan 1;97(9):383–6.

29. Madikane VE, Bhakta S, Russell AJ, Campbell WE, Claridge TDW, Elisha BG, Davies

SG, Smith P, Sim E p. Inhibition of mycobacterial arylamine N-acetyltransferase contributes to anti-mycobacterial activity of Warburgia salutaris. Bioorganic & Medicinal Chemistry. 2007 May;15(10):3579–86.

30. Obakiro SB, Kiprop A, Kowino I, Kigondu E, Odero MP, Omara T, Bunalema L. Ethnobotany, ethnopharmacology, and phytochemistry of traditional medicinal plants used in the management of symptoms of tuberculosis in East Africa: a systematic review. Tropical Medicine and Health. 2020 Aug 14;48(1).

CHAPTER 2
Literature Review

2.1 History of Tuberculosis

Tuberculosis (TB), which was previously referred to as consumption, has profoundly impacted the social and economic nature of human existence (1, 2). Since ancient times, TB, an illness resembling TB, has been documented in various civilizations. The Vedas contain an early description of the condition, referred to as "Yakshma," which translates to "wasting disease" (3). Literature from Chinese, Greek, and Arabic have records of TB-like disease (3, 4). For the past 150 million years, *Mycobacterium tuberculosis (M.tuberculosis)* has been in existence (5). Among others, mummies from the Egyptian pre-dynastic era exhibited typical tubercular lesions (6). The initial faint evidence of tuberculosis in humans is a bone lesion discovered in a 500-thousand-year-old skull in Turkey. The strongest and earliest evidence of human tuberculosis (TB) is the detection of TB in a Neolithic infant and woman from a 9000-year-old settlement in the Eastern Mediterranean using polymerase chain reaction (PCR)(6). Girolamo Fracastorius (1483-1553) demonstrated that certain ailments could be transmitted through "particles" through direct or indirect human contact. Miliary tuberculosis was initially characterized by Thomas Willis (1621-1675). Benjamin Marten (1690-1752) proposed the theory of "contagious living fluid," which postulated that minute living organisms induce tuberculosis. Jean Antoine Villemin (1827-1892), a French medic in the army, demonstrated tuberculosis transmission from humans to animals and animal to animal (6). The term "tuberculosis" is derived from the Latin word "tubercula," which is defined as "a small lump." This observation is present in all forms of the disease. Johann Lukas Schoenlein proposed this appellation in 1834 (7). In a meeting of the Berlin Society of Physiology on March 24, 1882, Robert Koch declared that he had identified the causative agent of pulmonary tuberculosis. In his published paper, he subsequently referred to it as the "tuberkel virus." In 1905, the German scientist was awarded the coveted Nobel Prize in Medicine for his innovative concepts regarding tuberculosis bacilli's staining and subsequent cultivation on bovine and/or sheep serum (7, 8). Between 1908 and 1921, Leon Charles Albert Calmette (1863–1933) established a vaccine against tuberculosis by subculturing *Mycobacterium bovis* more than 200 times in a guinea pig model (3,7).

2.2 Classification of Tuberculosis

Table 2.1: Taxonomy of *M. tuberculosis*.

Order	Actinomycetales
Class	Acinamyceles
Family	Mycobacteriaceae
Genus	*Mycobacterium*

2.3 Cell Wall of Mycobacterium tuberculosis

Mycobacterium tuberculosis (M. tuberculosis) is the causative agent of tuberculosis, a respiratory disease. TB is considered one of the most effective pathogens, and its success is attributed to the bacteria's capacity to influence and interfere with the host systems at various levels (10). It is an organism that has been extensively engineered to infect and flourish in mammalian tissue (11, 12). *M. tuberculosis* establishes and maintains the state of infection by interacting with the trafficking pathways of the host cells, including phagosome maturation (11, 13-15) and autophagy (16, 17); these interactions occur at the cellular level (10). The cellular surfaces of microbial pathogens have been modified to protect against host degradative enzymes, radical ion species, and antibiotics. The cell wall comprises numerous components that are essential to its life cycle. These components include glycolipids, which have been associated with microbial pathogenesis (18- 21). In *M. tuberculosis*, a sulfated glycolipid termed sulfolipid-1 (SL-1) has been recognized as a potential virulence factor (22).

M. tuberculosis is characterized by long-chain mycolic acids (Figure 2.1) that are covalently linked to the arabinogalactan core (AG). Mycolic acids are specialized lipid constituents of the mycobacterial cell membrane and are vital for the survival of *Mycobacterium* genus members (23). These acids noncovalently anchor an outer membrane of lipids and glycolipids (Figure 2.2). The host response is modulated by the interaction between immune cells and phenolic glycolipids (PGL), lipoarabinomannan (LAM), and trehalose dimycolate (TDM), which are components of the cell wall that have been implicated in modulating host-pathogen interactions (24-26).

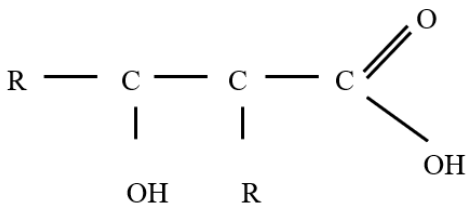

Figure 2.1: Structure of mycolic acid.

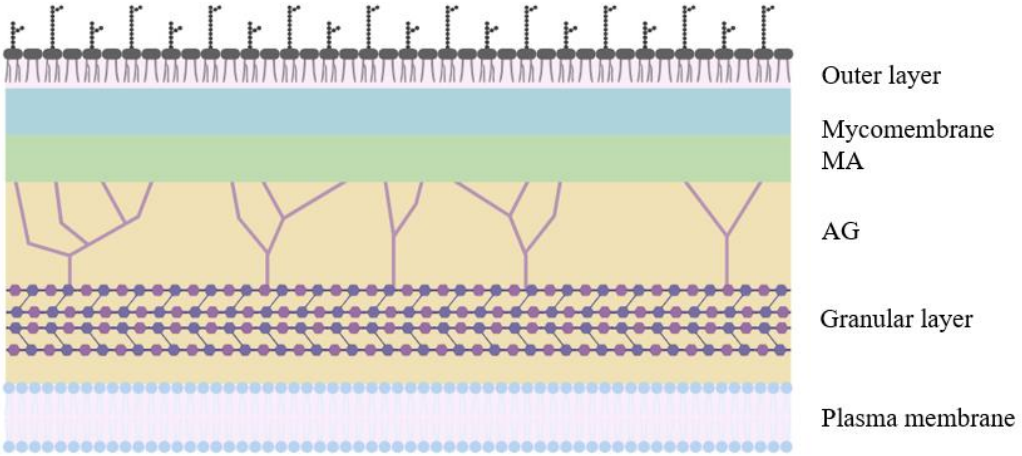

Figure 2.2: The cell wall of *M. tuberculosis* and its components. AG: arabinogalactan; MA: mycolic acid.

Although the bacteria exist in an arrested phagosome in vitro, *M. tuberculosis* infection may significantly affect the endo-lysosomal system due to the unique lipids of the surface component that concentrate in endosomes and lysosomes (27-30). Mycobacterial surface components, chiefly SL-1, facilitate the modifications in lysosomes. SL-1 independently stimulates lysosomal biogenesis across several cell types by modulating the mTORC1-TFEB axis in host cells and influences phagosome trafficking kinetics in macrophages. The findings endorse a concept wherein *M. tuberculosis* and lysosomes mutually regulate one another; specifically, *M. tuberculosis* infection prompts lysosomal biogenesis in macrophages, which in turn governs the trafficking and survival of the bacterium (10). *M. tuberculosis* possesses elevated concentrations of trehalose (a disaccharide) in its unbound state, along with the cord factor and SL-1 (31).

The increasing knowledge of the molecular, structural, and immunological foundations of *M. tuberculosis* pathogenicity presents novel prospects for therapeutic discovery. Lipid metabolism is essential for the bacillus's infectious and latent stages. Consequently, pharmaceuticals focusing on the lipid metabolic network serve as potent anti-tubercular medicines (32). Given that fatty acyl-AMP ligase (FAAL) inhibitors, such as acyl-sulfamoyl analogues, also inhibit fatty acyl-CoA ligases (FACLs), they are anticipated to affect various lipid biosynthesis and degradative processes (33, 34). This approach of concurrently blocking numerous enzymes has significant promise as a new class of multi-target pharmaceuticals.

2.4 Pathogenesis and Risk Factors

The bulk of droplet nuclei containing *M. tuberculosis* from infectious individuals are retained in the upper airway and ejected by ciliated mucosal cells, with just a small proportion reaching the alveoli. The mycobacteria then bind to the cell surface of alveolar macrophages through complement receptors, Type A scavenger receptors, or mannose receptors (6). After phagocytosis, mycobacteria diminish

acidity within the phagosome, and a cell wall constituent (i.e., lipoarabinomannan) disrupts the Ca+/calmodulin pathway, hence obstructing phagosome lysosome fusion. Upon successful inhibition of phagosome maturation, bacilli proliferation commences, leading to the final rupture of the macrophage, which releases the bacilli. Other macrophages subsequently internalize these bacilli, perpetuating the infection cycle and further disseminating the spread (35). The transmission of the bacteria is influenced by several parameters, including the number of bacilli in droplets, its virulence factors, exposure to UV light, aerosolization, and ventilation (36). In addition to primarily affecting the lungs within the respiratory system, the bacterium can disseminate to other body regions, leading to extrapulmonary or extrapulmonary tuberculosis (Figure 2.3). These encompass the regions of the bones, joints, lymphatic pleura, and meninges (37).

The Centre for Disease Control and Prevention (CDC) identifies risk factors such as a compromised immune system resulting from certain medications or health conditions, including diabetes, cancer, or human immunodeficiency virus (HIV), as well as employment in environments conducive to tuberculosis transmission, such as hospitals or correctional facilities, and frequent travel to regions where tuberculosis is prevalent, particularly in Asia, Africa, and Latin America (38). Identifying recently exposed people (close contacts) at elevated risk of advancement and providing them with prophylactic medication may constitute an effective technique to avert illness development. Biomarkers demonstrate the potential for identifying those at the greatest risk of development (39). A considerable body of research has examined how pathogen and host factors, such as local immune responses and disease tolerance, elucidate the pathogenesis and risk factors for developing tuberculosis while also identifying socioeconomic risk factors that may equally predict susceptibility to infection and illness from TB (40).

Individuals from low socio-economic status populations are at an elevated risk of contracting tuberculosis (41), and in nations with a low burden of tuberculosis, there have been significant reductions in morbidity and mortality due to modifications in overall living circumstances (42). A study in Peru identified modifiable socioeconomic risk variables, such as indoor air pollution, inadequate window provision per room, and household socioeconomic status, as significant predictors of tuberculosis infection and illness (43). Individuals with a history of tuberculosis are at an elevated risk of recurrence, perpetuating a detrimental cycle of tuberculosis and poverty (44). Addressing socioeconomic variables, such as smoking and indoor air pollution, is equally crucial as host and pathogen factors in mitigating the incidence of tuberculosis (40).

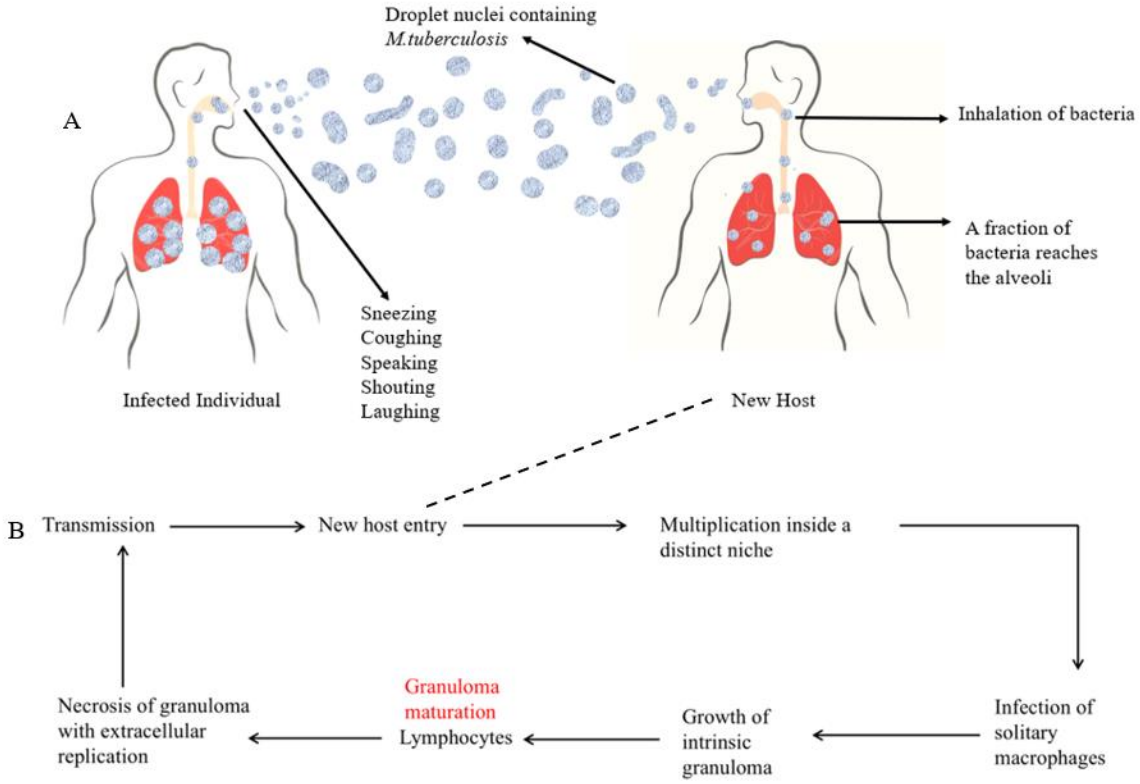

Figure 2.3: An overview of tuberculosis transmission, wherein (A) elucidates the mechanism by which infected individuals expel droplet nuclei into the atmosphere, facilitating the infection of new hosts, and (B) delineates the transmission cycle inside these new hosts, resulting in the further dissemination of bacteria into the air.

2.5 Symptoms

Symptoms vary according to the location and proliferation of the TB bacterium, which predominantly inhabits the lungs. A cough persisting for over three weeks indicates the presence of active tuberculosis in the lungs. Additionally, there is chest pain accompanied by haemoptysis and sputum production. Additional symptoms encompass weariness, weight reduction, chills, fever, and nocturnal perspiration. Tuberculosis in the lymph nodes frequently manifests as hard, red, and purple swelling beneath the skin.

Tuberculosis in the brain may result in headaches or confusion, whereas in the spine, individuals may exhibit back pain (38).

2.6 Treatment and Drug Resistance

Treatment comprises four medications: isoniazid, rifampicin, pyrazinamide, and ethambutol administered for two months, succeeded by isoniazid and rifampicin for an additional four months (38, 45). Daily delivery of therapy yields superior outcomes compared to thrice-weekly treatment, with the World Health Organisation (WHO) advocating for daily fixed-dose combination therapy for all patients diagnosed with tuberculosis (45). Recent therapeutic advancements in the management of drug-susceptible tuberculosis have concentrated on two domains: the administration of high-dose rifampicin and the incorporation or replacement of fluoroquinolones in the therapy regimen (40).

Isoniazid (INH): frequently utilized as a primary therapeutic agent and for tuberculosis prophylaxis. INH is a prodrug activated by KatG (46), a catalase-peroxidase, leading to forming various radicals and adducts that disrupt mycolic acid synthesis, impacting cell wall synthesis (47). A bactericidal action subsequently ensues. INH can also interfere with the synthesis and metabolism of lipids, deoxyribonucleic acid (DNA), carbohydrates, and nicotinamide adenine dinucleotide (NAD) (47). Resistance typically manifests and is commonly identified in KatG (48).

Rifampicin (RIF): An antibacterial agent effective against several gram-positive bacteria, *Mycobacterium* species, and certain gram-negative bacteria. It is recognized for its inhibition of bacterial DNA-dependent RNA polymerase (49) by binding within the DNA/ ribonucleic acid (RNA) channels of the polymerase subunit (50), so directly obstructing the elongating RNA at the 5’ end. Resistance arises from mutations that modify the residues of the rifampicin binding site on RNA polymerases (51), reducing affinity for rifampicin.

Pyrazinamide (PZA): an essential first-line tuberculosis medication that shortens the treatment period from 9-12 months to 6 months (52). PZA infiltrates the granuloma of *M. tuberculosis*, where it is converted into the active form of pyrazinoic acid by pyrazinamidase (53), encoded by the pncA gene. Pyrazinoic acid inhibits fatty acid synthase, hence preventing bacteria from synthesizing fatty acids (54). Pyrazinoic acid accumulates in Bacillus spp. under acidic circumstances with a pH range of 5 to 6 (53, 55). It has been suggested that the accumulation of pyrazinoic acid disturbs membrane potential and impedes energy production (56), both of which are essential for the survival of *M. tuberculosis* in an acidic infection site. The predominant cause of PZA resistance in *M. tuberculosis* strains is mutations in the pncA gene (57).

Ethambutol (EMB): A bacteriostatic agent utilized in treating pulmonary tuberculosis, in conjunction with isoniazid, pyrazinamide, and rifampicin, through the infiltration of mycobacterial cells. It inhibits arabinosyltransferases upon entering the cell, obstructing the synthesis of cell wall constituents such as

arabinogalactan and LAM, as well as cell division (58). Arabinosyltransferases are encoded by the embCAB operon (59). The number of binding sites for mycolic acid diminishes as the quantity of arabinogalactan in the cell wall decreases, accumulating mycolic acid, trehalose monomycolate, and TDM (60). Ethambutol resistance arises from mutations in the embB gene, particularly at the commonly mutated site embB306 (61).

Bedaquiline (BDQ) binds to the c- and ε-subunits of ATP synthase by imitating essential residues in the proton transfer chain, hence inhibiting the movement of the c-rotary subunits during ATP catalysis (62, 63). A critical survival pathway is impaired in both actively growing and non-growing bacteria (63). The uncoupling capabilities of BDQ, facilitated by the H+/K+ antiporter, result in ATP synthase inhibition, causing ATP depletion and membrane potential dissipation (64). Mutations arise in the coding gene atpE, specifically inside the F0 domain of ATP synthase (65, 66).

Any tuberculosis medication may induce a cutaneous rash. Alternative tuberculosis medications may induce gastrointestinal discomfort or nausea. Consuming tuberculosis medication with food can enhance its absorption in the body. The medications rifampin or rifapentine may cause certain bodily fluids to become orange (38).

Isoniazid-resistant strains of tuberculosis are the predominant types of drug-resistant tuberculosis worldwide (67). Presently, significant nations such as Russia, Myanmar, China, and South Africa have experienced a rise in the incidence of rifampicin-resistant tuberculosis (68). Drug-resistant tuberculosis signifies that the pathogens resist at least one of the most potent antitubercular medications. Multidrug-resistant tuberculosis (MDR TB) is induced by pathogens that resist two or more primary antitubercular agents: isoniazid and rifampin. Two additional severe variants of MDR TB are designated as pre-extensively drug-resistant TB (pre-XDR TB) and extensively drug-resistant TB (XDR TB). Pre-XDR and XDR tuberculosis are uncommon forms of illness that exhibit resistance to almost all pharmacological treatments for tuberculosis (38, 45). Non-adherence to the prescribed antibiotic regimen may play a lesser role in the emergence of drug resistance compared to other factors contributing to acquired drug resistance, such as inadequate serum drug concentrations, drug gradients in pulmonary tissue, and the presence of drug efflux pumps on bacterial surfaces (69) can cause drug resistance as well as having an episode of TB prior. Certain individuals get drug-resistant tuberculosis due to exposure to drug-resistant tuberculosis pathogens.

2.7 Genetics of Sulfolipid-1

The genes of the PE_PGRS family are associated with the pathogenesis of *M. tuberculosis*. These genes originate from genomic islands (GI) 1 and 2 and are implicated in SL-1 production. Sequence study indicated that the five PGRS genes exhibit greater polymorphism than other PGRS members in fully virulent *M. tuberculosis* complex strains. Besides serving as a virulence factor of the tubercle bacillus, sulfolipid-1 (SL-1) cluster genes influence the modulation of host-pathogen interactions (70).

There is five PE_PGRS family genes: PE_PGRS53 (Rv3507), PE_PGRS54 (Rv3508), PE_PGRS55 (Rv3511), PE_PGRS56 (Rv3512), and PE_PGRS57 (Rv3514) inside GI-1. GI-2 comprises four chromosomally adjacent genes: papA2 (Rv3820c), mmpL8 (Rv3823c), papA1 (Rv3824c), and psk2 (Rv3825c), which are involved in the synthesis of SL-1. Established research has revealed evidence that PE-PGRS family genes and genes involved in SL-1 production contribute to the pathogenesis of *M. tuberculosis* (70). PE_PGRS is the most significant subgroup of the PE family, characterized as an acidic, glycine-rich protein family exclusive to mycobacteria (71). Four genes within GI-2 have been shown to participate in the sequential production of the predominant sulfatide on the cell surface of *M. tuberculosis*, denoted as SL-1 (72-75). SL-1 and SL-A (a synthetic analogue of SL-1) produce a unique transcriptional signature distinct from established pro-inflammatory agonists (76).

2.8 Structure and Synthesis of SL-1

The structure of SL-1 comprises a disaccharide trehalose-2-sulfate (T2S) core, which is modified by four fatty acyl units, typically including two hydroxypthioceranic acid, one pthioceranic acid, and one palmitic acid (Figure 2.4) (77).

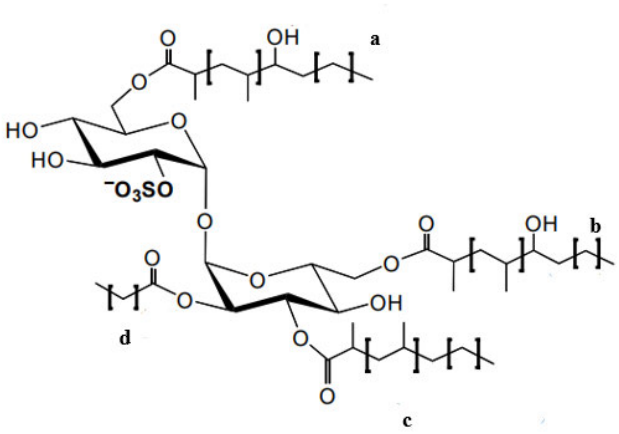

Figure 2.4: The structure of SL-1 and its four fatty acyl units. Hydroxypthioceranic acids at (a) and (b), pthioceranic acid (c) and palmitic acid (d).

SL-1 is synthesized in mycobacteria via an enzymatic pathway that begins with the sulfation of the symmetric disaccharide trehalose to trehalose-2-sulfate (T2S) by the enzyme sulfotransferase 0 (Stf0) (Figure 2.5A), followed by a sequence of acylation reactions (78). Genetic deletion of stf0 in *M. tuberculosis* leads to an inability to produce SL-1 (79). Sulfation of biomolecules is an effect that governs extracellular interactions by modifying the binding characteristics of the associated macromolecule (80, 81). Sulfation has been contrasted with phosphorylation, which, in turn, affects intracellular processes. Sulfotransferases (STs) are enzymes that facilitate the transfer of the sulfuryl group from the universal donor molecule, 3′-phosphoadenosine-5′-phosphosulfate (PAPS), to carbohydrates, proteins, and various low-molecular-mass metabolites (82-84).

Pks2 integrates methyl branches into the virulence lipid SL-1. MmpL8 is essential for fully synthesizing SL-1, and its biosynthetic precursor, SL_{1278}, accumulates within mmpL8- cells (73, 74). SL_{1278}, a diacylated intermediate in SL-1 production, has been demonstrated to trigger the adaptive immune response in human patients (72). The sulfotransferase Stf0 sulfates trehalose at position 2, resulting in the formation of trehalose-2-sulfate (T2S), which initiates SL-1 production (79). In addition, the polyketide synthase Pks2 produces phthioceranoyl and hydroxyphthioceranoyl lipids located at the 6-, 6-, and 3- locations of SL-1(73). The final characterized step in SL-1 biosynthesis is the transfer of SL_{1278} to the outer leaflet of the cell by MmpL8 (72); the enzymes responsible for the final acylation of SL_{1278} to SL-1 have yet to be determined (Figure 2.5B).

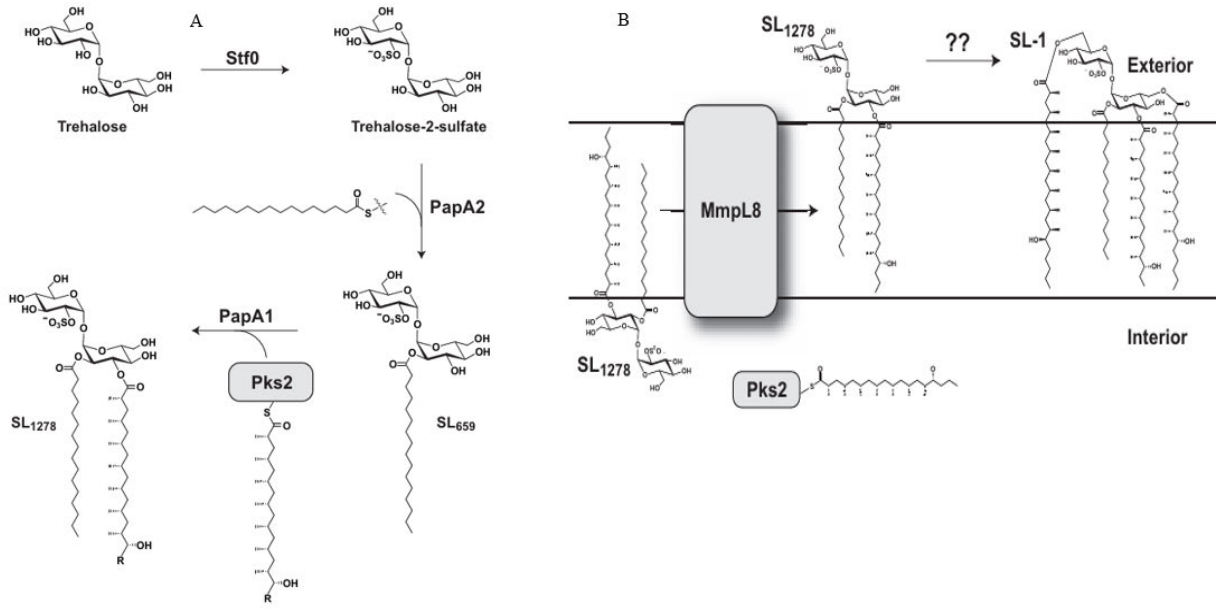

Figure 2.5: (A) The proposed synthesis pathway for SL-1. Stf0 initially sulfates Trehalose to produce T2S. PapA2 subsequently acylates the 2-position of T2S to yield SL659. A hydroxyphthioceranic acid is then synthesized by Pks2. (B) MmpL8 subsequently transports the diacylated SL1278 to the cell exterior, where the final acylations occur (72).

2.9 Properties and Functions of SL-1

SL-1 is exclusively expressed in pathogenic mycobacteria, with its levels positively associated with strain virulence; nonetheless, it is non-essential for the growth of *M. tuberculosis* (19, 85). It is located on the exterior membrane of the cell (Figure 2.6), enabling interaction with host cells during infection (76). The absence of SL-1, constituting roughly 1-2% of *M. tuberculosis* dry weight (22), could potentially disrupt cell membrane permeability and integrity, or surface lipid composition. Considering the efficacy of the latent phase in *M. tuberculosis* pathogenesis, it is unsurprising that *M. tuberculosis* has preserved mechanisms that may govern its intracellular proliferation. It is intriguing to consider why *M. tuberculosis* has preserved genes for SL-1 production, which appear to increase its vulnerability

to antimicrobial agents, and whether this suggests that SL-1 may fulfill additional roles advantageous to *M. tuberculosis* pathogenesis (76). *M. tuberculosis* may also possess mechanisms to modulate SL-1 levels by precisely regulating its production or relocation to the outer cell wall. Transcriptional and metabolic pathways exist that seem to regulate SL-1 synthesis (86-89).

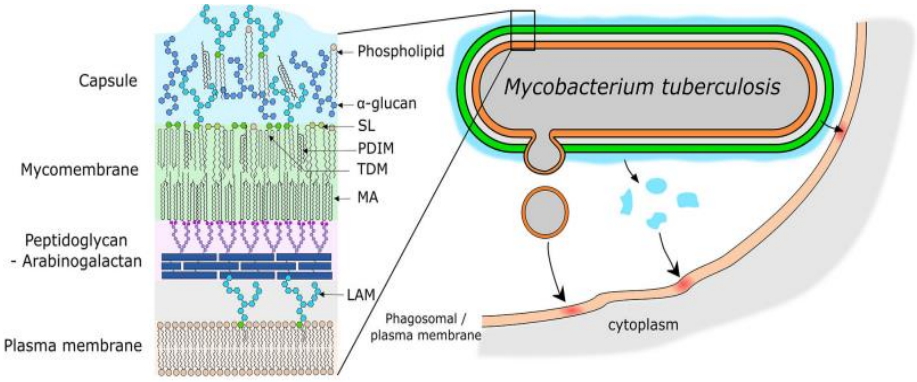

Figure 2.6: The model of the mycobacterial envelope and the lipid components, including SL-1 in the outer membrane (90).

The production of SL-1 during specific phases of the *M. tuberculosis* infection cycle may be crucial for resisting host defense responses that are not reliant on adenosine monophosphate (AMP) activity. Moreover, the production of SL 1 may have been preserved by *M. tuberculosis* to function as a molecular determinant specifically recognized by human cells (76). In cell culture models, pure SL-1 has been suggested to modify phagosome-lysosome fusion, impair mitochondrial oxidative phosphorylation, and stimulate and inhibit cytokine and reactive oxygen species generation by human leukocytes (91-97). The augmented production of SL-1 may fortify the tubercle bacillus's cell wall, enhancing its protective capacity against unfavourable growth conditions found in the host or in vitro environments. This impact may be significant for the formation or maintenance of persistent infection of *M. tuberculosis* during chronic infection (70). Numerous studies have demonstrated that SL-1 exerts various effects on the modulation of host-pathogen interactions, including the regulation of superoxide (O^{2-}) release, the prevention of cord factor-induced granuloma development, and the suppression of serum TNF-α release in mice (98).

SL-1 obstructs the fusion of mycobacteria containing phagosomes with lysosomes, a well-documented method of mycobacterial survival (13, 79, 93, 99). SL-1 stimulates lysosomal biogenesis through a mTORC1 TFEB-dependent mechanism (Figure 2.7), while a mutant strain of *M. tuberculosis* deficient in SL-1 exhibits a marked reduction in lysosomal homeostasis alterations both *in vitro* and *in vivo*. The attenuated lysosomal reconfiguration in the SL-1 mutant leads to diminished trafficking to lysosomes and increased intracellular survival of the mutant bacteria (10), consequently finding SL-1 is essential for adaptive lysosomal homeostasis in the context of infection.

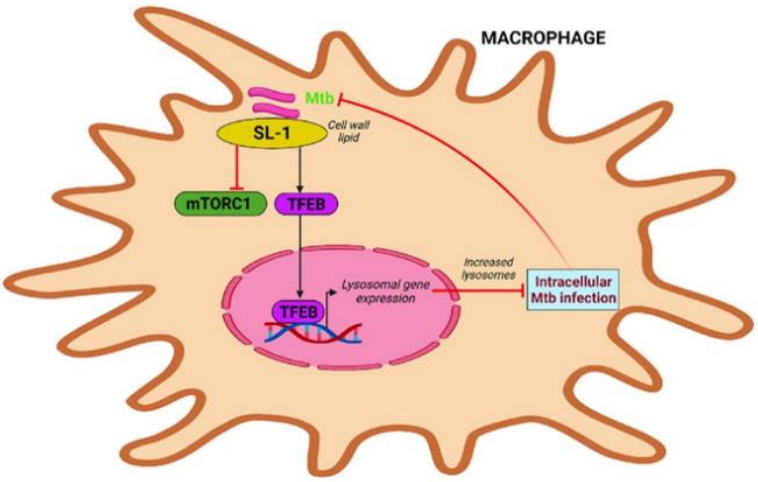

Figure 2.7: Lysosome biogenesis induction through sulfolipid-1 (100).

SL-1 exhibited a significant impact on host lysosomes. SL-1 production is regulated by many mechanisms and is upregulated during the infection of both human macrophages and mice (87-89, 101, 102). SL-1 has been proposed to contribute to phagosome acidification, as phagosomes with sulfolipid-coated silica beads exhibit more acidification than those with control lipids (91). The presence of lipids such as SL-1 on the surface may enable *M. tuberculosis* to regulate or fine-tune its survival via influencing host lysosomes and its intracellular trafficking.

Mammalian cells, such as oligodendrocytes and Schwann cells, synthesize a sulfated sphingolipid known as sulfatide (3-O-sulfogalactosylceramide), which constitutes 4% of myelin lipids (103). To establish if mammalian sulfatide may activate nociceptive neurons and further evaluate the chemical specificity of neuronal activation by exposing neurons to sulfatide, it was noted that neither sulfatide nor its non-sulfated analogue, galactocerebroside, elicited a response in successfully inducing elevated intracellular [Ca^{2+}]. SL-1 independently activates neurons, and the neuronal response to SL-1 does not indicate a universal reaction to non-sulfated mycobacterial cell wall glycolipids or sulfated monosaccharide lipids (104). The synthesis of SL1 is both essential and adequate for activating MED17.11 neurons in vitro, and the organically synthesized precursor T2S also stimulates MED17.11 neurons. Consequently, SL-1 can activate nociceptive neurons in both mice and humans. The coughing observed in *Mycobacterium tuberculosis*-infected guinea pigs is attributable to the synthesis of SL-1 (104). The genetic ablation of SL-1 production in *M. tuberculosis* inhibited neuronal activation and cough induction by *M. tuberculosis* extracts, but SL-1 alone was adequate to provoke cough in naive guinea pigs. Ultimately, guinea pigs inoculated with *M. tuberculosis* deficient in SL-1 synthesis exhibited a diminished cough response, although presenting a significant bacterial load and lung pathology indicative of active tuberculosis (104).

2.10 FadD

Examination of the mycobacterial genome has revealed that numerous genes, including FadD, are implicated in lipid metabolism (105). Modelling studies indicate that mycobacterial FadD proteins may possess extensive N-terminal domains accompanied by diminutive C-terminal domains (33). Genetic and biochemical investigations have demonstrated that polyketide synthases (Pks) and fatty acid synthases (FASs) collaborate with FAAL and FACL, as well as other enzymes related to lipid metabolism, to establish the lipid metabolic network for *M. tuberculosis* (106). PKSs are involved in the biosynthesis of specialized lipid metabolites, such as mycolic acids, phthiocerol dimycocerosates (PDIMs), sulfolipids, mannosyl-β1-phosphomycoketides (MPMs), and mycobactin (107-109). FAALs facilitate communication between FASs and PKSs by supplying an activated fatty acyl adenylate during lipid biosynthesis (33, 34). Assessing these lipids and their metabolic pathways provides a chance to identify and create innovative treatments capable of disturbing the lipid metabolic network.

Numerous FAAL members are near PKS and NRPS gene clusters within the *M. tuberculosis* genome. FAAL proteins facilitate the transfer of an activated fatty acid to PKSs, extending the chain and forming pathogenic lipids that constitute the cell wall. The metabolic future of the activated fatty acid is dictated by its conversion into an acyl-CoA thioester, facilitating energy production and the biosynthesis of phospholipids, or into acyl-AMP for the creation of complex lipids (32). Pks2 is located close to the FAAL-like enzyme FadD23 and possesses a complete PKS module with all six catalytic domains; consequently, pks2 would synthesize pthioceranic acids by employing seven methyl malonyl-CoA (MMCoA) extender substrates through an iterative biosynthetic process (32).

Lipid disintegration is essential because mycobacteria exploit host lipids (fatty acids and cholesterol) to energise key metabolic pathways and serve as substrates for many complex mycobacterial lipids (32, 106, 110, 111). The fadD gene family participates in lipid biosynthesis and catabolism. The mycobacterial fad genes are categorized into two subclasses: fatty acyl-CoA ligases (FACLs), which participate in lipid breakdown, and fatty acyl-AMP ligases (FAALs), which are responsible for lipid biosynthesis based on their activity (32, 71, 106, 111-114). FACLs and FAALs facilitate the ATP-dependent activation of fatty acid substrates to form an acyl-adenylate intermediate, subsequently transferring the acyl group to other substrates, using coenzyme A (CoA) for fatty acid chain lengthening enzymes (FACLs) and PKS for fatty acid acyl ligases (FAALs) (Figure 2.8) (105).

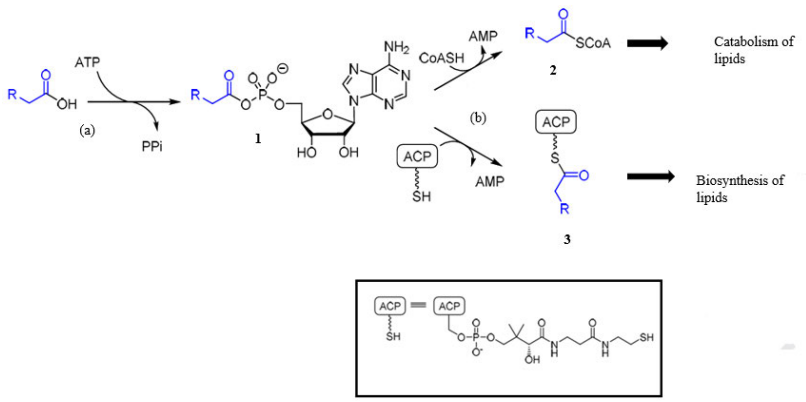

Figure 2.8: The enzymatic mechanism of FadD. FadD facilitates the two-step catalytic process. The initial step (a) entails the adenylation of a fatty acid to generate an acyl adenylate 1. The second reaction (b) involves the acylation of an acceptor molecule, resulting in the formation of thioesters 2 or 3. CoA esters (2) produced by FadD provide FACL, whereas FadDs that load the ACP domain of polyketide synthase enzymes to supply 3 are referred to as FAALs.

The specific metabolic functions of the 20 FACLs remain mostly unclear. FACL3, FACL17, and FACL19 have been biochemically confirmed as CoA ligases implicated in cholesterol breakdown (105). FACL6, FACL15, and FACL19 exhibited extensive substrate specificity (112). In comparison, the FAAL class of FadDs seems to be physiologically nonredundant and facilitates the connection between fatty acid and polyketide production in mycobacteria (33, 106). FadD10 is a FAAL that transfers fatty acids to an acyl carrier protein (Rv0100) (115). FAAL22 is crucial for forming phenolic glycolipids and facilitates the activation and transfer of 4-hydroxybenzoic acid to PKS15/1 (116-118). FAAL26, FAAL28, and FAAL29 are essential to produce PDIM, a significant virulent lipid in the cell wall (91-122). FAAL32 is necessary for activating the long meromycolic chain and is crucial for mycobacterial proliferation (123-126). FAAL23 was identified as participating in sulfolipid synthesis (127).

2.11 FadD23

FadD23 is vital for SL-1 synthesis. It is one of the 34 fatty acid adenylating enzymes in *M. tuberculosis*. FadD23 is a monomer that consists of a N-terminal domain (1-460) and a C-terminal domain (473-584) (Figure 2.9). These two domains are connected by flexible loops and an anti-parallel β sheet (465-472) (128). *M. tuberculosis* FadD23 has 14 helices, 23 β sheets, and irregular loops. The N-terminal is divided into three regions. Region B surrounds a cavity for substrate binding. The C terminal domain comprises 3 peripheral helices and inner sheets respectively. The adenosine binding pocket is located between the N and C- C-terminal domains. The N-terminal domain residues are predominantly involved in binding. Residues Asp222, Tyr376, His221, Ala328, and Ala332 were found to be important for binding.

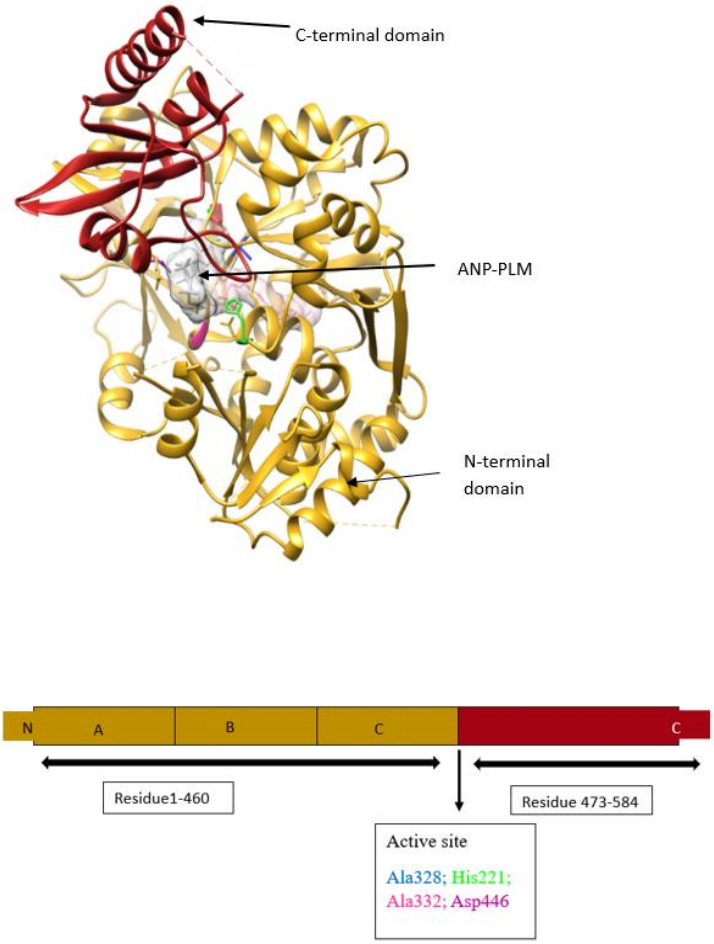

Figure 2.9: Structure of FadD23 in complex with ANP-PLM (PDB ID: 8hdf) with gold denoting N-terminal domain and brick red denoting C-terminal domain. The N-terminal domain comprises 3 regions (A, B, C). The catalytic acids include Ala, His, and Asp (Catalytic amino acids).

AMP-C16 is generated by the hydrolysis of ATP and palmitic acid (Figure 2.10), joining with AMP. The substrate is mainly located in the N-terminal domain. ATP or AMP-PNP is bound to the contact surface between the N (Region B & C)- terminal and C-terminal domains. The fatty acid part points to the β sheet of the N-terminal domain. Palmitic acid is suggested to be the optimal substrate for FadD23 (128). The C-terminal domain provided conformational stability, while the N-terminal domain could not capture fatty acids. The C-terminal domain may serve as a cover for fatty acid binding to FadD23. It resembles a lid that transitions from an open to a closed (stable) state. The anti β sheet stabilizes the overall structure in the closed conformation.

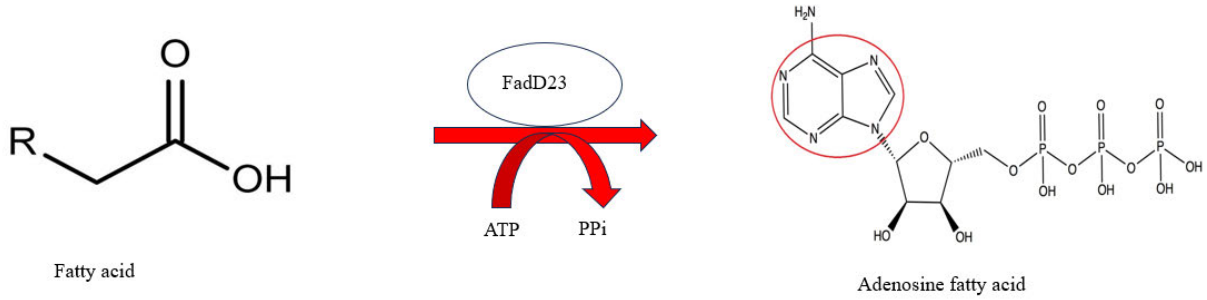

Figure 2.10: The activation of FadD23 using ATP and fatty acid to generate acyl adenylate and PPi products.

M. tuberculosis can transfer hexadecanoyl adenylate or AMP-C18 to Pks in vivo (73). His221 plays a key role in hydrolyzing ATP and product production. The C-terminal domain rotates after binding with ATP and induces full conformation change in the entire structure (Figure 2.11). ATP de-pyrophosphate combines with palmitic acid to form hexadecanoyl adenylate, which dissociates from FadD23 with the involvement of downstream proteins. FadD23 returns to the apo state and awaits substrate capture.

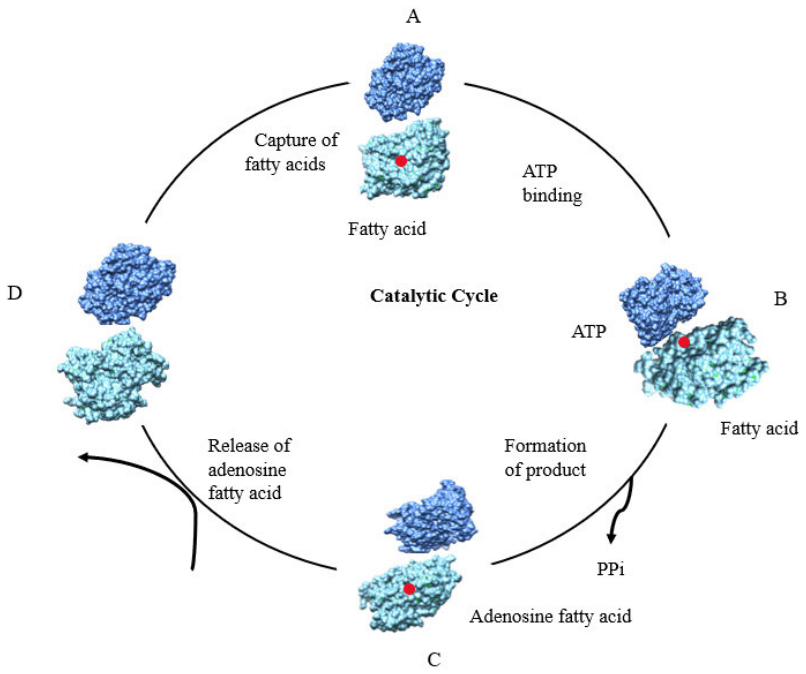

Figure 2.11: The FadD23 catalytic cycle consists of four steps. Fatty acids are sequestered (A). The binding of ATP induces rotation of the C-terminal (B). The synthesis of products is attributed to the proximity of the N and C-terminal domains. The final phase is the dissemination of the products (D).

2.12 Introduction to Computational Chemistry

Chemical concepts are inherently abstract and might be challenging to convey comprehensibly. A tripartite representation method presents a challenge to chemistry at the macroscopic, sub-microscopic, and symbolic levels (129). Chemical phenomena can be observable at the macroscopic level, whereas the sub-microscopic level elucidates the visible qualities of a substance through the interactions of atoms, molecules, and ions (e.g., molecular modelling). The symbolic level illustrates macro and micro phenomena via chemical symbols, formulas, and equations (130).

Introducing a novel pharmaceutical to the market entails significant expenditures in financial resources, human capital, and temporal investment. Computer-aided drug discovery (CADD) techniques employed by leading pharmaceutical corporations and research organizations have become indispensable in the initial phase of drug discovery, facilitating a more cost-effective drug development process and reducing failures in the final step. The application of rational drug design in CADD offers a knowledge-based methodology that can generate significant insights into the interaction dynamics between protein and ligand complexes, along with their binding affinity (131). The present state of the drug development encompasses multiple fields, including chemical and structural biology, computational chemistry, organic synthesis, and pharmacology, and consists of multiple stages. Modelling approaches are often classified into structure-based and ligand-based methods. The structure-based methodology involves utilizing the three-dimensional configuration of the target (enzyme/receptor) to generate or screen prospective ligands (modulators), succeeded by synthesis, biological evaluation, and optimization. Conversely, the ligand-based technique involves treating a collection of molecules exhibiting varied shapes and an established ability to use computational modelling techniques to formulate theoretical forecasting models (131).

Eli Lilly (LY-517717) exemplifies the integration of drug discovery for the prevention of venous thromboembolism in patients undergoing hip or knee surgery, incorporating *in silico de novo* drug design, structure-based lead optimization, iterative synthesis, and assay studies (132-134). To date, CADD has effectively facilitated the introduction of novel medicinal molecules for various diseases, including HIV-1 inhibitors (atazanavir (135), saquinavir (136), indinavir (137), and ritonavir (138)), anti-cancer agents (raltitrexed (139)), and antibiotics (norfloxacin (140)). Shaker et al. (141) have listed a variety of drugs and the year in which they were approved, and the respective drug target/disease. A study examined the disparities in inhibitor binding between wild-type and mutant structures of InhA, a prominent target for tuberculosis (142). Mutations in this protein resulted in reduced affinity for its cofactor, nicotinamide adenine dinucleotide (NADH), leading to isoniazid resistance. MD simulations of the wild-type and mutant structures of InhA complexed with NADH were conducted using Amber 6.0 (143) to elucidate the fundamental characteristics influenced by structural alterations. Schroeder and colleagues discovered that mutations in the glycine-rich loop (I21V and I16T) disrupted the NADH binding conformation, particularly affecting its pyrophosphate moiety, reducing direct and indirect

hydrogen bond interactions within the binding pocket. Isoniazid necessitates the creation of a covalent adduct with NADH at the InhA binding site. Alterations in binding interactions and conformation of NADH may adversely affect this, hence contributing to isoniazid resistance (142). Tuberculosis has been the focus of ongoing and extensive drug discovery research, encompassing thousands of published computer-aided drug design studies. Nonetheless, a study by Ekins et al. identified deficiencies in implementing these methodologies in tuberculosis research (144), leading to a sluggish introduction of candidates into the tuberculosis medication pipeline despite the evident necessity and urgency for addressing this disease. This indicates that more stringent efforts are required in tuberculosis drug discovery to fully leverage the benefits of computational techniques.

Computational chemistry is increasingly becoming a prominent branch in theoretical chemistry, concentrating on resolving chemical issues using computers in molecular drug design methods. Computational chemistry does not directly engage in developing theoretical methodologies; instead, it focuses on deriving results pertinent to chemical issues (145). Incorporating computational chemistry may facilitate the examination of emerging and persistent issues in the pursuit of effective solutions (146). Nonetheless, this is contingent upon the desired accuracy and the inherent properties of the system in question; acquiring significant information for systems consisting of several thousand particles is now feasible. The sole constraint of computational chemistry may lie in the selection of a suitable theory or approach for a specific problem, as well as the capacity to evaluate the quality of the results obtained (147). Two primary methodologies arise from computational chemistry: the first involves examining molecular chemistry at the electronic level, referred to as quantum mechanics; the second, molecular dynamics, disregards explicit electron interactions and emphasizes classical physics principles.

2.13 Force Fields

A force field comprises a collection of functions and constants, designated as parameters, which can be utilized to relate the system's energy to its particles (148). The parameters are designed to establish reference points and force constants, offering a characterization of the potential energy surface (PES) for diverse molecular systems with varying degrees of freedom, arising from incorporating attractive or repulsive atomic interactions. Force fields like AMBER (143), CHARMM (149), NAMD (150), and GROMOS (151) are widely utilized to establish parameters for the simulation of biomolecules. A diverse array of force fields can be utilized for a system; nevertheless, selecting an appropriate force field must be executed judiciously, as each force field encompasses distinct parameters tailored for molecular families (152). Consequently, selecting the appropriate force field is essential, as it can enhance the correctness and relevance of the theoretical structural function of a system under investigation.

2.14 Virtual Screening

Virtual screening (VS) is a methodology in drug discovery and design that utilizes small molecular libraries to identify novel compounds and chemotypes exhibiting desired biological activity as substitutes for ligands or to facilitate the search for ligands targeting uncharted potential drug targets for which crystal, solution, and high-confidence homology structures and models exist (153). VS enables the filtration of thousands of tiny molecules to produce a feasible selection of compounds that may function as lead drugs. This method, referred to as the 'similar property concept,' posits that molecules with analogous structures may exhibit comparable properties (139, 154, 155). Two methodologies are available for screening: ligand-based virtual screening (LBVS) and structure-based virtual screening (SBVS). LBVS uses a predefined array of activities, such as substrate searching, to find potential compounds. In contrast, SBVS utilizes the three-dimensional (3-D) structure of the biological target to dock candidate molecules and evaluate them according to their expected binding affinity or complementarity to the binding site (153).

2.15 Drug Repurposing

Drug repurposing, also known as drug repositioning, reprofiling, or re-tasking, is a process employed to discover novel applications for authorized or investigational medications that extend beyond their original indications (156). The duration of drug development may be shortened by the finalization of preclinical testing, safety evaluations, and formulation advancements, alongside significant cost reductions in preclinical and phase I and II expenditures. Repurposed pharmaceuticals may uncover novel therapeutic targets and routes for further investigation and utilization. Two methodologies for drug repurposing are computational approaches (such as molecular docking (157)) and experimental approaches (such as phenotypic screening (158)).

Some success stories include Acetylsalicylic acid (Aspirin), Zidovudine and Minoxidil, which were repositioned for other treatments than their original indications. Aspirin was initially sold as an analgesic agent but was subsequently repurposed as a cardiovascular drug due to inhibition of platelet aggregation during clinical and pharmacological analysis. It was approved for the management of colorectal cancer in 2015 due to its anti-inflammatory effects. Zidovudine was originally used in cancer treatment, but through in vitro screening of compounds, it was approved for HIV/AIDS treatment in 1987. This was the first anti-HIV drug to be approved by the FDA. Minoxidil was originally used for treatment in hypertensive patients, but retrospective clinical analysis identified that hair growth was an adverse effect. By 1988 Minoxidil was also used to treat alopecia (159).

2.16 Molecular Dynamics

Molecular dynamics (MD) is a computational method employed to simulate complex molecular systems at the atomic level and calculate individual molecules' movements (160). Molecular dynamics is a highly desired computational tool since it allows for assessing fluctuations in the system's motion over a specified duration. Molecular dynamics facilitates the determination of the kinetic and thermodynamic

parameters of the molecular system (161). The primary objective of utilizing this computational application is to apply Newton's equations to elucidate and comprehend the energy and structural variations that may arise within a molecular network system. Nevertheless, the subsequent initial particle states are necessary:

1. The position and velocity of each particle in the molecular network system.
2. A robust force field to differentiate the interactions between atoms, such as AMBER or CHARMM.
3. Boundary criteria must be defined.
4. The classical equation of motion can thereafter be resolved.

$$Fi = m_i \frac{d^2 r_{i\ (t)}}{dt^2}$$

In this context, $r_i(t)$ denotes the particle's position vector, t signifies the temporal evolution, m represents the particle's mass, and Fi indicates the force acting onto the particle.

The application of molecular dynamics can be organized into four continuous technical processes that form a trajectory (162). The four technical procedures encompass:

a. The essential states of the biomolecular system are delineated:
-The coordinates of each atom within the molecular dynamics system.
- The bond properties exhibited by each atom.
- The acceleration of every atom.

b. The potential energy of each atom must be calculated.

c. The equations of motion can be resolved by integrating the potential energy derived from step 2

d. The cycle will revert to step 1 after the new state of the system is saved and the coordinates of each atom are modified.

A quantitative analysis will be conducted on the system's temporal evolution upon trajectory completion.

2.17 Trajectory Analysis

Molecular dynamic trajectories are produced straight from the simulation's production run. The MD trajectories can be characterized as sequential snapshots defined by the coordinates and velocities of each atom in the simulated system, along with the temporal evolution of the system in phase space (163, 164). The subsequent criteria must be considered when selecting software for molecular dynamics analysis:

1. Superior qualitative visualization attributes to facilitate precise representation of the trajectory's video clips and the production of high-quality snapshots/images.
2. Software must efficiently manage and handle substantial volumes of data.
3. Provide various analytical tools readily available within a single application.

The methodologies selected for post-dynamic analysis must be directly contingent upon the characteristics of the MD investigation. While quantitative assessment is essential, comprehensive analysis is crucial to underpin any visual systematization. Consequently, post-dynamic examination of the anticipated trajectories is crucial for the following reasons:

1. To assess the energy and conformational stability of the simulated system.
2. To ascertain and delineate the binding landscape of tiny molecules and compute the thermodynamic energy fluctuations along the trajectory of the constructed system.
3. Illustrate the dynamic conformational alterations or variability that may transpire inside the biomolecular system during the MD trajectory.

2.18 References

1. Moonan PK. Tuberculosis—the face of struggles, the struggles we face, and the dreams that lie within. Emerging Infectious Diseases, 2018;(24, 592-93.

2. Daniel TM, Iversen PA. Hippocrates and tuberculosis. Int J Tuberc Lung Dis. 2015;19(4):373-4.

3. Sharma SK, Mohan A. Tuberculosis: From an incurable scourge to a curable disease - journey over a millennium. Indian J Med Res. 2013;137(3):455-93.

4. Rosenblatt MB. Pulmonary tuberculosis: evolution of modern therapy. Bull N Y Acad Med. 1973;49(3):163-96.

5. Hayman J. Mycobacterium ulcerans: an infection from Jurassic time? Lancet. 1984;2(8410):1015-6.

6. Natarajan A, Beena PM, Devnikar AV, Mali S. A systemic review on tuberculosis. Indian J Tuberc. 2020;67(3):295-311

7. Cambau E, Drancourt M. Steps towards the discovery of *Mycobacterium tuberculosis* by Robert Koch, 1882. Clin Microbiol Infect. 2014;20(3):196-201.

8. Ellis H. Robert Koch: pioneer of bacteriology and Nobel prize winner. Br J Hosp Med (Lond). 2010;71(4):223.

9. Rastogi N. An Introduction to Mycobacterial Taxonomy, Structure, Drug Resistance, and Pathogenesis. In: Dionisio D, editor. Textbook-Atlas of Intestinal Infections in AIDS. Milano: Springer Milan; 2003. p. 89-115.

10. Sachdeva K, Goel M, Sudhakar M, Mehta M, Raju R, Raman K, Singh A, Sundaramurthy V. *Mycobacterium tuberculosis* (Mtb) lipid mediated lysosomal rewiring in infected macrophages modulates intracellular Mtb trafficking and survival. J Biol Chem. 2020;295(27):9192-210.

11. Russell DG. *Mycobacterium tuberculosis*: here today, and here tomorrow. Nat Rev Mol Cell Biol. 2001;2(8):569-77.

12. McKinney JD, Höner zu Bentrup K, Muñoz-Elías EJ, Miczak A, Chen B, Chan WT, Swenson D, Sacchettini JC, Jacobs WR,Jr, Russell DG. Persistence of *Mycobacterium tuberculosis* in macrophages and mice requires the glyoxylate shunt enzyme isocitrate lyase. Nature. 2000;406(6797):735-8.

13. Armstrong JA, Hart PD. Response of cultured macrophages to *Mycobacterium tuberculosis*, with observations on fusion of lysosomes with phagosomes. J Exp Med. 1971;134(3 Pt 1):713-40.

14. Cambier CJ, Falkow S, Ramakrishnan L. Host evasion and exploitation schemes of *Mycobacterium tuberculosis*. Cell. 2014;159(7):1497-509.

15. Pieters J. *Mycobacterium tuberculosis* and the macrophage: maintaining a balance. Cell Host Microbe. 2008;3(6):399-407.

16. Gutierrez MG, Master SS, Singh SB, Taylor GA, Colombo MI, Deretic V. Autophagy is a defense mechanism inhibiting BCG and *Mycobacterium tuberculosis* survival in infected macrophages.

Cell. 2004;119(6):753-66.

17. Kumar D, Nath L, Kamal MA, Varshney A, Jain A, Singh S, Rao KVS. Genome-wide analysis of the host intracellular network that regulates survival of *Mycobacterium tuberculosis*. Cell. 2010;140(5):731-43.

18. Brennan PJ, Nikaido H. The envelope of mycobacteria. Annu Rev Biochem. 1995; 64:29-63.

19. Minnikin DE, Kremer L, Dover LG, Besra GS. The methyl-branched fortifications of *Mycobacterium tuberculosis*. Chem Biol. 2002;9(5):545-53.

20. Kaur D, Guerin ME, Skovierová H, Brennan PJ, Jackson M. Chapter 2: Biogenesis of the cell wall and other glycoconjugates of *Mycobacterium tuberculosis*. Adv Appl Microbiol. 2009; 69:23-78.

21. Glickman MS, Jacobs WR, Jr. Microbial pathogenesis of *Mycobacterium tuberculosis*: dawn of a discipline. Cell. 2001;104(4):477-85.

22. Goren MB. Sulfolipid I of *Mycobacterium tuberculosis*, strain H37Rv. I. Purification and properties. Biochim Biophys Acta. 1970;210(1):116-26.

23. Marrakchi H, Lanéelle MA, Daffé M. Mycolic acids: structures, biosynthesis, and beyond. Chem Biol. 2014;21(1):67-85.

24. Reed MB, Domenech P, Manca C, Su H, Barczak AK, Kreiswirth BN, Kaplan G, Barry CE. A glycolipid of hypervirulent tuberculosis strains that inhibits the innate immune response. Nature. 2004;431(7004):84-7.

25. Geijtenbeek TB, Van Vliet SJ, Koppel EA, Sanchez-Hernandez M, Vandenbroucke-Grauls CM, Appelmelk B, Van Kooyk Y. Mycobacteria target DC-SIGN to suppress dendritic cell function. J Exp Med. 2003;197(1):7-17.

26. Bowdish DM, Sakamoto K, Kim MJ, Kroos M, Mukhopadhyay S, Leifer CA, Tryggvason K, Gordon S, Russell DG. MARCO, TLR2, and CD14 are required for macrophage cytokine responses to mycobacterial trehalose dimycolate and *Mycobacterium tuberculosis*. PLoS Pathog. 2009;5(6): e1000474.

27. Russell DG, Mwandumba HC, Rhoades EE. Mycobacterium and the coat of many lipids. J Cell Biol. 2002;158(3):421-6.

28. Beatty WL, Russell DG. Identification of mycobacterial surface proteins released into subcellular compartments of infected macrophages. Infect Immun. 2000;68(12):6997-7002.

29. Beatty WL, Rhoades ER, Ullrich HJ, Chatterjee D, Heuser JE, Russell DG. Trafficking and release of mycobacterial lipids from infected macrophages. Traffic. 2000;1(3):235-47.

30. Beatty WL, Ullrich HJ, Russell DG. Mycobacterial surface moieties are released from infected macrophages by a constitutive exocytic event. Eur J Cell Biol. 2001;80(1):31-40.

31. Elbein AD, Pan YT, Pastuszak I, Carroll D. New insights on trehalose: a multifunctional molecule. Glycobiology. 2003;13(4):17r-27r.

32. Mohanty D, Sankaranarayanan R, Gokhale RS. Fatty acyl-AMP ligases and polyketide

synthases are unique enzymes of lipid biosynthetic machinery in Mycobacterium *tuberculosis*. Tuberculosis (Edinb). 2011;91(5):448-55.

33. Trivedi OA, Arora P, Sridharan V, Tickoo R, Mohanty D, Gokhale RS. Enzymic activation and transfer of fatty acids as acyl-adenylates in mycobacteria. Nature. 2004;428(6981):441-5.

34. Arora P, Goyal A, Natarajan VT, Rajakumara E, Verma P, Gupta R, Yousuf M, Trivedi OA, Mohanty D, Tyagi A, Sankaranarayanan R, Gokhale RS. Mechanistic and functional insights into fatty acid activation in *Mycobacterium tuberculosis*. Nat Chem Biol. 2009;5(3):166-73.

35. Raviglione MC. Tuberculosis. In: Jameson JL, Fauci AS, Kasper DL, Hauser SL, Longo DL, Loscalzo J, editors. Harrison's Principles of Internal Medicine, 20e. New York, NY: McGraw-Hill Education; 2018.

36. Montalla V. *Mycobacterium tuberculosis*: An Overview of its General Characteristics, Pathophysiology, and Future Directions2021.

37. Knechel NA. Tuberculosis: pathophysiology, clinical features, and diagnosis. Crit Care Nurse. 2009;29(2):34-43; quiz 4.

38. Centre For Disease Control 2024 [Available from: https://www.cdc.gov/tb/index.html.

39. Zak DE, Penn-Nicholson A, Scriba TJ, Thompson E, Suliman S, Amon LM, Mahomed H, Erasmus M, Whatney W, Hussey GD, Abrahams D, Kafaar F, Hawkridge T, Verver S, Hughes EJ, Ota M, Sutherland J, Howe R, Dockrell HM, Boom WH, Thiel B, Ottenhoff THM, Mayanja-Kizza H, Crampin AC, Downing K, Hatherill M, Valvo J, Shankar S, Parida SK, Kaufmann SHE, Walzl G, Aderem A, Hanekom WA; ACS and GC6-74 cohort study groups. A blood RNA signature for tuberculosis disease risk: a prospective cohort study. Lancet. 2016;387(10035):2312-22.

40. Furin J, Cox H, Pai M. Tuberculosis. Lancet. 2019;393(10181):1642-56.

41. Oxlade O, Murray M. Tuberculosis and poverty: why are the poor at greater risk in India? PLoS One. 2012;7(11):e47533.

42. Ortblad KF, Salomon JA, Bärnighausen T, Atun R. Stopping tuberculosis: a biosocial model for sustainable development. Lancet. 2015;386(10010):2354-62.

43. Saunders MJ, Wingfield T, Tovar MA, Baldwin MR, Datta S, Zevallos K, Montoya R, Valencia TR, Friedland JS, Moulton LH, Gilman RH, Evans CA. A score to predict and stratify risk of tuberculosis in adult contacts of tuberculosis index cases: a prospective derivation and external validation cohort study. Lancet Infect Dis. 2017;17(11):1190-9.

44. Batista J, de Albuquerque Mde F, Maruza M, Ximenes RA, Santos ML, Montarroyos UR, de Barros Miranda-Filho D, Lacerda HR, Rodrigues LC.. Incidence and risk factors for tuberculosis in people living with HIV: cohort from HIV referral health centers in Recife, Brazil. PLoS One. 2013;8(5):e63916.

45. World Health Organisation 2024 [Available from: https://www.who.int/news-room/fact sheets/detail/tuberculosis.

46. Unissa AN, Subbian S, Hanna LE, Selvakumar N. Overview on mechanisms of isoniazid action and resistance in *Mycobacterium tuberculosis*. Infect Genet Evol. 2016; 45:474-92.

47. Timmins GS, Deretic V. Mechanisms of action of isoniazid. Mol Microbiol. 2006;62(5):1220-7.

48. Zhang Y, Heym B, Allen B, Young D, Cole S. The catalase-peroxidase gene and isoniazid resistance of Mycobacterium tuberculosis. Nature. 1992;358(6387):591-3.

49. Centre For Disease Control: Treatment of Tuberculosis 2003 [Available from: Treatment of Tuberculosis American Thoracic Society, CDC, and Infectious Diseases Society of America]

50. Campbell EA, Korzheva N, Mustaev A, Murakami K, Nair S, Goldfarb A, Darst SA. Structural mechanism for rifampicin inhibition of bacterial rna polymerase. Cell. 2001;104(6):901-12.

51. Molodtsov V, Scharf NT, Stefan MA, Garcia GA, Murakami KS. Structural basis for rifamycin resistance of bacterial RNA polymerase by the three most clinically important RpoB mutations found in *Mycobacterium tuberculosis*. Mol Microbiol. 2017;103(6):1034-45.

52. Fox W, Ellard GA, Mitchison DA. Studies on the treatment of tuberculosis undertaken by the British Medical Research Council tuberculosis units, 1946-1986, with relevant subsequent publications. Int J Tuberc Lung Dis. 1999;3(10 Suppl 2): S231-79.

53. Whitfield MG, Soeters HM, Warren RM, York T, Sampson SL, Streicher EM, van Helden PD, van Rie A. A Global Perspective on Pyrazinamide Resistance: Systematic Review and Meta-Analysis. PLoS One. 2015;10(7): e0133869.

54. Zimhony O, Cox JS, Welch JT, Vilchèze C, Jacobs WR, Jr. Pyrazinamide inhibits the eukaryotic-like fatty acid synthetase I (FASI) of *Mycobacterium tuberculosis*. Nat Med. 2000;6(9):1043-7.

55. Zhang Y, Mitchison D. The curious characteristics of pyrazinamide: a review. Int J Tuberc Lung Dis. 2003;7(1):6-21.

56. Zhang Y, Wade MM, Scorpio A, Zhang H, Sun Z. Mode of action of pyrazinamide: disruption of *Mycobacterium tuberculosis* membrane transport and energetics by pyrazinoic acid. J Antimicrob Chemother. 2003;52(5):790-5.

57. Zhang Y, Shi W, Zhang W, Mitchison D. Mechanisms of Pyrazinamide Action and Resistance. Microbiol Spectr. 2014;2(4): Mgm2-0023-2013.

58. Palomino JC, Martin A. Drug Resistance Mechanisms in *Mycobacterium tuberculosis.* Antibiotics (Basel). 2014;3(3):317-40.

59. Safi H, Lingaraju S, Amin A, Kim S, Jones M, Holmes M, McNeil M, Peterson SN, Chatterjee D, Fleischmann R, Alland D. Evolution of high-level ethambutol-resistant tuberculosis through interacting mutations in decaprenylphosphoryl-β-D arabinose biosynthetic and utilization pathway genes. Nat Genet. 2013;45(10):1190-7.

60. North EJ, Jackson M, Lee RE. New approaches to target the mycolic acid biosynthesis pathway for the development of tuberculosis therapeutics. Curr Pharm Des. 2014;20(27):4357 78.

61. Zhang Y, Yew WW. Mechanisms of drug resistance in *Mycobacterium tuberculosis*: update 2015. Int J Tuberc Lung Dis. 2015;19(11):1276-89.

62. Biukovic G, Basak S, Manimekalai MS, Rishikesan S, Roessle M, Dick T, Rao SP, Hunke C, Grüber G. Variations of subunit {varepsilon} of *the Mycobacterium tuberculosis* F1Fo ATP synthase and a novel model for mechanism of action of the tuberculosis drug TMC207. Antimicrob Agents Chemother. 2013;57(1):168-76.

63. Koul A, Vranckx L, Dendouga N, Balemans W, Van den Wyngaert I, Vergauwen K, Göhlmann HWH, Willebrords R, Poncelet A, Guillemont J, Bald D, Andries K. Diarylquinolines are bactericidal for dormant mycobacteria as a result of disturbed ATP homeostasis. J Biol Chem. 2008;283(37):25273-80.

64. Hards K, McMillan DGG, Schurig-Briccio LA, Gennis RB, Lill H, Bald D, Cook GM. Ionophoric effects of the antitubercular drug bedaquiline. Proc Natl Acad Sci U S A. 2018;115(28):7326-31.

65. Villellas C, Coeck N, Meehan CJ, Lounis N, de Jong B, Rigouts L, Andries K. Unexpected high prevalence of resistance-associated Rv0678 variants in MDR-TB patients without documented prior use of clofazimine or bedaquiline. J Antimicrob Chemother. 2017;72(3):684-90.

66. Xu J, Wang B, Hu M, Huo F, Guo S, Jing W, Nuermberger E, Lu Y. Primary Clofazimine and Bedaquiline Resistance among Isolates from Patients with Multidrug-Resistant Tuberculosis. Antimicrob Agents Chemother. 2017;61(6).

67. Chien JY, Chen YT, Wu SG, Lee JJ, Wang JY, Yu CJ. Treatment outcome of patients with isoniazid mono-resistant tuberculosis. Clin Microbiol Infect. 2015;21(1):59-68.

68. Ismail NA, Mvusi L, Nanoo A, Dreyer A, Omar SV, Babatunde S, Molebatsi T, van der Walt M, Adelekan A, Deyde V, Ihekweazu C, Madhi SA. Prevalence of drug resistant tuberculosis and imputed burden in South Africa: a national and sub-national cross sectional survey. Lancet Infect Dis. 2018;18(7):779-87.

69. Dheda K, Lenders L, Magombedze G, Srivastava S, Raj P, Arning E, Ashcraft P, Bottiglieri T, Wainwright H, Pennel T, Linegar A, Moodley L, Pooran A, Pasipanodya JG, Sirgel FA, van Helden PD, Wakeland E, Warren RM, Gumbo T. Drug Penetration Gradients Associated with Acquired Drug Resistance in Patients with Tuberculosis. Am J Respir Crit Care Med. 2018;198(9):1208-19.

70. Yu G, Fu X, Jin K, Zhang L, Wu W, Cui Z, Hu Z, Li Y. Integrative analysis of transcriptome and genome indicates two potential genomic islands are associated with pathogenesis *of Mycobacterium tuberculosis*. Gene. 2011;489(1):21-9.

71. Cole ST, Brosch R, Parkhill J, Garnier T, Churcher C, Harris D, Gordon SV, Eiglmeier K, Gas S, Barry CE 3rd, Tekaia F, Badcock K, Basham D, Brown D, Chillingworth T, Connor R, Davies R, Devlin K, Feltwell T, Gentles S, Hamlin N, Holroyd S, Hornsby T, Jagels K, Krogh A, McLean J, Moule S, Murphy L, Oliver K, Osborne J, Quail MA, Rajandream MA, Rogers J, Rutter S, Seeger K,

Skelton J, Squares R, Squares S, Sulston JE, Taylor K, Whitehead S, Barrell BG. Deciphering the biology of *Mycobacterium tuberculosis* from the complete genome sequence. Nature. 1998;393(6685):537-44.

72. Kumar P, Schelle MW, Jain M, Lin FL, Petzold CJ, Leavell MD, Leary JA, Cox JS, Bertozzi CR. PapA1 and PapA2 are acyltransferases essential for the biosynthesis of the *Mycobacterium tuberculosis* virulence factor sulfolipid-1. Proc Natl Acad Sci U S A. 2007;104(27):11221-6.

73. Sirakova TD, Thirumala AK, Dubey VS, Sprecher H, Kolattukudy PE. The *Mycobacterium tuberculosis* pks2 gene encodes the synthase for the hepta- and octamethyl-branched fatty acids required for sulfolipid synthesis. J Biol Chem. 2001;276(20):16833-9.

74. Converse SE, Mougous JD, Leavell MD, Leary JA, Bertozzi CR, Cox JS. MmpL8 is required for sulfolipid-1 biosynthesis and *Mycobacterium tuberculosis* virulence. Proc Natl Acad Sci U S A. 2003;100(10):6121-6.

75. Domenech P, Reed MB, Dowd CS, Manca C, Kaplan G, Barry CE, III. The Role of MmpL8 in Sulfatide Biogenesis and Virulence of *Mycobacterium tuberculosis**. Journal of Biological Chemistry. 2004;279(20):21257-65.

76. Gilmore SA, Schelle MW, Holsclaw CM, Leigh CD, Jain M, Cox JS, Leary JA, Bertozzi CR. Sulfolipid-1 biosynthesis restricts *Mycobacterium tuberculosis* growth in human macrophages. ACS Chem Biol. 2012;7(5):863-70.

77. Layre E, Cala-De Paepe D, Larrouy-Maumus G, Vaubourgeix J, Mundayoor S, Lindner B, Puzo G, Gilleron M. Deciphering sulfoglycolipids of *Mycobacterium tuberculosis*. J Lipid Res. 2011;52(6):1098 110.

78. Seeliger JC, Holsclaw CM, Schelle MW, Botyanszki Z, Gilmore SA, Tully SE, Niederweis M, Cravatt BF, Leary JA, Bertozzi CR. Elucidation and chemical modulation of sulfolipid-1 biosynthesis in *Mycobacterium tuberculosis*. J Biol Chem. 2012;287(11):7990-8000.

79. Mougous JD, Petzold CJ, Senaratne RH, Lee DH, Akey DL, Lin FL, Munchel SE, Pratt MR, Riley LW, Leary JA, Berger JM, Bertozzi CR. Identification, function and structure of the mycobacterial sulfotransferase that initiates sulfolipid-1 biosynthesis. Nat Struct Mol Biol. 2004;11(8):721-9.

80. Hemmerich S, Rosen SD. Carbohydrate sulfotransferases in lymphocyte homing. Glycobiology. 2000;10(9):849-56.

81. Mougous JD, Green RE, Williams SJ, Brenner SE, Bertozzi CR. Sulfotransferases and sulfatases in mycobacteria. Chem Biol. 2002;9(7):767-76.

82. Moore KL. The biology and enzymology of protein tyrosine O-sulfation. J Biol Chem. 2003;278(27):24243-6.

83. Honke K, Taniguchi N. Sulfotransferases and sulfated oligosaccharides. Med Res Rev. 2002;22(6):637-54.

84. Coughtrie MW. Sulfation through the looking glass--recent advances in sulfotransferase research for the curious. Pharmacogenomics J. 2002;2(5):297-308.

85. Gangadharam PR, Cohn ML, Middlebrook G. Infectivity, Pathogenicity And Sulpholipid Fraction Of Some Indian And British Strains Of Tubercle Bacilli. Tubercle. 1963; 44:452–455. [PubMed: 14101326]

86. Jain M, Petzold CJ, Schelle MW, Leavell MD, Mougous JD, Bertozzi CR, Leary JA, Cox JS. Lipidomics reveals control of *Mycobacterium tuberculosis* virulence lipids via metabolic coupling. Proc Natl Acad Sci U S A. 2007;104(12):5133-8.

87. Gonzalo Asensio J, Maia C, Ferrer NL, Barilone N, Laval F, Soto CY, Winter N, Daffé M, Gicquel B, Martín C, Jackson M. The virulence associated two-component PhoP-PhoR system controls the biosynthesis of polyketide-derived lipids in *Mycobacterium tuberculosis*. J Biol Chem. 2006;281(3):1313-6.

88. Singh A, Crossman DK, Mai D, Guidry L, Voskuil MI, Renfrow MB, Steyn AJC. *Mycobacterium tuberculosis* WhiB3 maintains redox homeostasis by regulating virulence lipid anabolism to modulate macrophage response. PLoS Pathog. 2009;5(8):e1000545.

89. Walters SB, Dubnau E, Kolesnikova I, Laval F, Daffe M, Smith I. The *Mycobacterium tuberculosis* PhoPR two-component system regulates genes essential for virulence and complex lipid biosynthesis. Mol Microbiol. 2006;60(2):312-30.

90. Augenstreich J, Briken V. Host Cell Targets of Released Lipid and Secreted Protein Effectors of *Mycobacterium tuberculosis*. Front Cell Infect Microbiol. 2020; 10:595029.

91. Brodin P, Poquet Y, Levillain F, Peguillet I, Larrouy-Maumus G, Gilleron M, Ewann F, Christophe T, Fenistein D, Jang J, Jang MS, Park SJ, Rauzier J, Carralot JP, Shrimpton R, Genovesio A, Gonzalo-Asensio JA, Puzo G, Martin C, Brosch R, Stewart GR, Gicquel B, Neyrolles O. High content phenotypic cell-based visual screen identifies *Mycobacterium tuberculosis* acyltrehalose-containing glycolipids involved in phagosome remodeling. PLoS Pathog. 2010;6(9): e1001100.

92. Pabst MJ, Gross JM, Brozna JP, Goren MB. Inhibition of macrophage priming by sulfatide from *Mycobacterium tuberculosis*. J Immunol. 1988;140(2):634-40.

93. Goren MB, D'Arcy Hart P, Young MR, Armstrong JA. Prevention of phagosome-lysosome fusion in cultured macrophages by sulfatides of *Mycobacterium tuberculosis*. Proc Natl Acad Sci U S A. 1976;73(7):2510-4.

94. Brozna JP, Horan M, Rademacher JM, Pabst KM, Pabst MJ. Monocyte responses to sulfatide from *Mycobacterium tuberculosis*: inhibition of priming for enhanced release of superoxide, associated with increased secretion of interleukin-1 and tumor necrosis factor alpha, and altered protein phosphorylation. Infect Immun. 1991;59(8):2542-8.

95. Kato M, Goren MB. Synergistic action of cord factor and mycobacterial sulfatides on mitochondria. Infect Immun. 1974;10(4):733-41.

96. Zhang L, English D, Andersen BR. Activation of human neutrophils by *Mycobacterium tuberculosis*-derived sulfolipid-1. J Immunol. 1991;146(8):2730-6.

97. Zhang L, Goren MB, Holzer TJ, Andersen BR. Effect of *Mycobacterium tuberculosis* derived sulfolipid I on human phagocytic cells. Infect Immun. 1988;56(11):2876-83.

98. Okamoto Y, Fujita Y, Naka T, Hirai M, Tomiyasu I, Yano I. Mycobacterial sulfolipid shows a virulence by inhibiting cord factor induced granuloma formation and TNF-alpha release. Microb Pathog. 2006;40(6):245-53.

99. Sturgill-Koszycki S, Schlesinger PH, Chakraborty P, Haddix PL, Collins HL, Fok AK, Allen RD, Gluck SL, Heuser J, Russell DG. Lack of acidification in *Mycobacterium* phagosomes produced by exclusion of the vesicular proton-ATPase. Science. 1994;263(5147):678-81.

100. Dwivedi R, Baindara P. Differential Regulation of TFEB-Induced Autophagy during *Mtb* Infection and Starvation. Microorganisms. 2023;11(12).

101. Graham JE, Clark-Curtiss JE. Identification of *Mycobacterium tuberculosis* RNAs synthesized in response to phagocytosis by human macrophages by selective capture of transcribed sequences (SCOTS). Proc Natl Acad Sci U S A. 1999;96(20):11554-9.

102. Rodríguez JE, Ramírez AS, Salas LP, Helguera-Repetto C, Gonzalez-y-Merchand J, Soto CY, Hernández-Pando R. Transcription of genes involved in sulfolipid and polyacyltrehalose biosynthesis of *Mycobacterium tuberculosis* in experimental latent tuberculosis infection. PLoS One. 2013;8(3):e58378.

103. Takahashi T, Suzuki T. Role of sulfatide in normal and pathological cells and tissues. J Lipid Res. 2012;53(8):1437-50.

104. Ruhl CR, Pasko BL, Khan HS, Kindt LM, Stamm CE, Franco LH, Hsia CC, Zhou M, Davis CR, Qin T, Gautron L, Burton MD, Mejia GL, Naik DK, Dussor G, Price TJ, Shiloh MU. *Mycobacterium tuberculosis* Sulfolipid-1 Activates Nociceptive Neurons and Induces Cough. Cell. 2020;181(2):293-305.e11.

105. Baran M, Grimes KD, Sibbald PA, Fu P, Boshoff HIM, Wilson DJ, Aldrich CC. Development of small-molecule inhibitors of fatty acyl-AMP and fatty acyl-CoA ligases in *Mycobacterium tuberculosis*. Eur J Med Chem. 2020; 201:112408.

106. Gokhale RS, Saxena P, Chopra T, Mohanty D. Versatile polyketide enzymatic machinery for the biosynthesis of complex mycobacterial lipids. Nat Prod Rep. 2007;24(2):267-77.

107. Trivedi OA, Arora P, Vats A, Ansari MZ, Tickoo R, Sridharan V, Mohanty D, Gokhale RS. Dissecting the mechanism and assembly of a complex virulence mycobacterial lipid. Mol Cell. 2005;17(5):631 43.

108. Saxena P, Yadav G, Mohanty D, Gokhale RS. A new family of type III polyketide synthases in *Mycobacterium tuberculosis*. J Biol Chem. 2003;278(45):44780-90.

109. Krithika R, Marathe U, Saxena P, Ansari MZ, Mohanty D, Gokhale RS. A genetic locus

required for iron acquisition in *Mycobacterium tuberculosis*. Proc Natl Acad Sci U S A. 2006;103(7):2069-74.

110. Wilburn KM, Fieweger RA, VanderVen BC. Cholesterol and fatty acids grease the wheels of *Mycobacterium tuberculosis* pathogenesis. Pathog Dis. 2018;76(2).

111. Le NH, Molle V, Eynard N, Miras M, Stella A, Bardou F, Galandrin S, Guillet V, André-Leroux G, Bellinzoni M, Alzari P, Mourey L, Burlet-Schiltz O, Daffé M, Marrakchi H. Ser/Thr Phosphorylation Regulates the Fatty Acyl-AMP Ligase Activity of FadD32, an Essential Enzyme in Mycolic Acid Biosynthesis. J Biol Chem. 2016;291(43):22793-805.

112. Arora P, Vats A, Saxena P, Mohanty D, Gokhale RS. Promiscuous fatty acyl CoA ligases produce acyl-CoA and acyl-SNAC precursors for polyketide biosynthesis. J Am Chem Soc. 2005;127(26):9388-9.

113. Goyal A, Verma P, Anandhakrishnan M, Gokhale RS, Sankaranarayanan R. Molecular basis of the functional divergence of fatty acyl-AMP ligase biosynthetic enzymes of *Mycobacterium tuberculosis*. J Mol Biol. 2012;416(2):221-38.

114. Lux MC, Standke LC, Tan DS. Targeting adenylate-forming enzymes with designed sulfonyladenosine inhibitors. J Antibiot (Tokyo). 2019;72(6):325-49.

115. Liu Z, Ioerger TR, Wang F, Sacchettini JC. Structures of *Mycobacterium tuberculosis* FadD10 protein reveal a new type of adenylate-forming enzyme. J Biol Chem. 2013;288(25):18473-83.

116. Ferreras JA, Stirrett KL, Lu X, Ryu JS, Soll CE, Tan DS, Quadri LE. Mycobacterial phenolic glycolipid virulence factor biosynthesis: mechanism and small-molecule inhibition of polyketide chain initiation. Chem Biol. 2008;15(1):51-61.

117. Siméone R, Léger M, Constant P, Malaga W, Marrakchi H, Daffé M, Guilhot C, Chalut C. Delineation of the roles of FadD22, FadD26 and FadD29 in the biosynthesis of phthiocerol dimycocerosates and related compounds in *Mycobacterium tuberculosis*. Febs j. 2010;277(12):2715-25.

118. Samanta S, Singh A, Biswas P, Bhatt A, Visweswariah SS. Mycobacterial phenolic glycolipid synthesis is regulated by cAMP-dependent lysine acylation of FadD22. Microbiology (Reading). 2017;163(3):373-82.

119. Díaz C, Pérez Del Palacio J, Valero-Guillén PL, Mena García P, Pérez I, Vicente F, Martín C, Genilloud O, Sánchez Pozo A, Gonzalo-Asensio J. Comparative Metabolomics between *Mycobacterium tuberculosis* and the MTBVAC Vaccine Candidate. ACS Infect Dis. 2019;5(8):1317-26.

120. Koster K, Largen A, Foster JT, Drees KP, Qian L, Desmond EP, Wan X, Hou S, Douglas JT. Whole genome SNP analysis suggests unique virulence factor differences of the Beijing and Manila families of *Mycobacterium tuberculosis* found in Hawaii. PLoS One. 2018;13(7): e0201146.

121. Broset E, Martín C, Gonzalo-Asensio J. Evolutionary landscape of the *Mycobacterium tuberculosis* complex from the viewpoint of PhoPR: implications for virulence regulation and

application to vaccine development. mBio. 2015;6(5):e01289-15.

122. Vergnolle O, Chavadi SS, Edupuganti UR, Mohandas P, Chan C, Zeng J, Kopylov M, Angelo NG, Warren JD, Soll CE, Quadri LE. Biosynthesis of cell envelope-associated phenolic glycolipids in *Mycobacterium marinum*. J Bacteriol. 2015;197(6):1040-50.

123. Gavalda S, Léger M, van der Rest B, Stella A, Bardou F, Montrozier H, Chalut C, Burlet-Schiltz O, Marrakchi H, Daffé M, Quémard A. The Pks13/FadD32 crosstalk for the biosynthesis of mycolic acids in *Mycobacterium tuberculosis*. J Biol Chem. 2009;284(29):19255-64.

124. Léger M, Gavalda S, Guillet V, van der Rest B, Slama N, Montrozier H, Mourey L, Quémard A, Daffé M, Marrakchi H. The dual function of the *Mycobacterium tuberculosis* FadD32 required for mycolic acid biosynthesis. Chem Biol. 2009;16(5):510-9.

125. Kuhn ML, Alexander E, Minasov G, Page HJ, Warwrzak Z, Shuvalova L, Flores KJ, Wilson DJ, Shi C, Aldrich CC, Anderson WF. Structure of the Essential *Mtb* FadD32 Enzyme: A Promising Drug Target for Treating Tuberculosis. ACS Infect Dis. 2016;2(8):579-91.

126. Guillet V, Galandrin S, Maveyraud L, Ladevèze S, Mariaule V, Bon C, Eynard N, Daffé M, Marrakchi H, Mourey L. Insight into Structure-Function Relationships and Inhibition of the Fatty Acyl-AMP Ligase (FadD32) Orthologs from Mycobacteria. J Biol Chem. 2016;291(15):7973-89.

127. Lynett J, Stokes RW. Selection of transposon mutants of *Mycobacterium tuberculosis* with increased macrophage infectivity identifies fadD23 to be involved in sulfolipid production and association with macrophages. Microbiology (Reading). 2007;153(Pt 9):3133-40.

128. Yan M, Cao L, Zhao L, Zhou W, Liu X, Zhang W, Rao Z. The Key Roles of *Mycobacterium tuberculosis* FadD23 C-terminal Domain in Catalytic Mechanisms. Front Microbiol. 2023;14:1090534.

129. Johnstone AH. The development of chemistry teaching: A changing response to changing demand. Journal of Chemical Education. 1993;70(9):701.

130. Jalonen E, editor Computer-based molecular modelling: Towards deeper understanding of chemistry 2016.

131. Macalino SJ, Gosu V, Hong S, Choi S. Role of computer-aided drug design in modern drug discovery. Arch Pharm Res. 2015;38(9):1686-701.

132. Jones SD, Liebeschuetz JW, Morgan PJ, Murray CW, Rimmer AD, Roscoe JM, Waszkowycz B, Welsh PM, Wylie WA, Young SC, Martin H, Mahler J, Brady L, Wilkinson K. The design of phenylglycine containing benzamidine carboxamides as potent and selective inhibitors of factor Xa. Bioorg Med Chem Lett. 2001;11(5):733-6.

133. Liebeschuetz JW, Jones SD, Morgan PJ, Murray CW, Rimmer AD, Roscoe JM, Waszkowycz B, Welsh PM, Wylie WA, Young SC, Martin H, Mahler J, Brady L, Wilkinson K. PRO_SELECT: combining structure-based drug design and array-based chemistry for rapid lead discovery. 2. The development of a series of highly potent and selective factor Xa inhibitors. J Med Chem. 2002;45(6):1221-32.

134. Devabhakthuni S, Yoon CH, Pincus KJ. Review of the Target-Specific Oral Anticoagulants in Development for the Treatment and Prevention of Venous Thromboembolism. J Pharm Pract. 2016;29(4):392-405.

135. Robinson BS, Riccardi KA, Gong YF, Guo Q, Stock DA, Blair WS, Terry BJ, Deminie CA, Djang F, Colonno RJ, Lin PF. BMS-232632, a highly potent human immunodeficiency virus protease inhibitor that can be used in combination with other available antiretroviral agents. Antimicrob Agents Chemother. 2000;44(8):2093-9.

136. Krohn A, Redshaw S, Ritchie JC, Graves BJ, Hatada MH. Novel binding mode of highly potent HIV-proteinase inhibitors incorporating the (R)-hydroxyethylamine isostere. J Med Chem. 1991;34(11):3340-2.

137. Chen Z, Li Y, Chen E, Hall DL, Darke PL, Culberson C, Shafer JA, Kuo LC. Crystal structure at 1.9-A resolution of human immunodeficiency virus (HIV) II protease complexed with L-735,524, an orally bioavailable inhibitor of the HIV proteases. J Biol Chem. 1994;269(42):26344-8.

138. Kempf DJ, Marsh KC, Denissen JF, McDonald E, Vasavanonda S, Flentge CA, Green BE, Fino L, Park CH, Kong XP. ABT 538 is a potent inhibitor of human immunodeficiency virus protease and has high oral bioavailability in humans. Proc Natl Acad Sci U S A. 1995;92(7):2484-8.

139. Anderson AC. The process of structure-based drug design. Chem Biol. 2003;10(9):787 97.

140. Rutenber EE, Stroud RM. Binding of the anticancer drug ZD1694 to E. coli thymidylate synthase: assessing specificity and affinity. Structure. 1996;4(11):1317-24.

141. Shaker B, Ahmad S, Lee J, Jung C, Na D. In silico methods and tools for drug discovery. Comput Biol Med. 2021; 137:104851.

142. Schroeder EK, Basso LA, Santos DS, de Souza ON. Molecular dynamics simulation studies of the wild-type, I21V, and I16T mutants of isoniazid-resistant *Mycobacterium tuberculosis* enoyl reductase (InhA) in complex with NADH: toward the understanding of NADH InhA different affinities. Biophys J. 2005;89(2):876-84.

143. Case DA, Cheatham TE, 3rd, Darden T, Gohlke H, Luo R, Merz KM, Jr., Onufriev A, Simmerling C, Wang B, Woods RJ. The Amber biomolecular simulation programs. J Comput Chem. 2005;26(16):1668-88.

144. Ekins S, Freundlich JS, Choi I, Sarker M, Talcott C. Computational databases, pathway and cheminformatics tools for tuberculosis drug discovery. Trends Microbiol. 2011;19(2):65-74.

145. National Research Council Committee on Challenges for the Chemical Sciences in the 21st C. The National Academies Collection: Reports funded by National Institutes of Health. Beyond the Molecular Frontier: Challenges for Chemistry and Chemical Engineering. Washington (DC): National Academies Press (US) Copyright 2003 by the National Academy of Sciences. All rights reserved.; 2003[https://doi.org/10.17226/10633].

146. Ekins S, Mestres J, Testa B. In silico pharmacology for drug discovery: methods for virtual ligand screening and profiling. Br J Pharmacol. 2007;152(1):9-20.

147. Grant BJ, Gorfe AA, McCammon JA. Ras conformational switching: simulating nucleotide-dependent conformational transitions with accelerated molecular dynamics. PLoS Comput Biol. 2009;5(3):e1000325.

148. González MA, editor Force fields and molecular dynamics simulations2011.

149. Brooks BR, Brooks CL, 3rd, Mackerell AD, Jr., Nilsson L, Petrella RJ, Roux B, Won Y, Archontis G, Bartels C, Boresch S, Caflisch A, Caves L, Cui Q, Dinner AR, Feig M, Fischer S, Gao J, Hodoscek M, Im W, Kuczera K, Lazaridis T, Ma J, Ovchinnikov V, Paci E, Pastor RW, Post CB, Pu JZ, Schaefer M, Tidor B, Venable RM, Woodcock HL, Wu X, Yang W, York DM, Karplus M. CHARMM: the biomolecular simulation program. J Comput Chem. 2009;30(10):1545-614.

150. Phillips JC, Braun R, Wang W, Gumbart J, Tajkhorshid E, Villa E, Chipot C, Skeel RD, Kalé L, Schulten K. Scalable molecular dynamics with NAMD. J Comput Chem. 2005;26(16):1781-802.

151. Christen M, Hünenberger PH, Bakowies D, Baron R, Bürgi R, Geerke DP, Heinz TN, Kastenholz MA, Kräutler V, Oostenbrink C, Peter C, Trzesniak D, van Gunsteren WF. The GROMOS software for biomolecular simulation: GROMOS05. J Comput Chem. 2005;26(16):1719-51.

152. Ponder JW, Case DA. Force Fields for Protein Simulations. Advances in Protein Chemistry. 66: Academic Press; 2003. p. 27-85.

153. Lavecchia A, Di Giovanni C. Virtual screening strategies in drug discovery: a critical review. Curr Med Chem. 2013;20(23):2839-60.

154. Lionta E, Spyrou G, Vassilatis DK, Cournia Z. Structure-based virtual screening for drug discovery: principles, applications and recent advances. Curr Top Med Chem. 2014;14(16):1923-38

155. Vyas V, Jain A, Jain A, Gupta A. Virtual Screening: A Fast Tool for Drug Design. Scientia Pharmaceutica. 2008;76(3):333-60.

156. Ashburn TT, Thor KB. Drug repositioning: identifying and developing new uses for existing drugs. Nat Rev Drug Discov. 2004;3(8):673-83.

157. Kitchen DB, Decornez H, Furr JR, Bajorath J. Docking and scoring in virtual screening for drug discovery: methods and applications. Nat Rev Drug Discov. 2004;3(11):935-49.

158. Moffat JG, Vincent F, Lee JA, Eder J, Prunotto M. Opportunities and challenges in phenotypic drug discovery: an industry perspective. Nat Rev Drug Discov. 2017;16(8):531-43.

159 Pushpakom S, Iorio F, Eyers PA, Escott KJ, Hopper S, Wells A, Doig A, Guilliams T, Latimer J, McNamee C, Norris A, Sanseau P, Cavalla D, Pirmohamed M. Drug repurposing: progress, challenges and recommendations. Nat Rev Drug Discov. 2019;18(1):41-58.

160. Amadei A, Linssen AB, Berendsen HJ. Essential dynamics of proteins. Proteins. 1993;17(4):412-25.

161. Petrenko R, Meller J. Molecular Dynamics. eLS.

162. Becker OM, MacKerell Jr., A.D., Roux, B., & Watanabe, M. (Eds.). Computational Biochemistry and Biophysics (1st ed.). (2001).

163. Likhachev IV, Balabaev NK, Galzitskaya OV. Available Instruments for Analyzing Molecular

Dynamics Trajectories. Open Biochem J. 2016; 10:1-11.
164. Meller Ja. Molecular Dynamics. eLS2001

CHAPTER 3

Research Paper

Repositioning FDA-approved drugs to identify potential mycobacterial FadD23 inhibitors

Chitra Dipika Pillay[1] and Ndumiso N Mhlongo[1*]

[1]School of Laboratory Medicine and Medical Sciences, University of KwaZulu-Natal

Durban 4001, South Africa

*Corresponding author: Dr Ndumiso N Mhlongo

Email: MhlongoN4@ukzn.ac.za

Telephone:+2731 260 2428

Fax:+2731 260 7792

Abstract

Mycobacterium tuberculosis (M.tuberculosis) is the etiological agent of Tuberculosis (TB) and continues to present difficulties to health security in the Asian and African areas due to the prevalence of developing countries. The annual increase in infection rates necessitates an inquiry into prospective treatments targeting druggable pathways involved in pathogenesis. Research has demonstrated that SL-1 can trigger the cough reflex, establishing a direct connection to tuberculosis pathogenesis, as coughing is a primary symptom and a means of TB transmission. The protein FadD23 was recognised as a crucial enzyme in manufacturing SL-1 and presents a novel target to mitigate TB development. Currently, there is no known inhibitor for FadD23. Drug repurposing refers to of applying a medication for a purpose other than its originally intended use, hence minimizing costs and time, which are critical factors in the drug discovery and design process. This study aimed to find possible inhibitors from medications that have already received FDA approval. Various in silico approaches were employed, including molecular docking, molecular dynamics simulations, MM/PBSA and decomposition calculations, and DSSP, to identify a possible inhibitor. The findings indicated that Simeprevir exhibited the most potential as an inhibitor, with a binding affinity of -33.87 kcal/mol. Most of its binding affinity resulted from hydrophobic interactions, which rendered the complex compact and stable, consistent with the secondary structure per residue analysis, indicating that Simeprevir exhibited significant occupancy in the binding site. Thr176, Thr766, and Arg460 were identified as the primary contributions to the total binding energy. Interestingly, although ANP created numerous hydrogen bonds, its binding energy suggests that these bonds may not have been strong, indicating that quantity is not the sole determinant of strength. Additionally, it is noteworthy that Simeprevir may maintain stability at the binding site residue while simultaneously promoting significant mobility in its catalytic C-terminal domain, thereby impairing performance. Our research establishes a foundation for promoting FadD23 as a novel target for Simeprevir for further experimental assessment in pursuit of TB treatment.

Keywords: FDA, *M. tuberculosis*, molecular docking, MD simulation, drug repositioning, FadD23

3.1 Introduction

In 1882, Robert Koch discovered *Mycobacterium tuberculosis (M. tuberculosis*) as the etiological agent of tuberculosis (TB) (1). TB is a contagious airborne illness that ranks among the deadliest infections globally, resulting in mortality. It predominantly impacts the respiratory system (pulmonary TB), yet other body areas may be involved (extra-pulmonary TB). The World Health Organisation (WHO) reported 10.8 million cases in 2023, with approximately 1.25 million fatalities documented. TB has likely resumed its status as the foremost cause of mortality from a singular infectious agent after three years, during which it was supplanted by coronavirus disease (COVID-19). It remains the primary cause of death among individuals with HIV and a significant contributor to fatalities associated with antibiotic resistance (2). Transmission occurs by aerosol droplets containing *M. tuberculosis*, which are expelled into the air when infected individuals talk, sneeze, or cough ((3,4)No existing vaccinations can effectively prevent tuberculosis disease in adults, either before or after exposure to *M. tuberculosis*.

Tuberculosis possesses a robust waxy cell wall that hinders drug penetration to molecular targets and contains efflux pumps that confer drug resistance (5). The tuberculosis bacteria affect the host system at a cellular level (6) to facilitate success and sustain infection by interacting with host mechanisms such as autophagy (7,8). The cell wall comprises several glycolipids, including trehalose dimycolate (TDM), lipomannan (LM), and mycolic acids essential for its lifespan and microbial pathogenicity. The cellular membrane has been modified to safeguard against reactive ion species, antibiotics, and host-derived degradative enzymes (9-12). Sulfolipid-1(SL-1) is a sulfated glycolipid implicated as a virulence factor in the initial stages of microbial infection (13,14).

SL-1 constitutes roughly 1-2% of the dry cell wall's weight (13), rendering it the predominant sulfatide on the outer membrane of the cell wall, where it can engage with host cells during infections (15). SL-1 possesses a trehalose-2-sulfate (T2S) core modified by four fatty acyl units (Figure 3.1) (16,17).

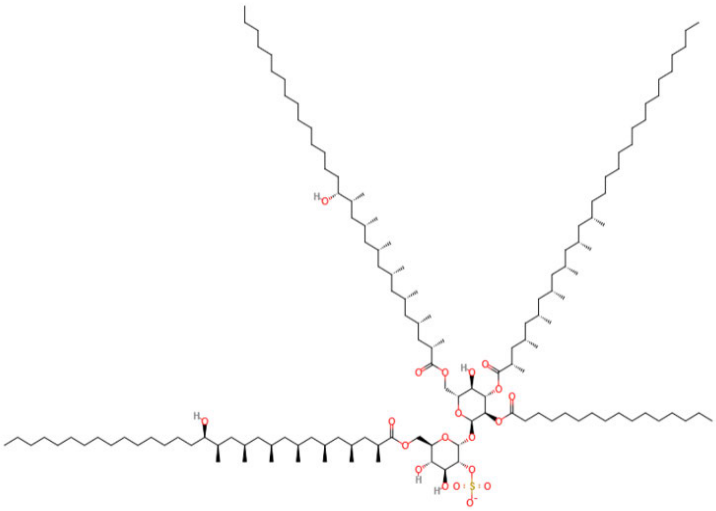

Figure 3.1: Composition of SL-1 featuring fatty acyl substituents: three extensively methyl-branched (hydroxy) phthioceranoic acids and palmitic acid.

SL-1 was recognized for its involvement in nociceptive neural activity and cough induction (18), a characteristic symptom of tuberculosis, hence implicating the sulfatide in TB transmission and pathogenesis. This glycolipid hasthe capacity to disrupt mitochondrial oxidative phosphorylation, the interaction of the phagosome and lysosome, and alterations in phagocytic cells (19-21). Polyketide synthase 2 (Pks2) synthesizes methyl-branched (hydroxy) pthioceranoyl chains, as depicted in Figure 3.2, due to the presence of a starting unit through FadD23 (17,22,23). . FadD23 and pks2 are important to SL-1 biosynthesis (24). *M. tuberculosis* FadD23 is one of 34 fatty acid adenylating (FadDs) enzymes in *M. tuberculosis* (25) that are responsible for synthesizing lipids that impart virulence and metabolism of lipids (26). FadD23 is classified within the fatty acid-AMP ligases (FAAL) category of FadDs, which facilitate the activation and transfer of fatty acids to the corresponding polyketide synthases

A distinguishing characteristic of FAALs and Fatty acyl-coenzyme A ligases (FACLs) is their substantial N-terminal domains, accompanied by smaller C-terminal domains. FadD23 has been identified as a novel drug target, as illustrated in Figure 3.2, to develop potential drugs against TB, and Yan et al. (27) proposed that the C-terminal domain may function as a cover for the substrate during binding. Figure 3.2 additionally depicts the structure as a monomer with the N-terminal domain (1-460) and the C-terminal domain (473-584) (27). Another study conducted by Yan et al. (28) noted the residues that defined the three regions of the N-terminal, as illustrated in Figure 3.2

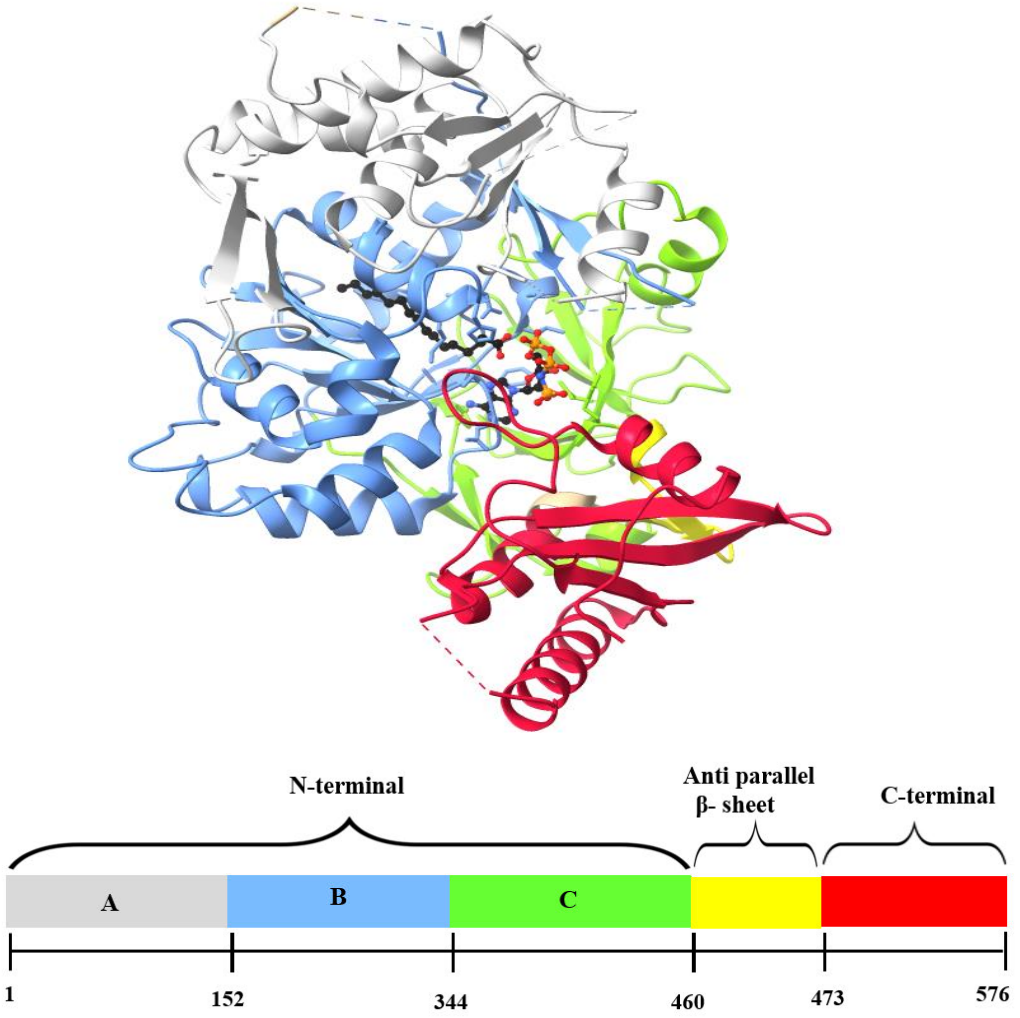

Figure 3.2: Structure of FadD23 (PDB ID: 8hdf), with an overview of the residues that make up its structure.

Computational chemistry enhances the drug discovery process by significantly shortening the drug development timeline (29). Novel therapeutic agents are necessary for the successful treatment and prevention of TB transmission, therefore incorporating computational techniques that facilitate the development of TB treatments is economical. Computational methods, including molecular modelling (30,31), docking (32,33), virtual screening (34,35), and molecular dynamics simulations (36,37), enable medicinal chemists and biological scientists to evaluate millions of molecules, refining and selecting just the viable lead medications for subsequent experimental validation (38). . This work sought to employ *in silico* approaches to identify possible inhibitors of FadD23 by utilizing drugs that have already received FDA approval for repurposing purposes. Using these methods, our goal was to determine how an FDA-approved drug interacts with FadD23 compared to palmitic acid at the molecular level. This work aims to yield results that may enhance the design and development of new inhibitors for FadD23 and the FadD class and urge FadD23 as a new drug target. This study elucidates how FDA-approved drugs may potentially impair FadD23 action. We employed the computational

methodologies and determined that Simeprevir, a drug utilized in HCV treatment, emerged as the most promising candidate for potential inhibition. The results indicated that the robust hydrophobic interactions of Simeprevir result in a higher binding affinity than Phosphoaminophosphonic acid-adenylate (ANP), with which it seems to compete at the binding site. The findings derived from the work necessitate experimental validation and raise curiosities regarding the C-terminal domain of the protein and its loop dynamics.

3.2 Methodology

3.2.1 Molecular Systems Preparation

The X-ray crystal structure of FadD23 (PDB ID: 8HDF) was acquired from the Protein Data Bank (PDB). The small molecules were obtained from the ZINC database (39,40), utilizing a filter for drugs approved by the FDA. The small molecules and protein structures were prepared using UCSF Chimera (41). Accessory molecules were removed, and hydrogen atoms were removed from the proteins and incorporated into the ligands in preparation for docking and molecular dynamics simulations (MDS). ANP and palmitic acid were extracted from the crystal structure and prepared for molecular docking and molecular dynamics simulations.

3.2.2 Molecular Docking

AutoDock Vina (42,43) was used to perform molecular docking. Gasteiger partial charges, as well as atom types between protein and ligand, were assigned. The grid box was defined with the parameters: x = 96 Å, y = 108 Å, z = 100 Å, and the centre coordinates were x = 39 Å, y = 34.047 Å, z = 208.864 Å, with an exhaustiveness of 10. The specified coordinates were employed to blindly dock candidate inhibitors from the ZINC database against FadD23. The docked conformations were produced with a Lamarckian genetic method. The conformations aligned with the docking scores (RMSD = 0.00 Å) in descending order. Docking scores were visualized using UCSF Chimera, and a complex of the highest docking score ligand was generated and preserved for molecular dynamics simulations.

3.2.3 Molecular Dynamics Simulations

MD simulations were conducted using AMBER 18 (44) software package with ff14SB forcefield on Sander (45,46). The LEAP module (47) was employed to incorporate hydrogen atoms into the protein and to add counter ions for system neutralization. The protein atoms were situated 12 Å from the protein surface to the box boundary in each system within the TIP3P water box (47). All systems incorporated boundary conditions of cubic periodicity. Using the particle mesh Ewald approach, a non-bonding cut-off distance of 12 Å was employed to address long-range electrostatic interactions (48). The entire system was energy-minimised using a restraint potential of 500 kcal $mol^{-1}Å^{-2}$ for 1000 steps. The SANDER module was utilized to execute unrestrained conjugate gradient minimization for 1000 steps across the entire system. Utilizing the Langevin thermostat (49) canonical ensemble (NVT), molecular dynamics simulations were conducted for 50 ps at a random collision frequency of 1 ps, during which

the system was incrementally heated from 0 to 300 K, applying harmonic restraints of 5 kcal $mol^{-1}Å^{-2}$ to the solute atoms. The molecular dynamics production simulation was conducted at a constant temperature of 300 K and a constant pressure of 1 atm, utilizing a time step of 2 fs and the Berendsen (50) barostat for pressure regulation. MD simulations lasting 600 ns were conducted to achieve sufficient sampling and system convergence, and MD trajectories were saved every 1 ps for analysis.

3.2.4 Trajectory Analysis

Following the completion of the 600 nanosecond simulations, MD trajectories underwent post-MD analysis computations utilizing the PTRAJ and CPPTRAJ (51) modules of Amber18. The aforementioned techniques are utilized in the analysis of molecular systems, including MM-PBSA (molecular mechanics Poisson–Boltzmann surface area), per-residue free energy decomposition analysis, hydrogen bonding analysis, RMSD (root mean square deviation), RMSF (root mean square fluctuation), Radius of Gyration (Rg), and Secondary Structure Elements (DSSP).

3.2.5 Binding-Free Energy

The MM/PBSA methodology was employed to compute the binding affinity between a ligand and a protein. Equations (1) and (5), as presented below, were employed to compute the binding free energy from MD trajectories. The computation of binding free energy is a thermodynamic approach that provides a valuable understanding of the interaction between a protein and a ligand. The MM/PBSA methodology was additionally employed to ascertain the specific energetic contributions of particular amino acid residues to the overall binding free energy. The visualization of protein-ligand interactions was accomplished through the utilization of LigPlus software.

$$\Delta G_{binding} = G_{complex} - [G_{receptor} + G_{ligand}] \quad (1)$$

$$\Delta G_{binding} = \Delta G_{MM} + \Delta G_{sol} - T\Delta S \quad (2)$$

$$\Delta G_{MM} = \Delta G_{vdW} + \Delta G_{ele} \quad (3)$$

$$\Delta G_{sol} = \Delta_{polar} + \Delta G_{non\text{-}polar} \quad (4)$$

The variable $\Delta G_{binding}$, as depicted in equation 1, represents the binding free energy associated with forming the protein and ligand complex. In the second equation, each term was explicitly and precisely defined. The binding free energy can be expressed as the aggregate of the free energy derived from molecular mechanics (ΔG_{MM}), the entropy contribution ($-T\Delta S$), and the solvation-free energy. The free energy associated with molecular mechanics is denoted as ΔG_{MM} in equation 2. The system's composition is determined by the combined influence of van der Waals interactions and electrostatic interactions ($\Delta G_{vdW} + \Delta G_{ele}$), as depicted in the third equation. Equation 4 was employed to determine the solvation-free energy by incorporating both polar and non-polar contributions, denoted as ΔG_{polar} and $G_{non\text{-}polar}$, respectively.

Per-residue energy breakdown refers to the process of determining the contribution of each amino acid to the overall binding free energy. The estimation is conducted with the MM/PBSA approach. The equation below illustrates the energy interactions between the ligand and residues. The overall Gibbs free energy change (ΔG) can be attributed to many factors, including the van der Waals contribution (ΔG_{vdW}), the electrostatic contribution (ΔG_{ele}), as well as the polar (ΔG_{polar}) and non-polar ($\Delta G_{non\text{-}polar}$) contributions.

$$\Delta G_{inhibitor}\text{-residue} = \Delta G_{vdW} + \Delta G_{ele} + \Delta G_{polar} + \Delta G_{non\text{-}polar} \quad (5)$$

The change in Gibbs free energy of the inhibitor-residue interaction can be expressed as the sum of the changes in van der Waals, electrostatic, polar, and non-polar energy.

3.2.6 Root Mean Square Deviation (RMSD)

The structural deviation of the complex may be determined by the spatial differentiation between two static structures of the same trajectory. The RMSD of a trajectory is defined as:

$$RMSD = \left[\frac{\Sigma_n \left(R_i - R_1^O\right)^2}{n}\right]^{1/2} \quad (6)$$

Where n is the total number of atoms in a complex, Ri represents the vector position of the Cα atoms of particles, *i* is the conformational reference calculated after aligning the structure to an initial conformation (O) using the least fitting square protocol. The average RMSD of a complex can be defined by taking the average structural deviation over the number of frames in each trajectory, which is calculated for receptors, ligands, and complexes in a simulation.

3.2.7 Radius of Gyration (Rg)

The Rg is a parameter used to describe the equilibrium conformation of a simulated system to gain insight into its stability during MD simulations. The Rg is used to describe the RMSD of atoms from the centre of gravity of a protein. This method allowed us to evaluate the compactness of the protein structure along the trajectory of the MD simulation. It is based on the following equation:

$$r^2 gy^r = \frac{\left(\sum_i^n -1 W_i (r_i - r^-)^2\right)}{\sum_i^n -1 W_i} \quad (7)$$

3.2.8 Root Mean Square Fluctuation (RMSF)

A particle's root mean square fluctuations (RMSF) describe the fluctuations of Cα atom residues relative to the average protein structure during the system's trajectory. This suggests the flexible nature of a protein based on the calculated RMSF (52). The subsequent equation is utilized to get a standardized RMSF:

$$sRMSF_i = \frac{RMSF_i - RMSF}{\sigma\,(RMSF)} \quad (8)$$

sRMSFi denotes the standardized RMSF, RMSFi represents the RMSF of the ith residue, RMSF signifies the average RMSF, and σ (RMSF) indicates the standard deviation of RMSF. The calculation of RMSF differs from that of RMSD and Rg, as it quantifies the total residue fluctuation throughout the trajectory rather than being assessed at each frame.

3.2.9 Hydrogen Bond Analysis

The impact of ligands on the protein binding site is assessed by using hydrogen bond analysis. The study examines the geometries and intensities of intramolecular hydrogen bonds that occur between a bound ligand and a protein. This is because ligands can bind to proteins by establishing hydrogen bonds. The conformational stability of the docked complex is substantially influenced by hydrogen bonds formed between the protein and ligand (53).

3.2.10 Secondary Structure Elements (DSSP)

Proteins are classified based on structural traits, such as helix turns, and physicochemical properties, such as polarity. Both are manifestations of the system's free energy. The energetics of interactions between the backbone and side chains across various conformers dictates the arrangement of amino acids. Conversely, polarity is dictated by the energetic interactions of different groups with solvents and among themselves. An amino acid sequence assumes a certain conformation corresponding to a thermodynamic minimum for that sequence (54).

The assignment of secondary structure is crucial for simplifying and characterizing protein structure. DSSP (55) provides a concise description of hydrogen bonding (HB), a commonly employed algorithm that designates secondary structural elements (SSE) to proteins. HB are assigned according to electrostatic energy between backbone carbonyl and amide groups. The electrostatic energy is calculated by summing the interactions between the carbon (C) and oxygen (O) of the carbonyl group and the hydrogen (H) and nitrogen (N) of the amide group; the assigned charges for each atom are 0.42, −0.42, 0.2, and −0.2 in units of electron charge. The hydrogen atom, usually absent from X-ray crystal formations, is incorporated. Only the two most stably interacting carbonyl groups are selected for each amide group 55,56). There are four parameters in DSSP: the energy cutoff, the limit of two nearest acceptors, and the two charge magnitudes.

3.3 Results and Discussion

3.3.1 Simeprevir potentially competes with ANP for a binding site

Molecular docking models determine the ideal binding mode of a ligand to a target and potential binding affinity based on their atomic composition and structural conformation. Among the 1276 leads produced, the top 9 compounds are presented in Table 3.1, exhibiting docking scores that range from -

10.5 to 10.0 kcal/mol. The pharmacological indications of each drug, as noted by DrugBank, are also displayed. Simeprevir, a drug used to treat the Hepatitis C virus (HCV), docked into the N and C-domain with the highest docking score of -10.5 kcal/mol, interacting with key residues in the FadD23 function. The other 8 molecules docked around the same location with distinct conformations (Figure 3.4). Figure 3.3 depicts the binding of Simeprevir in comparison to ANP on FadD23.

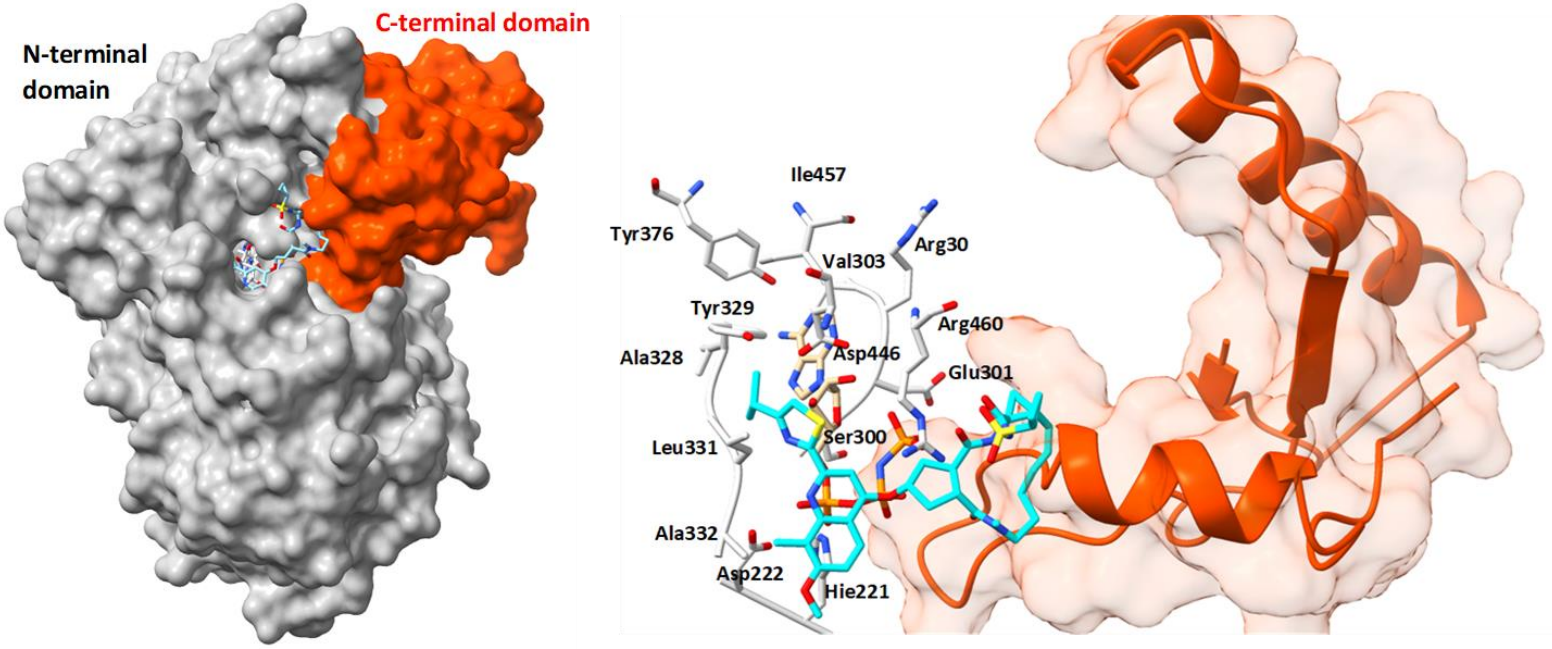

Figure 3.3: Validation of docking model. FadD23 (light grey) complexed with Simeprevir (cyan) and ANP (ecru) at the B and C regions of the N-terminal domain.

Even though we applied a blind docking strategy in this study, Simeprevir and other molecules opted to optimally bind in the ANP binding site of FadD23, thus indirectly validating our docking strategy. Since there is no approved drug that targets FadD23, we used ANP as a reference molecule. For the docked molecules to interfere with the normal function of FadD23, they must either bind on the ANP binding site and compete with ANP for a binding site or bind to the substrate (PLM) binding site. However, the PLM binding site is embedded deep at the core of FadD23 and would only permit binding molecules that structurally resemble PLM or are smaller than PLM.

Phosphoaminophosphonic acid-adenylate ester is an organic molecule including an adenylate moiety, a phosphonic acid, and a carbon-nitrogen bond linking the two. It is a bioactive compound that has been discovered in various creatures, encompassing plants, microbes, and mammals. It is an ATP analogue, which is necessary to activate FadD enzymes.

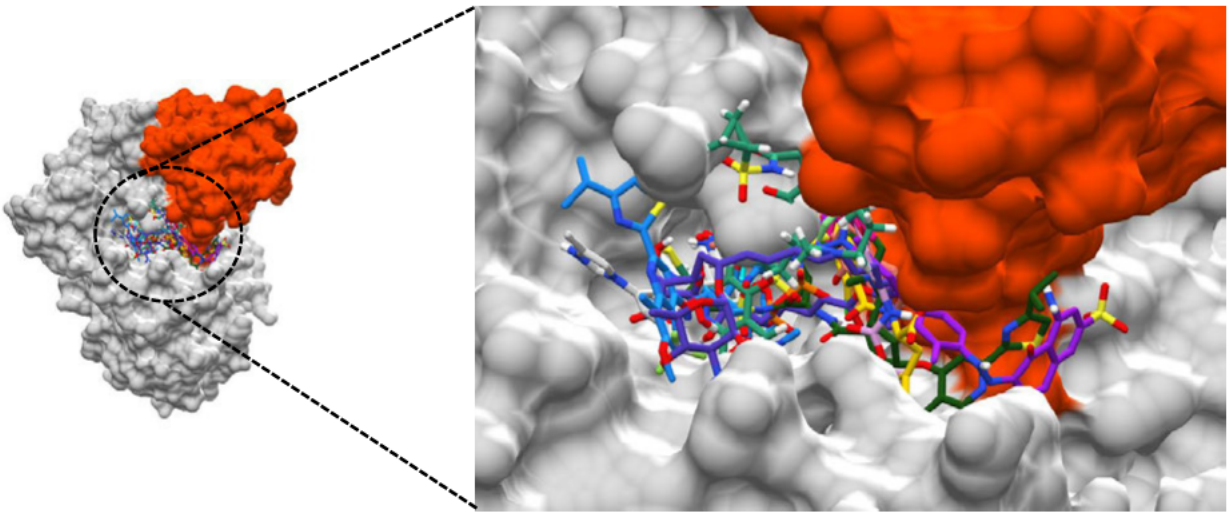

Figure 3.4: The top 9 compounds docked to FadD23 (left), with an overview of the orientations of the compounds (right).

Although the binding scores are similar and vary by decimal points, it is crucial to recognize that their structure and size influence their positioning within the pockets of FadD23. Simeprevir exhibited a high docking score attributable to its larger structure and cyclic ring. Conversely, Natamycin, despite also possessing a cyclic ring, registered a lower docking score, likely due to its smaller size and the absence of the two sulfur atoms present in Simeprevir, which contribute to non-covalent interactions that enhance protein structure stability.

Docking scores may be unreliable as they do not account for the presence of protons in the target, rendering the derived scores inauthentic. For validity, docked complexes are subjected to MD simulations, which produce precise binding affinity scores by accounting for protons and solvent molecules.

Table 3.1 Molecular docking scores for the top 9 compounds.

Zinc ID	Drug Name	Docking score (kcal/mol)	Pharmacology / Indication	2-D Structure
ZINC000164760756	Simeprevir	-10.5	Treatment of individuals with chronic hepatitis C virus (HCV) infection	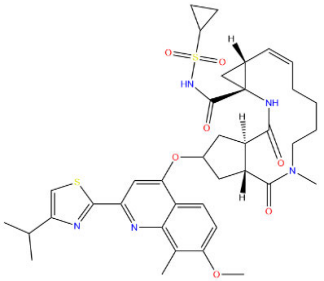
ZINC000000896717	Zafirlukast	-10.4	Long-term management of asthma.	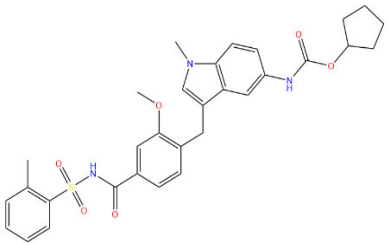

ZINC000006716957	Nilotinib	-10.3	For the prospective treatment of several leukaemias, including chronic myeloid leukaemia (CML)	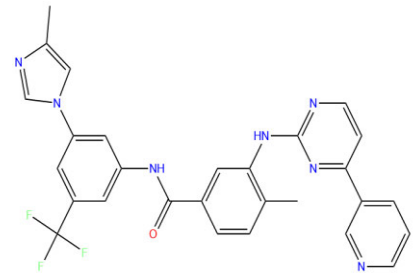
ZINC000013831130	Raltegravir	-10.2	Treatment of HIV-1 infection in combination with other antiretroviral agents.	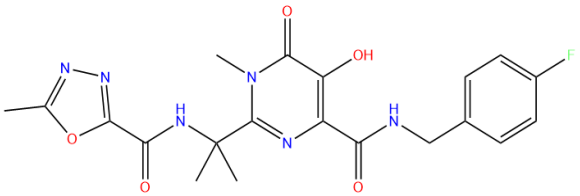
ZINC000253632968	Cromolyn	-10.1	For the treatment of individuals with bronchial asthma. Additionally, employed in managing vernal keratoconjunctivitis, vernal conjunctivitis, and vernal keratitis.	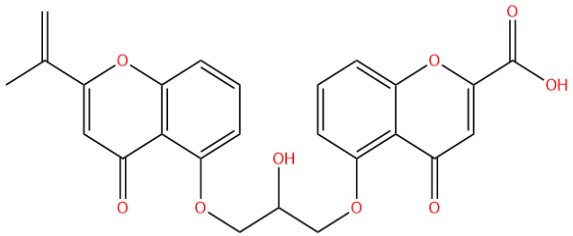

ZINC000003917708	Daunorubicin	-10.1	For remission induction in acute nonlymphocytic leukemia (of adults) and acute lymphocytic leukemia of children and adults.	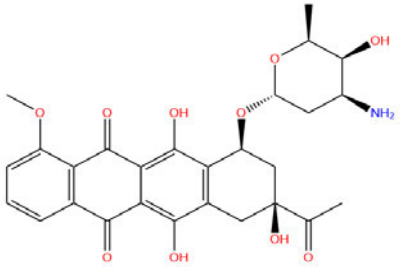
ZINC000169621220	Natamycin	-10.1	Treatment of fungal blepharitis, conjunctivitis, and keratitis induced by susceptible organisms, including *Fusarium solani* keratitis.	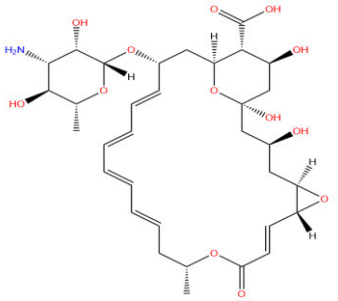
ZINC000001542113	Vilazodone	-10.1	Treatment of major depressive disorder.	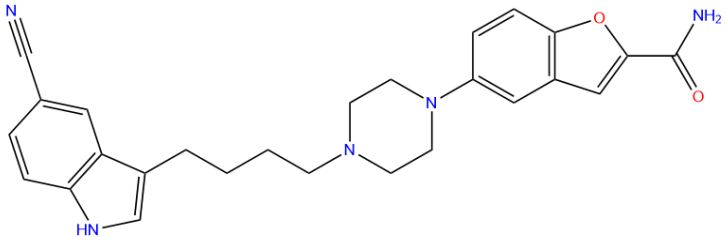

ZINC000084668739	Lifitegrast	-10.0	For the treatment of signs and symptoms of keratoconjunctivitis sicca.	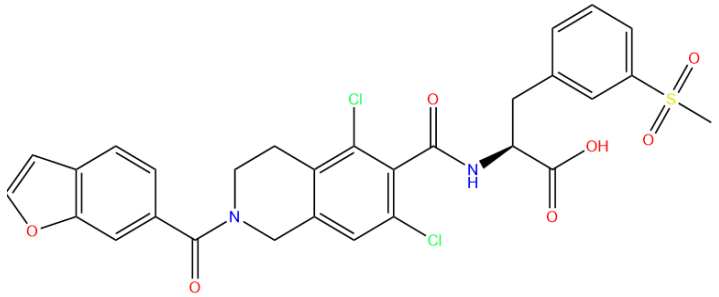

3.3.2 A bulky hydrophobic conformation of Simeprevir governs its complex stability

The RMSD quantifies conformational alterations in a structure by assessing the deviation of Cα atoms of residues situated in the backbone. It indicates the level of stability of a simulated system. An optimal RMSD value is less than 3Å, signifying the robust stability of a system (57,58). Figure 3.5 illustrates the impact of ligand conformational evolution on the protein structure. All systems exhibited considerable stability during an MD trajectory (**S5**), with average RMSD values of 1.92 Å, 2.23 Å, and 1.88 Å for ANP, Simeprevir, and PLM, respectively. PLM exhibited stability for a period of 300 ns, with a maximum RMSD value of 2.5 Å recorded at 50 ns, coinciding with the initial phase of the simulation when the ligand and protein were distantly apart. At the onset of simulations, significant stability was noted for both ANP and Simeprevir complexes, likely attributable to the distance between the ligands and the protein. Between 50 ns and 200 ns, FadD23+Simeprevir exhibited maximum stability at 600 ns, except for a minor surge at 100 ns, which we propose may result from the rotation of Simeprevir as it attempts to establish contacts with FadD23.

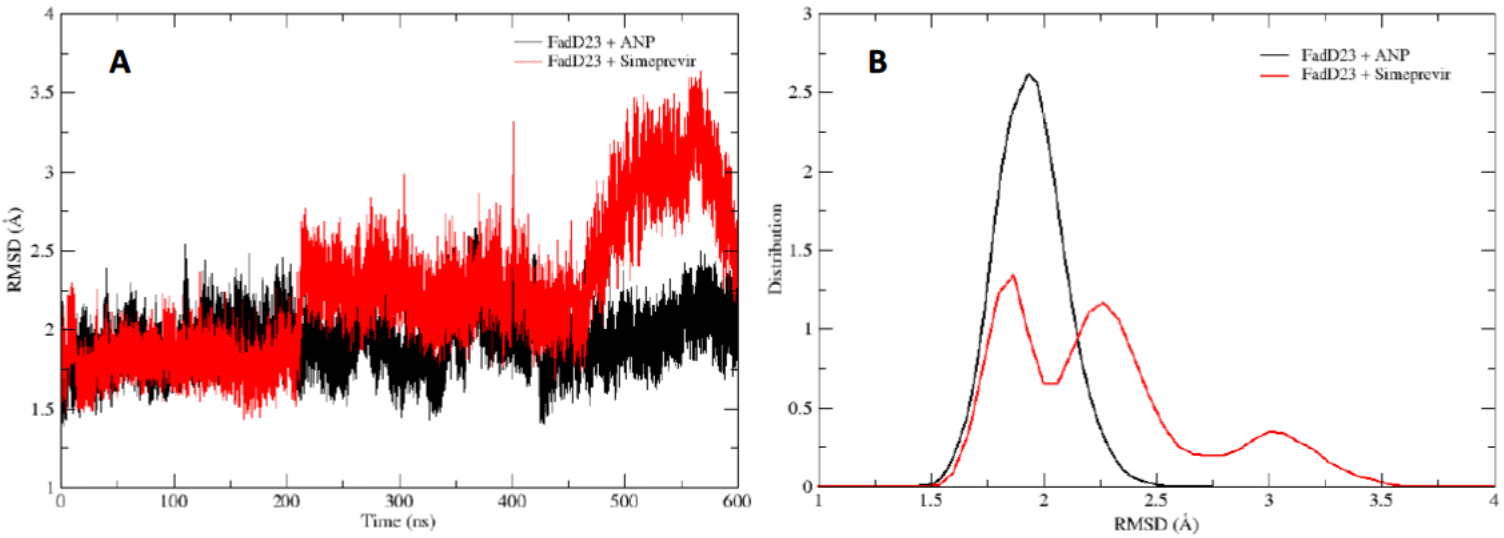

Figure 3.5: RMSD of FadD23 in complex with ANP (black) and Simeprevir (red).

During this period, we noted that FadD23+ANP had the highest RMSD of 2.54 Å in the simulation, which remained stable. Between 200 ns and 400 ns, FadD23+ANP exhibited greater stability than FadD23+Simeprevir, potentially attributable to ΔG_{sol}. In contrast, FadD23 experienced three significant spikes in its RMSD at 216ns, 275ns, 305ns, and 401ns, with the RMSD increasing from 2.77 Å to 3.31 Å, likely due to the augmented distance between FadD23 and Simeprevir and the conformational changes associated with Simeprevir. At 428 ns, FadD23 exhibited its maximum stability for this system, with an RMSD of 1.41 Å. Meanwhile, between 403 ns and 466 ns, the RMSD values for FadD23 + Simeprevir returned to approximately 2.2 Å and 2.4 Å, potentially indicating another conformational

change that reduced the distance between the protein and ligand, thereby achieving a stable system. From 467 ns to 600 ns, ANP exhibited stability with small peaks, indicating little interaction between the protein and ligand accompanied by conformational changes. FadD23+Simeprevir, however, reached its most unstable state at 563 ns with a peak of 3.72 Å, attributable to a conformational shift that occurred. It failed to regain stability before the conclusion of the simulation. Simeprevir exhibits more stability than ANP, as seen by the average RMSD values of 1.90Å and 2.10Å for the ligand. It demonstrates the alterations induced by Simeprevir, attributable to its size and cyclization. From 300 ns to 480 ns, it exhibited greater stability than ANP, with an RMSD of approximately 1.5 Å. Subsequently, a spike occurred due to a conformational shift, after which it stabilized from 540 ns to 600 ns. The ligand RMSD corresponds with the predicted binding affinity. The hydrophobic interactions suggest that van de Waals forces may have enhanced the stability of the protein by compacting the non-polar amino acids within the protein core, thus diminishing the distance between molecules. **S7** shows changes in the conformation, which led to lower RMSD, and increasing binding affinity as more energy is required to break the nucleus. The RMSD distribution exhibited a unimodal pattern ranging from 1.5Å to 2.5Å for all three ligands when in complex with FadD23 (Figure 3.5B and **S5**). We observed that Simeprevir demonstrated a multi-modal distribution.

3.3.3 Simeprevir affinity for FadD23 is driven by electrostatic and van der Waals forces

The MM/PBSA (59) method was employed to elucidate the energy profiles of FadD23 in complex with ANP, PLM, and Simeprevir, thereby offering insights into the binding process between the drug target and a candidate molecule by integrating enthalpic and entropic contributions. In this study binding free energy calculations were performed from MD trajectories and are presented in Table 3.2.

Table 3.2. Calculated binding energies (kcal/mol) between FadD23 and ANP, PLM, and Simeprevir, respectively.

Complex	$\Delta \boldsymbol{E}_{\mathbf{vdw}}$	$\Delta \boldsymbol{E}_{\mathbf{ele}}$	$\Delta \boldsymbol{G}_{\mathbf{gas}}$	$\Delta \boldsymbol{G}_{\mathbf{sol}}$	$\Delta \boldsymbol{G}_{\mathbf{bind}}$
FadD23 + ANP	-39.61 ± 0.15	84.49 ± 3.44	44.88 ± 3.43	-62.83 ± 2.88	-17.95 ± 0.63
FadD23 + PLM	-51.43 ± 0.11	-14.25 ± 0.22	-65.68 ± 0.22	15.84± 0.18	-49.84 ± 0.14
FadD23 + Simeprevir	-55.92 ± 0.22	-41.99 ± 0.41	-97.91 ± 0.49	64.04± 0.41	-33.87 ± 0.18

ΔE_{vdw} = van der Waals; ΔE_{ele} = Electrostatic; ΔG_{gas} = gas-phase energy; ΔG_{sol} = solvation energy; ΔG_{bind} = total binding energy.

PLM was included in the calculations to show differences in binding site preference of the docked molecules to its binding site. Since Simeprevir did not bind in the PLM site, PLM was therefore excluded from further calculations beyond binding free energy. PLM had the highest binding energy of -49.84 kcal/mol, while ANP demonstrated the lowest binding energy of -17.65 kcal/mol. It was noted that Simeprevir exhibited the highest binding energy of -33.87 kcal/mol, which surpassed that of ANP but was inferior to that of PLM. Most of the energy profiles for Simeprevir is exothermic, indicating that greater energy is necessary to dissociate Simeprevir from its binding to FadD23 compared to ANP,

with which it appears to compete, as illustrated in Figure 3.3. ΔG_{gas} influenced the overall binding free energy for PLM and Simeprevir, with values of -65.68 kcal/mol and -97.91 kcal/mol, indicating a transition from a less ordered state to an ordered state, accompanied by energy release in the system, whereas the ANP system exhibited the contrary effect. We concentrated on the contributions of ΔE_{vdw} and ΔE_{ele} to the overall binding energy. ANP exhibited the minimal contribution of ΔE_{vdw}, recorded at -39.61 kcal/mol, suggesting restricted interactions with the hydrophobic residues of the FadD23 protein, in contrast to other proteins.

Conversely, PLM's ΔE_{vdw} profile of -51.43 kcal/mol is warranted, as it is situated within a hydrophobic pocket. The structure of Simeprevir is comparatively big relative to these ligands and features a cyclic ring, which may have resulted in substantial interactions with FadD23. The sulfur atoms in Simeprevir may influence interactions due to their increased polarizability relative to other atoms, resulting in a greater ΔE_{vdw} of -55.92 kcal/mol. In the case of ΔE_{ele}, energy may have been required to surmount the repulsive forces, resulting in a net value of 84.49 kcal/mol. Conversely, Simeprevir exhibited the highest ΔE_{ele} of -41.99 kcal/mol, as the inherent attraction facilitated energy release when atoms approached bond formation. This value surpasses that of PLM (-14.25 kcal/mol) due to structural differences and size; the distance between PLM and FadD23 may have been greater, thereby diminishing energy according to Coulomb's law, where F is inversely proportional to r^2. We also acquired insights into the MM/PBSA for each frame **(S2-4**). Initially, we observed significant contributions from electrostatic interactions for ANP in comparison to Simeprevir and PLM, which ceased around 200 ns, at which point the values for ANP and Simeprevir began to stabilize, aligning with the energy profiles presented in Table 3.2. We observed the unpredictable behaviour of van der Waals for PLM, likely attributable to the hydrophobic pocket in which it was situated, enhancing its binding affinity.

3.3.4 Protein-Ligand Interaction

Both ANP and Simeprevir bind at the ATP binding site (28), while PLM resides in a hydrophobic pocket of FadD23 (27). We performed per-residue energy decomposition and hydrogen bond formation analyses to gain insight into the interactions between the protein and ligand. Table 3.3 below shows the residues that interacted with the ligand at their respective binding sites.

Table 3.3: Binding site residues that interacted with ANP, PLM, and Simeprevir.

Complex	Residues
FadD23+ ANP	Glu301, Tyr329, Arg302, Ala328, Tyr376, Gly330, Ser300, Asp446, Arg460, Hie221, Arg555, Lys553, Thr549
FadD23+ PLM	Hie221, Asp222, Leu331, Ala328, Ser300, Val336, Met195, Met223, Gly330, Tyr199, Leu297, Phe265, Leu227, Val235, Val226, Phe200

FadD23+ Simeprevir	Arg460, Arg128, Ala557, Arg556, Arg555, Glu558, Asp463, Lys462, Ala332, Thr444, Thr446, Tyr175, Gln174, Asp446, Gly330, Glu333, Leu331, Tyr329

Simeprevir exhibited more residues for interaction, likely attributable to its wider binding site. All three ligands interacted with Gly330. while ANP and Simeprevir also shared interactions with Arg460, Asp446, Tyr329, and Arg555. Figure 3.6 illustrates the interactions referenced in the preceding table; however, it precisely delineates the nature of the interactions and the binding modality.

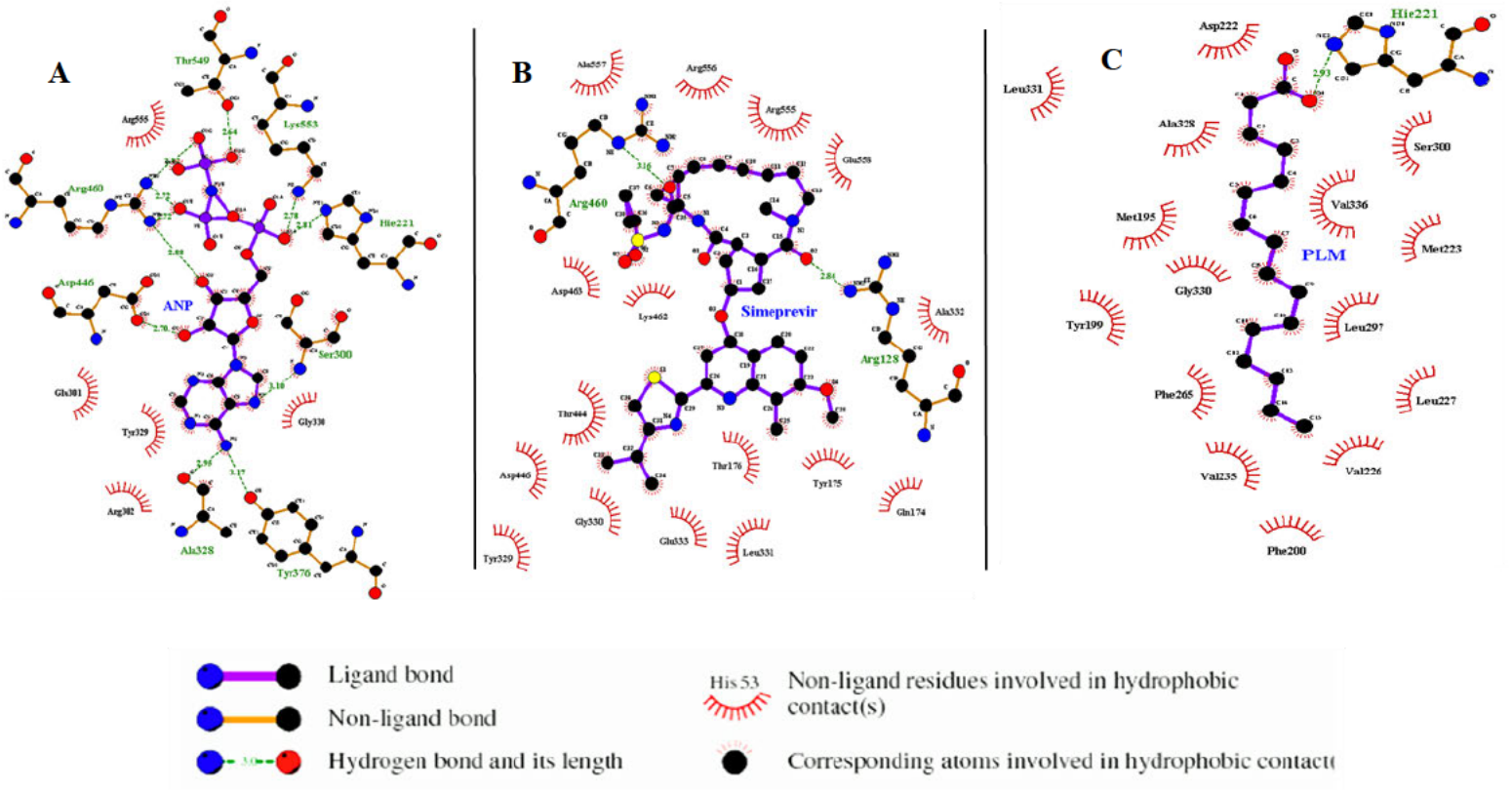

Figure 3.6: Interaction residue profile of ANP (A) Simeprevir (B) and PLM (C)

The interaction profile indicates that Simeprevir exhibited the highest hydrophobic interactions, resulting in a significant van der Waals energies contribution to total binding energy, whereas ANP demonstrated the lowest hydrophobic interactions among the three ligands, as evidenced by its minimal van der Waals contribution relative to PLM and Simeprevir. ANP exhibited substantial hydrogen bonding, corroborated by the hydrogen bond analysis **(Table S4-S6)** and protein-ligand contact information **(Table S7-9)**. ANP was observed to form more hydrophobic interactions towards the end of the simulation (**S1**).

Figure 3.7 delineates the contributions of binding energies, categorized by the specific amino acid contributions associated with their respective binding sites within the protein. A table detailing these contributions is included **(Table S1-S3)**. Arg460, Arg555, and Tyr329 mostly influenced ANP's overall binding energy. Arginine is a polar residue capable of forming up to six hydrogen bonds due to the guanidinium group at the terminus of its aliphatic chain; despite its polarity, it may also engage in van der Waals interactions.

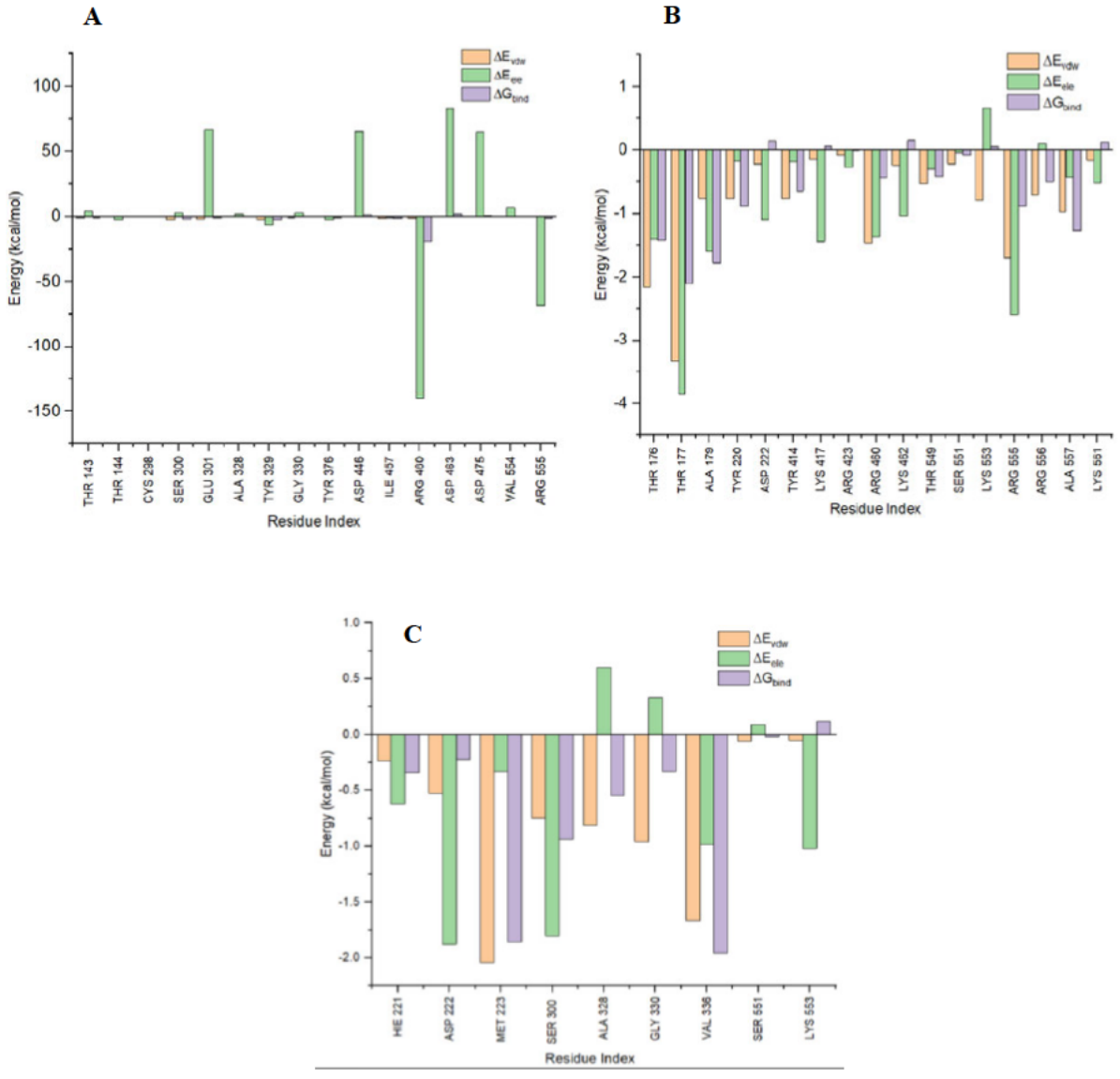

Figure 3.7: Per residue decomposition analysis for ANP (A), Simeprevir (B), and PLM (C).

Tyrosine is polar and has a phenyl group in its sidechain and an OH group capable of forming hydrogen bonds. Asp446 had the highest number of hydrogen bonding interactions **(Table S9)** with 1131 contacts. Aspartic acid possesses a carboxyl group on its side chain, which tends to establish hydrogen bonds

with the backbones of adjacent amides. Contributions from Thr177, Thr176, Arg555, Ala179, Lys553, and Arg460 influence Simeprevir's total binding energy. The side chains of Arginine have already been addressed. The side chain of Threonine possesses a hydroxyl group (OH), rendering it polar and uncharged; hence, the electrostatic contribution is elevated due to the unequal electron density distribution, resulting in partial positive and negative charges. Alanine is nonpolar and linked to a methyl group; its diminutive size facilitates compact packing and contributes to protein stability, as evidenced by the RMSD and Rg of Simeprevir. Lysine is polar, yet it can interact with hydrophobic molecules due to its aliphatic carbon chain. It participates in electrostatic interactions because of its positively charged amino group. Simeprevir's main hydrogen bond contacts were Arg460, Thr176, and Thr177 (**Table S8**). However, we noted that Arg128 was involved in hydrogen bonding (**Table S5**); this happens to be a residue from region A of the N-terminal domain, which Yan et al. (28) reported to not have binding functionality. We report that region A of the N-terminal domain may serve as a site for hydrogen bonding, which may have impacted the binding energy.

Met223, Val336, Asp222, and Ser300 were the main contributors to PLM overall binding energy. Methionine is a non-polar residue, and its side chain includes a sulfur atom, which may enhance interactions through van der Waals forces - its primary mode of interaction with other molecules. Valine is a non-polar, rather bulky, and hydrophobic residue, mostly engaging in van der Waals interactions. Serine is a polar residue with a hydroxyl group, facilitating the formation of hydrogen bonds. Aspartic acid possesses a carboxyl group, is polar, and functions as a hydrogen donor and acceptor. These residues participate in hydrogen bond formation as indicated by the simulation (**Tables S4-S6**). Asp222 had more hydrogen bond contacts than Val336 (**Table S7**). The residues identified from the hydrogen bond and contact information are consistent with the decomposition obtained, reflecting our binding energy profiles above. Simeprevir and PLM exhibited more significant contributions from van der Waals and electrostatic interactions compared to ANP. Simeprevir exhibited a greater number of interactions with residues from the C-terminal domain in comparison to ANP or PLM. This contrasts with the findings obtained by Yan et al. (28) regarding Phu-AMS. They observed that their inhibitor had no direct interaction with the C-terminal domain.

3.3.5 Simeprevir induces a compact conformation on the FadD23 structure.

The equilibrium conformation of a whole system can be characterized by the Radius of gyration (Rg) parameter. This measure is used to assess the compactness of the protein structure during MD simulations. The Rg for ANP and Simeprevir in complex with FadD23 are presented in Figure 3.8.

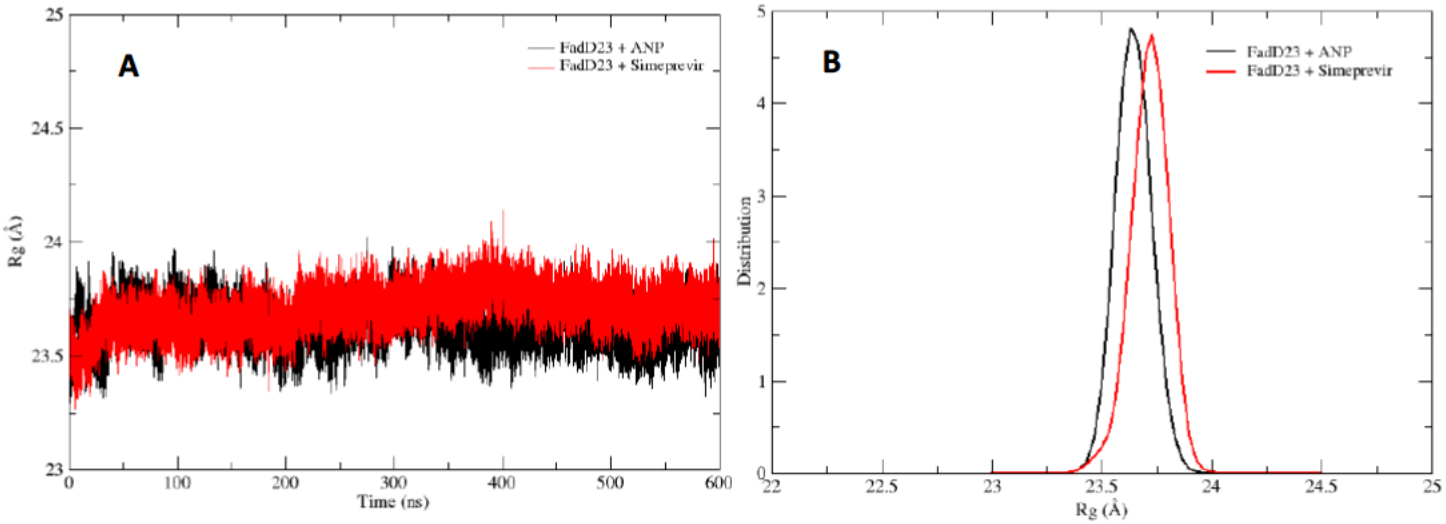

Figure 3.8: Radius of Gyration of FadD23 in complex with ANP (black) vs Simeprevir (red).

The findings indicate that FadD23 is influenced by Simeprevir as a ligand, with its compactness correlating to a 1.90Å RMSD (**S9**). At around 401-402 nanoseconds, the Rg measured 24.44 Å, likely attributable to the presence of bulky amino acids such as phenylalanine, leucine, valine, tryptophan, isoleucine, and alanine. The configuration of Simeprevir, along with its ring structure, renders it both compact and stable, which is indicates of our overall binding energy; hence, greater energy is required to dissociate Simeprevir from its binding site on FadD23. PLM also exhibited a peak at 187-253 ns likely attributable to bulky amino acids such as Ala, Val, Ile, and Phe, which have been shown to constitute the hydrophobic pocket that accommodates PLM (27). The nonpolar amino acid residues possess bulky side chains, characterized by branching in leucine and isoleucine, while phenylalanine and tryptophan feature aromatic rings as side chains. We observed that Simeprevir is relatively compact due to van der Waals interactions, which compel the amino acids to minimize the volume it occupies because of hydrophobicity. Our binding energy profile, breakdown residues, and RMSD analysis corroborate this Rg. The distribution for both complexes was unimodal, ranging from 23.5Å to 24Å (Figure 3.8B).

3.3.6 Simeprevir suppresses residue displacement in the N-terminal domain and induces notable residue displacement in the C-terminal domain

RMSF characterizes the dynamics of individual amino acids in protein structure by calculating Cα fluctuations during simulations, hence providing insight into protein flexibility (60). The RMSF for ANP and Simeprevir complexes are illustrated in Figure 3.9.

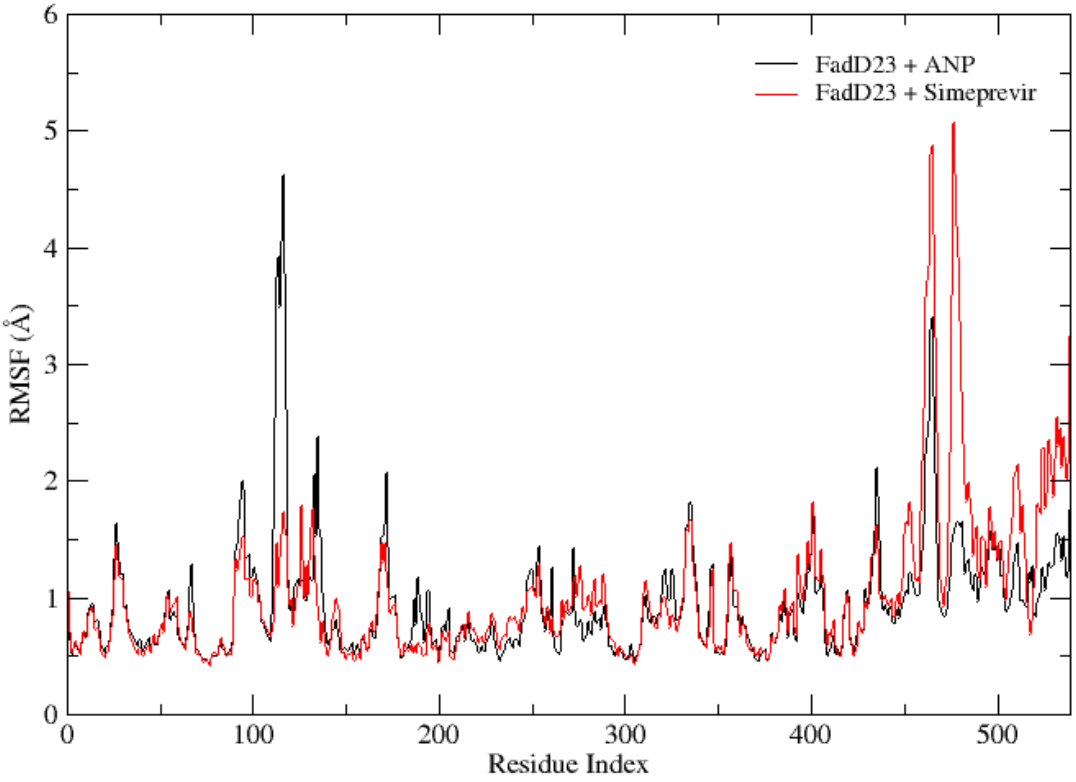

Figure 3.9: Residue mobility in FadD23 complexed with ANP and Simeprevir, respectively.

Prominent variations in amino acid displacement were observed in FadD23 complexes. Simeprevir was noted to diminish the mobility of amino acid residues at positions 94-157, which constitutes region A of the N-terminal domain, along with a reduction in mobility at residue Glu517. We observed several alterations in the binding site regions B and C of the N-terminal domain compared to Yan et al (28), specifically concerning the residues Tyr170, Phe200, Asn319, Ala328, and Glu422. These findings indicate that Simeprevir can obstruct the protein's binding site region and its interaction with ANP by diminishing the mobility of amino acids, therefore affecting both function and the conformational shift that is expected to occur. High displacement of Val166 in the FadD23+ANP system was observed, possibly due to the presence of isopropyl which is hydrophobic and is readily able to interact with the surrounding environment. The C-terminal residues exhibited significant displacement due to the presence of Simeprevir, particularly from Ser473 onwards, which appeared to enhance the mobility of

amino acids relative to ANP. This alteration may disrupt the C-terminal (residue 473-576) (28), implicated in the catalytic mechanism of FadD23(27), potentially obstructing product formation, impeding conformational changes in FadD23, and hinder crosstalk with pks2. Simeprevir potentially restricts residual flexibility at the binding site while simultaneously allowing the C-terminal residues to exhibit considerable mobility. Changes in the dynamics of the loop were also observed from 0ns, 300ns, and 600ns due to Simeprevir binding (**S7)**.

3.3.7 Simeprevir potentially arrests FadD23 function by altering secondary structure elements

The Secondary Structure Elements (SSE) were examined to identify structural changes induced by ligand binding on a protein. SSE provides insight into the correlation between protein function and fundamental structure (61). They produce forecasts on protein-protein interactions, structural classification, and comparative analysis. This is predicated on identifying hydrogen bonds that conform to electrostatic criteria. Figure 3.10 depicts changes in secondary structure elements in FadD23 comparatively induced by ANP and Simeprevir.

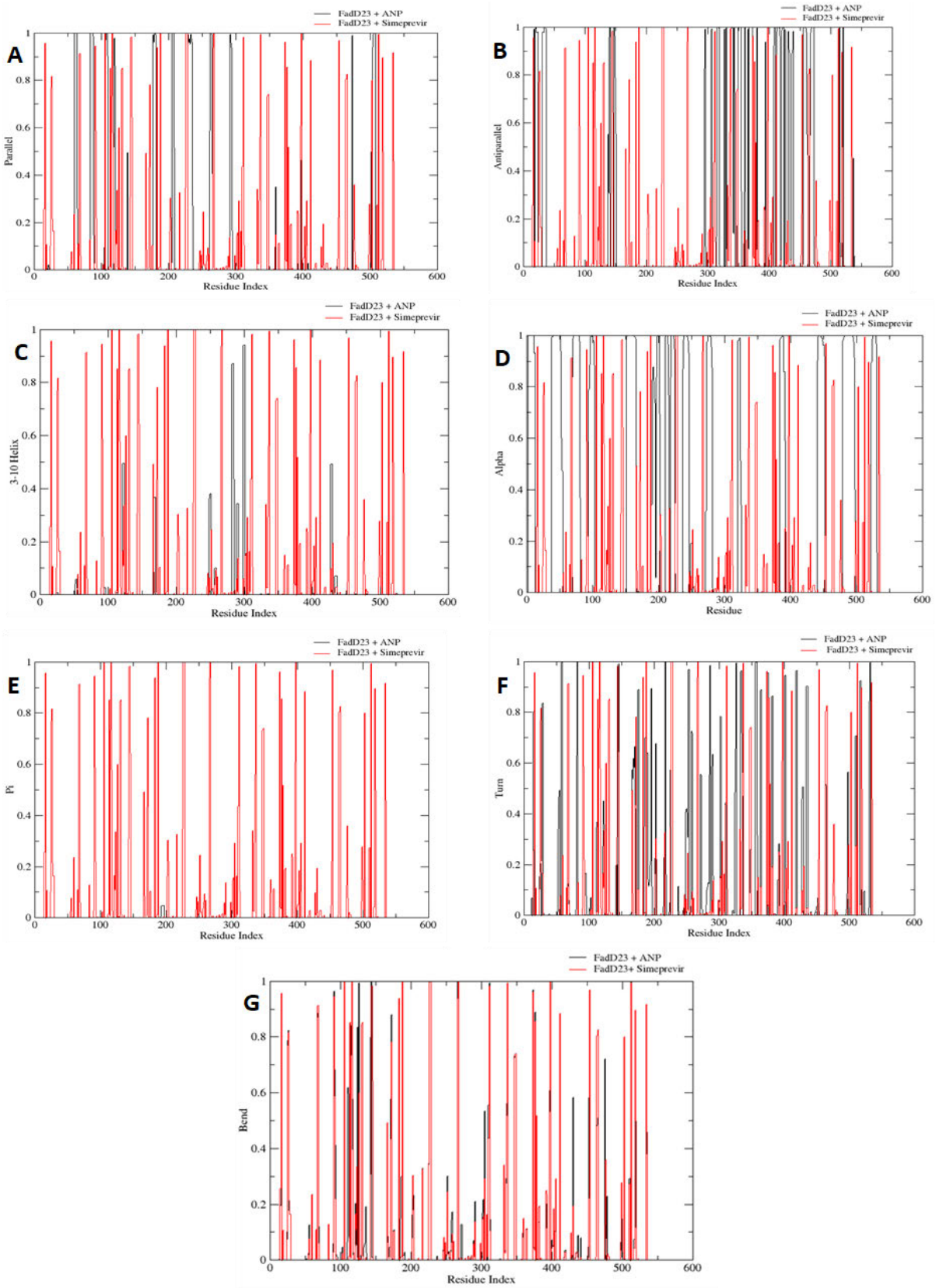

Figure 3.10: Changes in FadD23 Secondary Structure Elements from Parallel (A) to Bend (G).

Simeprevir induced a notable increase in Parallel (A), 3-10 (C), alpha (D), Pi (E), and bend (G) SSEs in in FadD23. In contrast, ANP showed higher Anti-parallel (B) and Turn (F) formation than Simeprevir, which exhibited a significant drop in occupancy. In Figure 3.12A, substantial alterations at the following residues: Ala59, Ala65, Val66, Leu83, Ile88, Ser120, Ser138, Thr177, Val181, Ala205, Leu209, Val235, Glu261, Ala264, Leu290, Thr295, Gly360, Pro396, Thr399, Asp408, His472, Lys501, and Glu507 for ANP were observed. Structural modifications of parallel sheets did not impact the residues constituting the ligand binding site but did influence residues located in those areas and the C-terminal. Thr177 (an active site residue) formed hydrogen bonds with both ANP and Simeprevir, suggesting that the disruption of hydrogen bonding, along with Glycine and Proline, impedes sheet formation.

In Figure 3.12B, the most significant alterations transpired at Gly330, Ser341, Glu348, Gln380, Asn392, Thr393, Gly407, Cys365, Lys417, Pro418, Pro440, Ile466, Asp515, Leu536, and Ser537. Gly330 was observed to establish hydrogen bonds with ANP. From residue 300 to 539, there was an increase in anti-parallel sheets attributed to the formation of stronger hydrogen bonds, compared to Simeprevir, as the latter had stronger hydrophobic interactions.

In Figure 3.12C, we observed alterations for ANP at the residues Ala53, Thr199-Ile122, Phe247-Arg250, Gln256, Leu290, Gly426, and Ala434. No hydrogen bond formation was seen with these amino acids, nor any impact on binding affinity. Changes in Figure 3.12D for ANP were observed at positions 100, Phe192, Met195, Trp216, Phe247, Leu248, Asn270, Arg385, Thr480, Gly498, and Thr523. No decomposition towards binding energy was observed for the specified amino acids, nor did hydrogen bonds form with these residues. These residues may disrupt hydrogen bonding or cause steric clashes compared to Simeprevir due to potential alterations at interaction sites, resulting in diminished binding affinity. In E, alterations transpired at Ile188-Phe192; however, the most significant modification was at Met195 for ANP. The absence of a pi helix may be attributed to the interruption caused by methionine, a non-polar amino acid, due to its side chain, which features a sulfur atom bonded to a methyl group. When situated near a hydrogen bonding site, its hydrophobic characteristics inhibit interactions. In F, alterations were noted at the following residues: Val14, Ser32, His58, Ser93, Glu102, Ile122, Val144, Tyr167, 176, Pro178, Pro218, Gly236, Arg250, Phe271, Ala286, Glu301-His304, Ala328, Leu378, Gln380, Pro389, Ile400, Ala428, Val450, Leu465, Asn497, 512, Glu517, Thr523. Ser531, Thr532, and Ser533 for ANP enhanced the turn helix's occupancy. We observed that the active site residues Ala328 and Glu301 were impacted, with Glu301 specifically forming hydrogen bonds. Simeprevir occupied fewer turn helices since it did not promote hydrogen bonding compared to ANP (**S8-9**). Ultimately, for G, we observed variations at Ile122, 124-128, Asp145, Ala252, Met258, Ala272, Leu290, Val303, Glu402-Ala306, Leu429, Pro440, Asp476, and Glu517 for ANP in contrast to Simeprevir, which exhibited multiple bends likely due to steric clashes aimed at optimizing the arrangement of hydrophobic residues within the protein. These observations indicate that Simeprevir

induces fewer alterations in protein structure, especially at the active site, than ANP. Simeprevir exhibited higher occupancies across all elements except for turn helices and anti-parallel sheets. Nevertheless, the robust hydrophobic and electrostatic interactions facilitated a binding affinity of -33.87 kcal/mol, in contrast to ANP's affinity of -17.95 kcal/mol. We observed multiple hydrogen bonds created by ANP (**Table S6 and S9**); nonetheless, the strength of each individual bond is significant, given the poor binding of ANP.

3.3.8 Distance Analysis

The distance was calculated for residues Glu301-Asp222, Asp446-His221, Glu301-Asp446, His221-Arg460, and Lys553 and Arg460 to gain insight into the effect that ANP and Simeprevir may have had on the distance between these two amino acid residues.

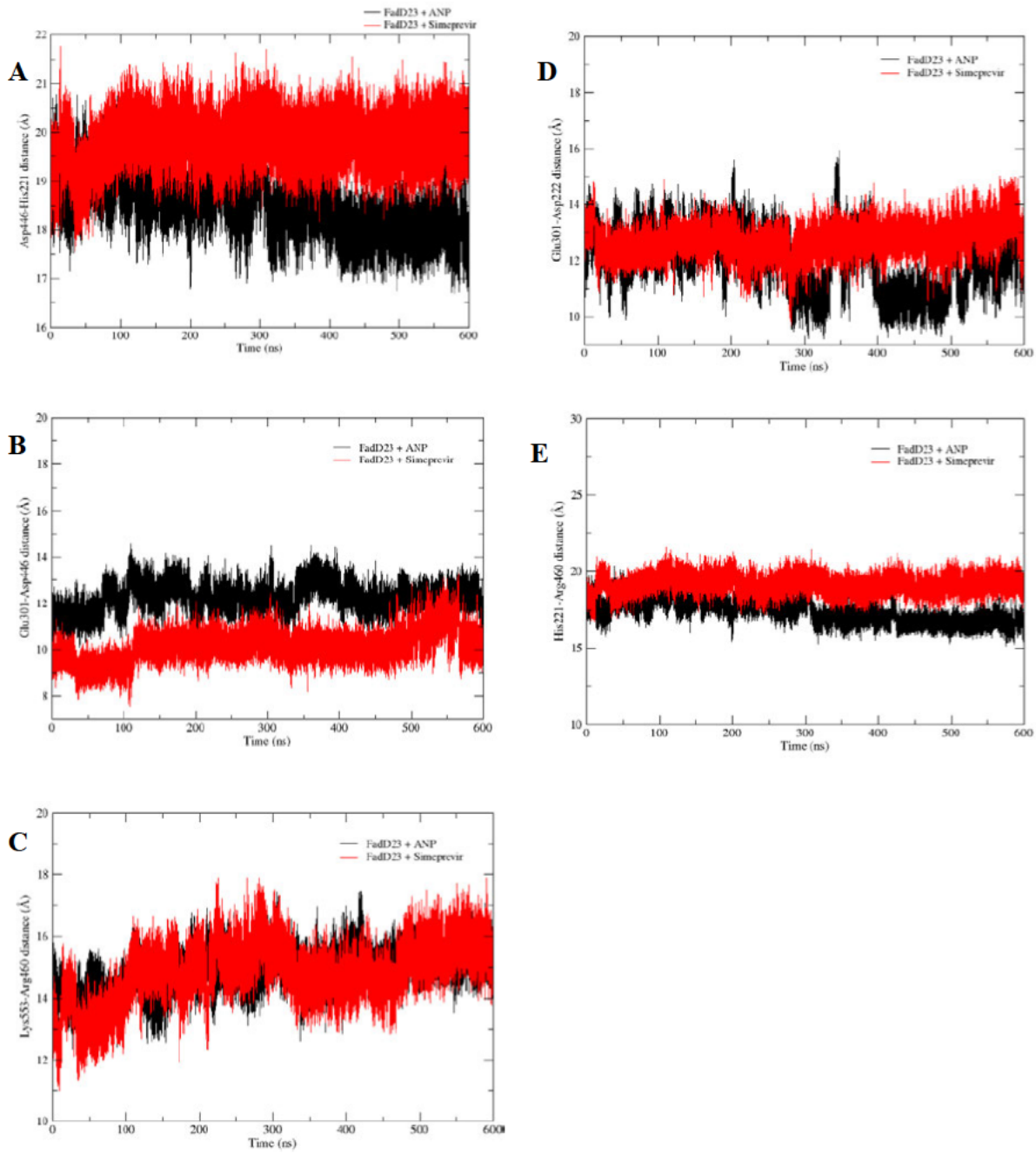

Figure 3.11 Distance Analysis measured from Cα atoms for residues Asp, Arg, Glu, His, and Lys.

We noted that the distances had increased for residues Glu301-Asp422, Asp446-His221, and His221-Arg460. The distance for Lys553-Arg460 displayed minimal differences in distance. However, Glu301-Asp446 saw the distance decrease significantly with Simeprevir was involved. Table 3.4 highlights the average distances for these residues. These differences may have been due to changes in the secondary structures of the protein, as seen in Figure 3.11, where we noticed significant changes to the FadD23+Simeprevir system. The changes in the distance may impact the binding site volume pocket. The side chains of the amino acids determine the distances between the pair of residues. Glu has a carboxylate group and readily forms hydrogen bonds; Asp also has a carboxyl group and is noted for

having an acidic side chain; Arg has three carbons attached to a guanidium group and is highly hydrophilic, His has an imidazole ring, and we notice they had increased distance in the case of Simeprevir, Lys has an amino group and is polar. It appears the interactions with the ligands influenced the distances as a larger molecule like Simeprevir increased the distance between residues compared to ANP

Table 3.4: Average distance between ANP and Simeprevir for residues Glu301, Asp222, His221, Lys553, and Arg460

	Glu301-Asp422	Asp446-His221	Glu301-Asp446	His221-Arg460	Lys553-Arg460
ANP	11.99Å	18.56Å	12.24Å	17.43Å	14.86Å
Simeprevir	12.72Å	19.82Å	10.14Å	19.16Å	14.82Å

3.4 Conclusion

Tuberculosis has persisted as a worldwide health security challenge for generations. Currently, the African and Asian regions appear to be the most afflicted. No existing vaccination can safeguard against pulmonary tuberculosis, nor is there any drug known to inhibit the transmission of tuberculosis, as evidenced by the millions claimed to be afflicted each year. These statistics necessitate intervention and measures to mitigate TB transmission. Our computational work aimed to identify FDA-approved medications that could potentially block FadD23, a crucial enzyme in SL-1 production. SL-1 has been shown to affect the onset of tuberculosis by influencing nociceptive neural activity and inducing cough. Molecular docking, molecular dynamics simulations, RMSD, Rg, RMSF, MM/PBSA, decomposition analysis, hydrogen bond analysis, and secondary structure elements (DSSP) was some of the computational applications used to explore potential inhibitors. HCV and TB have a complex relationship and can sometimes co-occur, leading to severe complications and disease due to compromised immunity. Simeprevir can disrupt the viral replication cycle, leading to impaired viral replication and reduced viral load in the patient's body. This could help improve immune function, which helps to reduce the risk of TB or developing active TB infection. Administering Simeprevir to those patients with HCV/TB could impact TB-specific T cells and potentially impact the immune response against TB. The findings of our investigation indicated that Simeprevir, a drug used for HCV treatment, exhibits superior binding affinity to FadD23 in comparison to ANP (an ATP analogue), which is implicated in FadD activation and appears to be a competitive antagonist based on blind docking studies. The elevated binding energy resulted from the multitude of hydrophobic contacts. The Simeprevir ligand significantly influenced RMSD at 1.90Å, exhibiting compactness and inducing considerable mobility in the C-terminal domain residues, perhaps compromising its catalytic function. Simeprevir demonstrated significant occupancy in the secondary structural analysis, leading to better binding affinity than ANP, contributing to its stability, particularly at the binding site, and revealing increased distances between amino acids, which may influence the volume of the binding site. Thr176, Thr177, and Arg460 exhibited the highest frequency of hydrogen bonds; however, we did not perform a toxicity investigation as this drug has already received FDA approval. The preliminary results require experimental validation to substantiate the findings and advocate for FadD23 as a fresh target for exploration alongside other FadD enzymes.

3.5 References

1. Kaufmann SH, Schaible UE. 100th anniversary of Robert Koch's Nobel Prize for the discovery of the tubercle bacillus. Trends Microbiol. 2005;13(10):469-75.

2. World Health Organisation 2024 [Available from: https://www.who.int/news-room/fact-sheets/detail/tuberculosis.

3. Leung AN. Pulmonary tuberculosis: the essentials. Radiology. 1999;210(2):307-22.

4. Raviglione MC. Tuberculosis. In: Jameson JL, Fauci AS, Kasper DL, Hauser SL, Longo DL, Loscalzo J, editors. Harrison's Principles of Internal Medicine, 20e. New York, NY: McGraw-Hill Education; 2018.

5. Singh V. Tuberculosis treatment-shortening. Drug Discov Today. 2024;29(5):103955.

6. Sachdeva K, Goel M, Sudhakar M, Mehta M, Raju R, Raman K, Singh A, Sundaramurthy V. *Mycobacterium tuberculosis* (Mtb) lipid mediated lysosomal rewiring in infected macrophages modulates intracellular Mtb trafficking and survival. J Biol Chem. 2020;295(27):9192-210.

7. Gutierrez MG, Master SS, Singh SB, Taylor GA, Colombo MI, Deretic V. Autophagy is a defense mechanism inhibiting BCG and Mycobacterium tuberculosis survival in infected macrophages. Cell. 2004;119(6):753-66.

8. Kumar D, Nath L, Kamal MA, Varshney A, Jain A, Singh S, Rao KV. Genome-wide analysis of the host intracellular network that regulates survival of Mycobacterium tuberculosis. Cell. 2010;140(5):731-43.

9. Brennan PJ, Nikaido H. The envelope of mycobacteria. Annu Rev Biochem. 1995;64:29-63.

10. Minnikin DE, Kremer L, Dover LG, Besra GS. The methyl-branched fortifications of Mycobacterium tuberculosis. Chem Biol. 2002;9(5):545-53.

11. Glickman MS, Jacobs WR, Jr. Microbial pathogenesis of Mycobacterium tuberculosis: dawn of a discipline. Cell. 2001;104(4):477-85.

12. Kaur D, Guerin ME, Skovierová H, Brennan PJ, Jackson M. Chapter 2: Biogenesis of the cell wall and other glycoconjugates of Mycobacterium tuberculosis. Adv Appl Microbiol. 2009;69:23-78.

13. Goren MB. Sulfolipid I of Mycobacterium tuberculosis, strain H37Rv. I. Purification and properties. Biochim Biophys Acta. 1970;210(1):116-26.

14. Okamoto Y, Fujita Y, Naka T, Hirai M, Tomiyasu I, Yano I. Mycobacterial sulfolipid shows a virulence by inhibiting cord factor induced granuloma formation and TNF-alpha release. Microb Pathog. 2006;40(6):245-53.

15. Gilmore SA, Schelle MW, Holsclaw CM, Leigh CD, Jain M, Cox JS, Leary JA, Bertozzi CR. Sulfolipid-1 biosynthesis restricts Mycobacterium tuberculosis growth in human macrophages. ACS Chem Biol. 2012;7(5):863-70.

16. Layre E, Cala-De Paepe D, Larrouy-Maumus G, Vaubourgeix J, Mundayoor S, Lindner B, Puzo G, Gilleron M. Deciphering sulfoglycolipids of *Mycobacterium tuberculosis*. J Lipid Res. 2011;52(6):1098-110.

17. Seeliger JC, Holsclaw CM, Schelle MW, Botyanszki Z, Gilmore SA, Tully SE, Niederweis M, Cravatt BF, Leary JA, Bertozzi CR. Elucidation and chemical modulation of sulfolipid-1 biosynthesis in Mycobacterium tuberculosis. J Biol Chem. 2012;287(11):7990-8000.

18. Ruhl CR, Pasko BL, Khan HS, Kindt LM, Stamm CE, Franco LH, Hsia CC, Zhou M, Davis CR, Qin T, Gautron L, Burton MD, Mejia GL, Naik DK, Dussor G, Price TJ, Shiloh MU. Mycobacterium tuberculosis Sulfolipid-1 Activates Nociceptive Neurons and Induces Cough. Cell. 2020;181(2):293-305.e11.

19. Kato M, Goren MB. Synergistic action of cord factor and mycobacterial sulfatides on mitochondria. Infect Immun. 1974;10(4):733-41.

20. Goren MB, D'Arcy Hart P, Young MR, Armstrong JA. Prevention of phagosome-lysosome fusion in cultured macrophages by sulfatides of Mycobacterium tuberculosis. Proc Natl Acad Sci U S A. 1976;73(7):2510-4.

21. Zhang L, Goren MB, Holzer TJ, Andersen BR. Effect of Mycobacterium tuberculosis-derived sulfolipid I on human phagocytic cells. Infect Immun. 1988;56(11):2876-83.

22. Gokhale RS, Saxena P, Chopra T, Mohanty D. Versatile polyketide enzymatic machinery for the biosynthesis of complex mycobacterial lipids. Nat Prod Rep. 2007;24(2):267-77.

23. Sirakova TD, Thirumala AK, Dubey VS, Sprecher H, Kolattukudy PE. The Mycobacterium tuberculosis pks2 gene encodes the synthase for the hepta- and octamethyl-branched fatty acids required for sulfolipid synthesis. J Biol Chem. 2001;276(20):16833-9.

24. Lynett J, Stokes RW. Selection of transposon mutants of Mycobacterium tuberculosis with increased macrophage infectivity identifies fadD23 to be involved in sulfolipid production and association with macrophages. Microbiology (Reading). 2007;153(Pt 9):3133-40.

25. Cole ST, Brosch R, Parkhill J, Garnier T, Churcher C, Harris D, Gordon SV, Eiglmeier K, Gas S, Barry CE 3rd, Tekaia F, Badcock K, Basham D, Brown D, Chillingworth T, Connor R, Davies R, Devlin K, Feltwell T, Gentles S, Hamlin N, Holroyd S, Hornsby T, Jagels K, Krogh A, McLean J, Moule S, Murphy L, Oliver K, Osborne J, Quail MA, Rajandream MA, Rogers J, Rutter S, Seeger K, Skelton J, Squares R, Squares S, Sulston JE, Taylor K, Whitehead S, Barrell BG. Deciphering the biology of Mycobacterium tuberculosis from the complete genome sequence. Nature. 1998;393(6685):537-44.

26. Baran M, Grimes KD, Sibbald PA, Fu P, Boshoff HIM, Wilson DJ, Aldrich CC. Development of small-molecule inhibitors of fatty acyl-AMP and fatty acyl-CoA ligases in Mycobacterium tuberculosis. Eur J Med Chem. 2020;201:112408.

27. Yan M, Cao L, Zhao L, Zhou W, Liu X, Zhang W, Rao Z. The Key Roles of Mycobacterium tuberculosis FadD23 C-terminal Domain in Catalytic Mechanisms. Front Microbiol. 2023;14:1090534.

28. Yan M, Ma M, Chen R, Cao Y, Zhang W, Liu X. Structural basis for the development of potential inhibitors targeting FadD23 from Mycobacterium tuberculosis. Acta Crystallogr F Struct Biol Commun. 2023;79(Pt 8):208-16.
29. Macalino SJ, Gosu V, Hong S, Choi S. Role of computer-aided drug design in modern drug discovery. Arch Pharm Res. 2015;38(9):1686-701.
30. K I R, Deepa G, Namboori DK. Computational chemistry and molecular modeling: Principles and applications2008. 1-397 p.
31. Forster MJ. Molecular modelling in structural biology. Micron. 2002;33(4):365-84.
32. Meng XY, Zhang HX, Mezei M, Cui M. Molecular docking: a powerful approach for structure-based drug discovery. Curr Comput Aided Drug Des. 2011;7(2):146-57.
33. McConkey B, Sobolev V, Edelman M. The performance of current methods in ligand-protein docking. Current Science. 2002;83.
34. Langer T, Hoffmann RD. Virtual screening: an effective tool for lead structure discovery? Curr Pharm Des. 2001;7(7):509-27.
35. Lavecchia A, Di Giovanni C. Virtual screening strategies in drug discovery: a critical review. Curr Med Chem. 2013;20(23):2839-60.
36. Amadei A, Linssen AB, Berendsen HJ. Essential dynamics of proteins. Proteins. 1993;17(4):412-25.
37. Petrenko R, Meller J. Molecular Dynamics. eLS.
38. Chen C, Nguyen DT, Lee SJ, Baker NA, Karakoti AS, Lauw L, et al. Accelerating Computational Materials Discovery with Machine Learning and Cloud High-Performance Computing: from Large-Scale Screening to Experimental Validation. Journal of the American Chemical Society. 2024;146:20009-18.
39. Sterling T, Irwin JJ. ZINC 15--Ligand Discovery for Everyone. J Chem Inf Model. 2015;55(11):2324-37.
40. Irwin JJ, Sterling T, Mysinger MM, Bolstad ES, Coleman RG. ZINC: a free tool to discover chemistry for biology. J Chem Inf Model. 2012;52(7):1757-68.
41. Pettersen EF, Goddard TD, Huang CC, Couch GS, Greenblatt DM, Meng EC, et al. UCSF Chimera--a visualization system for exploratory research and analysis. J Comput Chem. 2004;25(13):1605-12.
42. Eberhardt J, Santos-Martins D, Tillack AF, Forli S. AutoDock Vina 1.2.0: New Docking Methods, Expanded Force Field, and Python Bindings. J Chem Inf Model. 2021;61(8):3891-8.
43. Trott O, Olson AJ. AutoDock Vina: improving the speed and accuracy of docking with a new scoring function, efficient optimization, and multithreading. J Comput Chem. 2010;31(2):455-61.
44. Wang J, Wolf RM, Caldwell JW, Kollman PA, Case DA. Development and testing of a general amber force field. J Comput Chem. 2004;25(9):1157-74.

45. Galindo-Murillo R, Robertson JC, Zgarbová M, Šponer J, Otyepka M, Jurečka P, et al. Assessing the Current State of Amber Force Field Modifications for DNA. J Chem Theory Comput. 2016;12(8):4114-27.
46. Maier JA, Martinez C, Kasavajhala K, Wickstrom L, Hauser KE, Simmerling C. ff14SB: Improving the Accuracy of Protein Side Chain and Backbone Parameters from ff99SB. Journal of Chemical Theory and Computation. 2015;11(8):3696-713.
47. Jorgensen WL, Chandrasekhar J, Madura JD, Impey RW, Klein ML. Comparison of simple potential functions for simulating liquid water. The Journal of Chemical Physics. 1983;79(2):926-35.
48. Harvey MJ, De Fabritiis G. An Implementation of the Smooth Particle Mesh Ewald Method on GPU Hardware. J Chem Theory Comput. 2009;5(9):2371-7.
49. Johnson A, Johnson, T., & Khan, A. Thermostats in Molecular Dynamics

Simulations An Interest in Thermostats. 1st edn ed: University of Massachusetts Amherst; 2012. p. 1–23..
50. Berendsen HJC, Postma JPM, Gunsteren WFv, Dinola A, Haak JR. Molecular dynamics with coupling to an external bath. Journal of Chemical Physics. 1984;81:3684-90.
51. Roe DR, Cheatham TE, 3rd. PTRAJ and CPPTRAJ: Software for Processing and Analysis of Molecular Dynamics Trajectory Data. J Chem Theory Comput. 2013;9(7):3084-95.
52. Bornot A, Etchebest C, de Brevern AG. Predicting protein flexibility through the prediction of local structures. Proteins. 2011;79(3):839-52.
53. Kumari M, Singh R, Subbarao N. Exploring the interaction mechanism between potential inhibitor and multi-target Mur enzymes of mycobacterium tuberculosis using molecular docking, molecular dynamics simulation, principal component analysis, free energy landscape, dynamic cross-correlation matrices, vector movements, and binding free energy calculation. J Biomol Struct Dyn. 2022;40(24):13497-526.
54. Wrabl JO, Larson SA, Hilser VJ. Thermodynamic propensities of amino acids in the native state ensemble: implications for fold recognition. Protein Sci. 2001;10(5):1032-45.
55. Kabsch W, Sander C. Dictionary of protein secondary structure: pattern recognition of hydrogen-bonded and geometrical features. Biopolymers. 1983;22(12):2577-637.
56. Haghighi H, Higham J, Henchman RH. Parameter-Free Hydrogen-Bond Definition to Classify Protein Secondary Structure. J Phys Chem B. 2016;120(33):8566-70.
57. Xiang Z, Soto CS, Honig B. Evaluating conformational free energies: the colony energy and its application to the problem of loop prediction. Proc Natl Acad Sci U S A. 2002;99(11):7432-7.
58. Dixit SB, Ponomarev SY, Beveridge DL. Root mean square deviation probability analysis of molecular dynamics trajectories on DNA. J Chem Inf Model. 2006;46(3):1084-93.
59. Genheden S, Ryde U. The MM/PBSA and MM/GBSA methods to estimate ligand-binding affinities. Expert Opin Drug Discov. 2015;10(5):449-61.

60. Sneha P, Doss CG. Molecular Dynamics: New Frontier in Personalized Medicine. Adv Protein Chem Struct Biol. 2016;102:181-224.
61. Yoo P, Zhou B, Zomaya A. Machine Learning Techniques for Protein Secondary Structure Prediction:An Overview and Evaluation. Current Bioinformatics. 2008;3:74-86.

Chapter 4
General Conclusions and Future Studies

4.1 General Conclusions

This study employed molecular docking and molecular dynamics simulations of Simeprevir, selected as the premier molecule, ANP, and PLM to investigate their molecular interactions with FadD23, aiming to discover a viable inhibitor from an already FDA-approved medicine. This study has accomplished the aim of identifying Simeprevir as a potential inhibitor against FadD23 among various FDA-approved drugs. Molecular dynamics helped explain how Simeprevir interacts with FadD23 compared to ANP and FadD23. Most of our research questions were answered as we found that Simeprevir bound to the ATP binding site, which may allow it to compete for ANP, and possibly block loading of the acyl chain to pks2. Simeprevir demonstrates superior potential as an inhibitor of FadD23, evidenced by its total binding energy, stability, and compactness. It exhibits high secondary structure occupancy per residue while preserving the rigidity of active site amino acids, concurrently inducing significant mobility in the C-terminal domain, thereby compromising its function. This data may be a potential reference for designing a chemical with suitable thermodynamic properties to inhibit FadD23. This study represents the initial application of *in silico* methods to identify drugs approved by the FDA as possible inhibitors of FadD23 while detailing the structural and thermodynamic alterations of the ligands over time.

4.2 Future Studies

Future studies involve the purification and expression of FadD23 for experimental purposes; however, tuberculosis proteins are known for their poor solubility, which adversely affects both purification and expression, ultimately impacting protein output. While protein purification is difficult for infectious diseases we could potentially apply surface plasmon resonance, isothermal titration calorimetry, track receptor dynamics and perform circular dichroism to study the Simeprevir and FadD23 interaction, and examine Simeprevir binding affinity on FadD23 through microscale thermophoresis. This molecule may be a scaffold for drug design against FadD23 compared to Phu-Ams. Prospective *in silico* investigations for FadD23 encompass examining the Apo structure relative to ATP and PLM, as well as investigating the interaction between FadD23 and pks2. To potentially utilise quantum computations to examine the structural alteration of FadD23 upon activation and its subsequent effects. Ultimately, it may be essential to examine the C-terminal domain and its loop mechanism, as it facilitates the catalytic activity of FadD23.

Supplementary Information

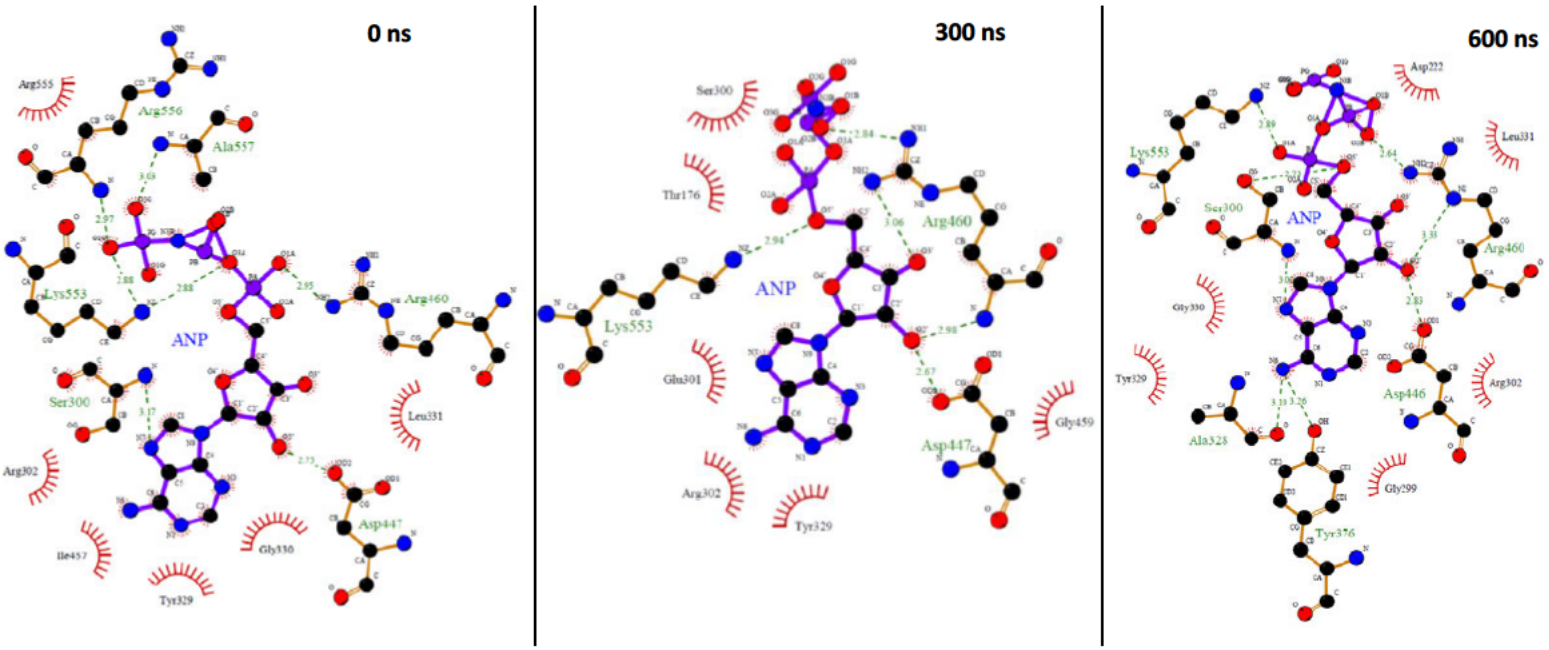

S1: Snapshots of FadD23-ANP interaction sampled at 0 ns, 300 ns and 600 ns time frames.

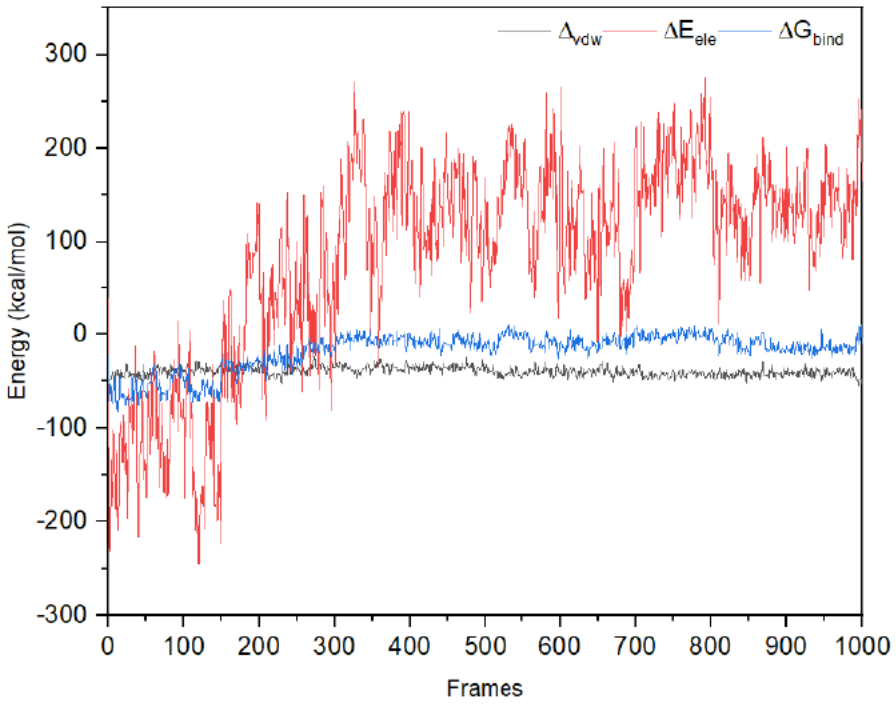

S2: Binding free energy evolution in FadD23-ANP system sampled over 1000 frames.

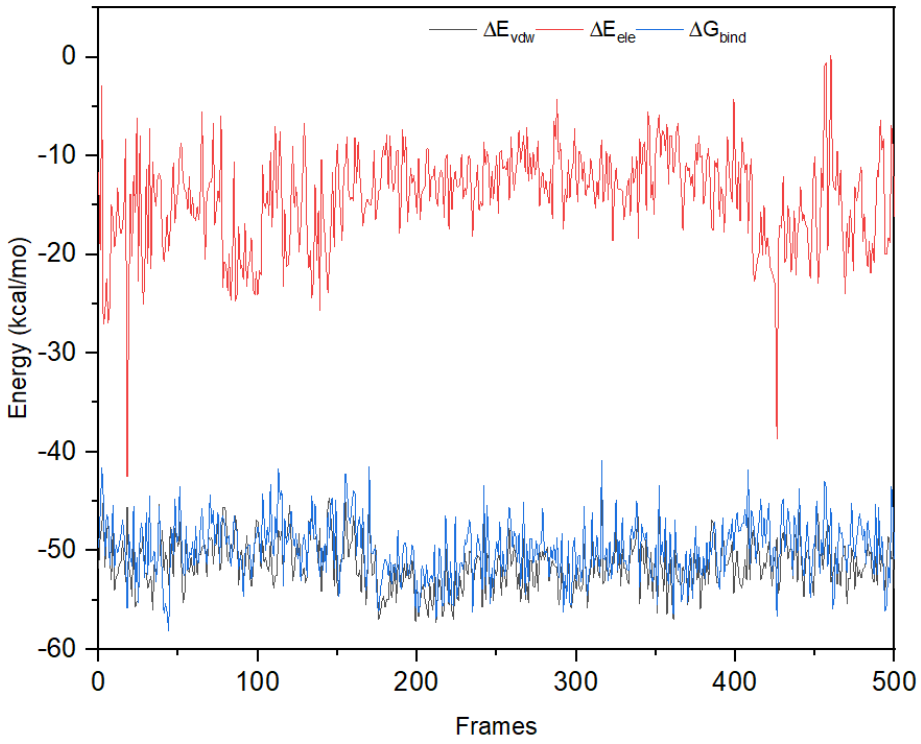

S3: Binding free energy evolution in FadD23-PLM system sampled over 1000 frames.

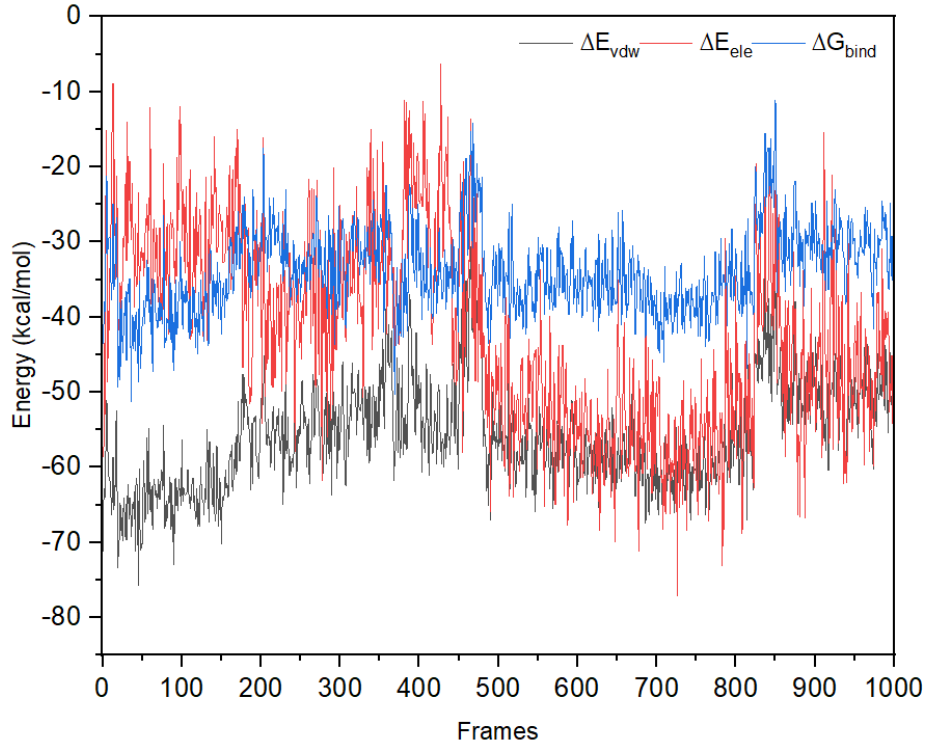

S4: Binding free energy evolution in FadD23-Simeprevir system sampled over 1000 frames.

Table S1: Per-residue Energy Decomposition in a FadD23-PLM system.

Residue	van der Waals	Electrostatic	Polar Solvation	Non-Polar Solv.	Total
HIE 221	-0.235± 0.205	-0.620± 0.638	0.521± 0.531	-0.006± 0.012	-0.340±0.309
ASP 222	-0.524± 0.364	-1.878± 1.961	2.235± 1.947	-0.059 ± 0.042	-0.226±0.357
MET 223	-2.044± 0.436	-0.332± 0.573	0.680± 0.422	-0.164± 0.029	-1.859±0.553
SER 300	-0.745± 0.454	-1.802± 1.231	1.737± 0.802	-0.130± 0.053	-0.940±0.545
ALA 328	-0.813± 0.193	0.602± 0.600	-0.271± 0.479	-0.063± 0.018	-0.545 ±0.340
GLY 330	-0.958± 0.278	0.332± 1.168	0.393± 0.762	-0.095± 0.034	-0.328±0.539
VAL 336	-1.667± 0.359	-0.987± 0.910	0.842± 0.328	-0.147± 0.025	-1.957±0.737
SER 551	-0.058± 0.114	0.089± 0.308	-0.045± 0.272	-0.003± 0.010	-0.017±0.121
LYS 553	-0.053± 0.097	-1.021± 1.209	1.204± 1.166	-0.010± 0.022	0.120±0.230

Table S2: Per-residue Energy Decomposition in a FadD23-Simeprevir system.

Residue	van der Waals	Electrostatic	Polar Solvation	Non-Polar Solv.	Total
ARG 128	-2.488± 1.738	-1.349± 1.834	3.060± 2.838	-0.417± 0.281	-1.195± 0.975
GLN 174	-0.180± 0.184	-0.070± 0.417	0.293± 0.374	-0.006± 0.013	0.038± 0.137
THR 176	-2.169± 0.641	-1.403± 1.707	2.487± 1.026	-0.341± 0.091	-1.426± 1.291
THR 177	-3.326± 0.694	-3.842± 1.481	5.482± 1.008	-0.421± 0.073	-2.106± 1.067

ALA 179	-0.769± 0.423	-1.594± 0.661	0.694± 0.301	-0.114± 0.030	-1.783± 0.450
TYR 220	-0.938± 0.487	-0.167± 0.228	0.386± 0.275	-0.167± 0.069	-0.886± 0.520
ASP 222	-0.216± 0.337	-1.095 1.345	1.461± 1.206	-0.014± 0.030	0.136± 0.304
TYR 414	-0.768± 0.321	-0.177 0.378	0.419± 0.396	-0.111± 0.039	-0.638± 0.354
LYS 417	-0.133± 0.077	-1.439 1.054	1.636± 1.118	-0.006± 0.014	0.058± 0.090
ARG 422	-0.075± 0.101	-0.270± 0.847	0.345± 0.803	-0.008± 0.029	-0.008± 0.097
ARG 460	-1.461± 0.509	-1.368± 3.512	2.800± 3.429	-0.412± 0.105	-0.442± 0.583
LYS 462	-0.229± 0.247	-1.035± 2.000	1.447± 2.075	-0.038± 0.085	0.145± 0.295
THR 549	-0.529± 0.465	-0.305± 0.182	0.496± 0.210	-0.077± 0.087	-0.415± 0.513
SER 551	-0.208± 0.176	-0.035± 0.200	0.193± 0.289	-0.024± 0.032	-0.073± 0.170
LYS 553	-0.798± 0.938	0.668± 1.985	0.304± 2.629	-0.127± 0.126	0.047± 0.578
ARG 555	-1.703± 0.983	-2.600± 1.268	3.707± 1.870	-0.294± 0.164	-0.890± 0.830
ARG 556	-0.697± 0.558	0.103± 1.078	0.215± 1.000	-0.115± 0.107	-0.495± 0.504
ALA 557	-0.973± 0.389	-0.424± 0.508	0.457± 0.403	-0.338± 0.095	-1.278± 0.557
LYS 561	-0.151± 0.186	-0.515± 2.528	0.828± 2.500	-0.044± 0.085	0.118± 0.409

Table S3: Per-residue Energy Decomposition in a FadD23-ANP system.

Residue	**van der Waals**	**Electrostatic**	**Polar Solvation**	**Non-Polar Solv.**	**Total**
THR 176	-0.769 ± 0.428	4.124± 3.176	-3.726± 2.310	-0.162± 0.055	-0.533± 1.190
THR 177	-0.229± 0.115	-2.155± 1.790	2.011± 1.656	-0.011± 0.015	-0.384 ± 0.276

CYS 298	-0.180± 0.095	-0.428± 0.789	0.417± 0.770	-0.004± 0.005	-0.195± 0.148
SER 300	-2.211± 0.598	2.926± 3.001	-2.242± 2.428	-0.242± 0.073	-1.768± 1.116
GLU 301	-1.733± 0.529	67.090± 4.390	-66.096± 4.105	-0.099± 0.049	-0.838± 0.736
ALA 328	-0.291± 0.318	1.849± 0.574	-1.721± 0.376	-0.019± 0.015	-0.181± 0.337
TYR 329	-2.027± 0.575	-5.814± 0.648	5.677± 0.456	-0.162± 0.030	-2.327± 0.752
GLY 330	-0.582± 0.328	2.683± 0.480	-2.303± 0.467	-0.086± 0.039	-0.288± 0.317
TYR 376	-0.304± 0.269	-2.175± 1.743	2.091± 1.104	-0.063± 0.028	-0.452± 0.709
ASP 446	-0.171± 0.676	65.814± 3.425	-64.186± 2.827	-0.078± 0.024	1.379± 0.813
ILE 457	-1.172± 0.559	-0.539± 0.655	0.586± 0.594	-0.107± 0.048	-1.232± 0.565
ARG 460	-0.951± 1.186	-139.804± 4.930	122.044± 2.814	-0.547± 0.128	-19.258± 2.758
ASP 463	-0.275± 0.102	82.563± 6.172	-80.629± 5.525	-0.024± 0.023	1.635± 0.714
ASP 475	-0.147± 0.114	65.344± 4.124	-64.521± 3.888	-0.011± 0.023	0.665± 0.226
VAL 554	-0.154± 0.129	6.528± 1.759	-6.152± 1.346	-0.011± 0.016	0.212± 0.372
ARG 555	-0.260 ± 0.366	-68.386± 14.742	67.62 ± 13.375	-0.055± 0.084	-1.072± 1.890

Table S4: Hydrogen Bond Formation Analysis in a FaD23-PLM system.

Acceptor	**Donor H**	**Donor**	**Frames**	**Distance$_{avg}$**	**Lifetime$_{avg}$**
PLM@O1	SER_300@H	SER_300@N	83328	2.8779	2.1555
PLM@O1	SER_300@HG	SER_300@OG	54713	2.7612	5.6922
VAL_336@O	PLM_573@H31	PLM_573@O	12049	2.7574	5.7240
GLY_330@O	PLM_573@H31	PLM_573@O	8463	2.7658	3.8242
PLM@O	SER_300@HG	SER_300@OG	6764	2.8531	1.5578
PLM@O	SER_300@H	SER_300@N	4473	2.9143	1.1852
ASP_222@OD1	PLM_573@H31	PLM_573@O	2096	2.6583	7.9696
PLM@O	LYS_553@HZ2	LYS_553@NZ	921	2.8685	1.7280

PLM@O	LYS_553@HZ3	LYS_553@NZ	900	2.8676	1.7274
PLM@O	SER_551@HG	SER_551@OG	868	2.8440	1.5201
PLM@O	LYS_553@HZ1	LYS_553@NZ	705	2.8695	1.8031
ASP_222@OD2	PLM_573@H31	PLM_573@O	550	2.6510	6.7901
PLM@O1	HIE_221@HE2	HIE_221@NE2	193	2.8738	1.3688
PLM@O1	LYS_553@HZ2	LYS_533@NZ	133	2.8407	1.4149
PLM@O1	LYS_533@HZ3	LYS_533@NZ	120	2.8378	1.4458
PLM@O	HIE_221@HE2	HIE_221@NE2	113	2.9053	1.0762
PLM@O1	LYS_553@HZ1	LYS_553@NZ	77	2.8410	1.6042
PLM@O1	GLY_330@H	GLY_330@N	68	2.9165	1.0000
PLM@O	GLY_330@H	GLY_330@N	21	2.9030	1.0500
PLM@O1	MET_223@H	MET_223@N	17	2.9278	1.0000
SER_300@OG	PLM_573@H31	PLM_573@O	14	2.7946	1.5556
PLM@O1	SER_551@HG	SER_551@OG	14	2.8591	1.0000
ASP_222@O	PLM_573@H31	PLM_573@O	6	2.8736	2.0000
PLM@O	MET_223@H	MET_223@N	5	2.9414	1.0000
ALA_328@O	PLM_573@H31	PLM_573@O	3	2.8008	1.5000
SER_551@O	PLM_573@H31	PLM_573@O	1	2.8590	1.0000

Table S5: Hydrogen Bond Formation Analysis in a FadD23-Simeprevir system.

Acceptor	**Donor H**	**Donor**	**Frames**	**Distance$_{avg}$**	**Lifetime$_{avg}$**
THR_177@O	LIG@HN	LIG@N5	237537	2.8632	3.1466
LIG@O6	ALA_179@H	ALA_179@N	236410	2.8774	2.6443
LIG@O7	ALA_179@H	ALA_179@N	82507	2.8741	2.7793
LIG@O6	THR_176@HG1	THR_176@OG1	81847	2.7521	6.5520
LIG@O5	ARG_460@HH22	ARG_460@NH2	16170	2.8242	4.9450
LIG@O5	ARG_460@HH11	ARG_460@NH1	9021	2.8380	1.7981
LIG@O2	LYS_561@HZ2	LYS_561@NZ	8381	2.8172	3.2025
LIG@O2	LYS_561@HZ1	LYS_561@NZ	7502	2.8158	3.2860
LIG@O2	LYS_561@HZ3	LYS_561@NZ	5608	2.8177	2.9392
LIG@O5	ARG_460@HH12	ARG_460@NH1	2886	2.8586	1.7261
LIG@O3	ARG_555@HH21	ARG_555@NH2	2239	2.8853	1.1308
LIG@O2	ALA_557@H	ALA_557@N	1779	2.9240	1.1418
LIG@O2	THR_177@HG1	THR_177@OG1	1755	2.6983	6.7500
LIG@O4	ARG_555@HH11	ARG_555@NH1	1077	2.8864	1.5298
THR_176@OG1	LIG@HN	LIG@N5	735	2.8863	2.2615
LIG@O4	ARG_555@HH21	ARG_555@NH2	700	2.8720	1.4374
LIG@O6	ARG_460@HH12	ARG_460@NH1	633	2.8629	1.9906
LIG@O2	THR_176@HG1	THR_176@OG1	531	2.7231	6.8961

LIG@O6	ARG_460@HH22	ARG_460@NH2	401	2.8518	2.0355
LIG@O6	LYS_462@HZ2	LYS_462@NZ	295	2.8176	2.5000
LIG@O4	ARG_555@HE	ARG_555@NE	278	2.8981	1.5027
LIG@O4	ARG_128@H	ARG_128@N	241	2.9432	1.0343
LIG@O6	LYS_462@HZ3	LYS_462@NZ	199	2.8242	1.9135
LIG@O5	LYS_462@HZ3	LYS_462@NZ	190	2.8300	2.1591
THR_176@O	LIG@HN	LIG@N5	185	2.9091	1.2585
LIG@O5	LYS_462@HZ2	LYS_462@NZ	183	2.8426	1.8673
LIG@O5	LYS_462@HZ1	LYS_462@NZ	153	2.8353	2.2174
LIG@O6	LYS_462@HZ1	LYS_462@NZ	150	2.8292	2.4194
LIG@O4	GLN_174@HE22	GLN_174@NE2	131	2.9154	1.1696
LIG@O7	LYS_462@HZ3	LYS_462@NZ	126	2.8035	2.2500
LIG@O4	ARG_128@HH11	ARG_128@NH1	121	2.8970	1.1863
LIG@O2	THR_177@H	THR_177@N	120	2.9123	1.1009
LIG@O7	LYS_462@HZ2	LYS_462@NZ	119	2.8278	2.3333
LIG@O7	LYS_462@HZ1	LYS_462@NZ	104	2.8167	2.2609
LIG@O4	GLN_174@HE21	GLN_174@NE2	97	2.8893	1.9020
LIG@O4	LYS_561@HZ3	LYS_561@NZ	79	2.8740	1.5192
LIG@O4	THR_549@HG1	THR_549@OG1	75	2.9086	1.1719
LIG@O4	SER_123@HG	SER_123@OG	59	2.8351	1.6857
LIG@O4	LYS_568@HZ2	LYS_568@NZ	59	2.8833	1.5946
LIG@O7	ARG_460@HE	ARG_460@NE	58	2.8693	1.4500
LIG@O3	ARG_555@HE	ARG_555@NE	52	2.9022	1.3333
LIG@O7	TYR_414@HH	TYR_414@OH	44	2.7867	2.0952
LIG@O4	SER_551@HG	SER_551@OG	38	2.8724	1.1515
LIG@O4	ARG_128@HH12	ARG_128@NH1	36	2.8869	1.0909
LIG@N4	ARG_128@HH11	ARG_128@NH1	31	2.9372	1.2917
LIG@O4	LYS_561@HZ1	LYS_561@NZ	28	2.8832	1.4000
LIG@O7	THR_176@HG1	THR_176@OG1	24	2.8257	1.6000
LIG@O5	ARG_460@HE	ARG_460@NE	20	2.9037	1.1111
LIG@O2	ARG_555@HH21	ARG_555@NH2	18	2.8687	1.1250
LIG@N4	THR_177@HG1	THR_177@OG1	18	2.9184	1.0588
LIG@N3	THR_177@HG1	THR_177@OG1	18	2.9368	1.0588
LIG@O3	ARG_555@HH22	ARG_555@NH2	14	2.8786	1.0769
LIG@O4	ASP_222@H	ASP_222@N	12	2.9532	1.0000
LIG@O3	ARG_128@HH21	ARG_128@NH2	11	2.8655	1.1000
LIG@O2	ARG_128@HH21	ARG_128@NH2	8	2.8623	1.0000
LIG@O7	LYS_417@HZ1	LYS_417@NZ	8	2.8647	1.1429
LIG@O3	ARG_128@HH22	ARG_128@NH2	8	2.8667	1.0000
LIG@N3	ARG_555@HH21	ARG_555@NH2	8	2.9520	1.0000

LIG@O6	TYR_414@HH	TYR_414@OH	7	2.8176	1.0000
LIG@O4	ARG_128@HH22	ARG_128@NH2	7	2.8682	1.4000
LIG@O7	ARG_460@HH11	ARG_460@NH1	6	2.8682	1.2000
LIG@O7	LYS_417@HZ2	LYS_417@NZ	5	2.7998	1.2500
LIG@O4	ARG_555@HH22	ARG_555@NH2	5	2.9334	1.0000
LIG@O1	THR_176@HG1	THR_176@OG1	4	2.7910	1.0000
LIG@O4	ARG_555@HH12	ARG_555@NH1	4	2.8641	1.0000
LIG@O2	ARG_556@H	ARG_556@N	4	2.8759	1.3333
LIG@O2	LYS_553@HZ1	LYS_553@NZ	4	2.8783	1.3333
LIG@O6	ARG_423@HH22	ARG_423@NH2	4	2.8811	1.0000
LIG@O3	ARG_128@HH12	ARG_128@NH1	4	2.9185	1.0000
LIG@N3	ARG_128@HH22	ARG_128@NH2	4	2.9273	1.0000
LIG@O3	ARG_128@HH11	ARG_128@NH1	4	2.9274	2.0000
LIG@O4	TYR_220@HH	TYR_220@OH	3	2.8254	1.0000
LIG@O6	ARG_423@HH12	ARG_423@NH1	3	2.8448	1.0000
LIG@O7	ARG_423@HH22	ARG_423@NH2	3	2.8590	1.5000
LIG@O4	ARG_128@HE	ARG_128@NE	3	2.8989	1.0000
LIG@N3	ARG_128@HH21	ARG_128@NH2	3	2.9287	1.0000
LIG@O3	ARG_555@HH12	ARG_555@NH1	2	2.8040	1.0000
LIG@O2	ARG_128@HH12	ARG_128@NH1	2	2.8454	1.0000
LIG@N4	ARG_460@HH11	ARG_460@NH1	2	2.8838	1.0000
LIG@O2	LYS_553@HZ3	LYS_553@NZ	2	2.8976	1.0000
LIG@N2	LYS_561@HZ3	LYS_561@NZ	2	2.9485	1.0000
LIG@N3	ARG_128@HE	ARG_95@NE	2	2.9525	1.0000
LIG@N2	LYS_561@HZ2	LYS_561@NZ	2	2.9546	1.0000
LIG@O4	ARG_556@H	ARG_556@N	2	2.9793	1.0000
LIG@O4	ARG_128@HH21	ARG_128@NH2	1	2.7795	1.0000
LIG@O2	ARG_555@HH22	ARG_555@NH2	1	2.7955	1.0000
LIG@O6	ARG_423@HH21	ARG_423@NH2	1	2.8142	1.0000
LIG@N3	ARG_128@HH12	ARG_128@NH1	1	2.8233	1.0000
LIG@N3	LYS_555@HZ1	LYS_555@NZ	1	2.8520	1.0000
LIG@O2	ARG_128@HH22	ARG_128@NH2	1	2.8850	1.0000
LIG@O4	ALA_557@H	ALA_557@N	1	2.9193	1.0000
LIG@N4	ARG_555@HH12	ARG_555@NH1	1	2.9447	1.0000
LIG@O4	THR_177@HG1	THR_177@OG1	1	2.9455	1.0000
LIG@O2	GLU_558@H	GLU_558@N	1	2.9539	1.0000
LIG@N4	ARG_128@HE	ARG_128@NE	1	2.9742	1.0000
LIG@N4	LYS_553@HZ2	LYS_553@NZ	1	2.9853	1.0000
LIG@N3	LYS_553@HZ3	LYS_553@NZ	1	2.9897	1.0000
LIG@N4	ARG_555@HE	ARG_555@NE	1	2.9950	1.0000

LIG@N2	LYS_561@HZ1	LYS_561@NZ	1	2.9970	1.0000

Table S6: Hydrogen Bond Formation Analysis in a FadD23-ANP system.

Acceptor	**Donor H**	**Donor**	**Frames**	**Distance$_{avg}$**	**Lifetime$_{avg}$**
ANP@O1B	ARG_460@HH22	ARG_460@NH2	528150	2.7919	14.5797
ANP@O2B	ARG_460@HH12	ARG_460@NH1	450773	2.7517	28.4274
ASP_446@OD2	ANP@HO2'	ANP@O2'	359512	2.6958	18.8919
ASP_446@OD1	ANP@HO2'	ANP@O2'	157608	2.7071	10.7436
ANP@O1B	ARG_460@HH12	ARG_460@NH1	118983	2.8326	2.9587
ALA_328@O	ANP@H61	ANP@N6	82515	2.8739	1.7298
ALA_328@O	ANP@H62	ANP@N6	82462	2.8727	1.7827
ANP@O3'	ARG_460@HH21	ARG_460@NH2	81674	2.8566	1.5974
ANP@O1A	LYS_553@HZ1	LYS_553@NZ	75244	2.7750	3.0607
ANP@O1A	LYS_553@HZ2	LYS_553@NZ	73737	2.7769	2.9635
ANP@O1A	LYS_553@HZ3	LYS_553@NZ	71741	2.7760	2.9508
ANP@O3A	ARG_460@HH12	ARG_460@NH1	71092	2.8140	4.1297
ANP@O3A	ARG_460@HH22	ARG_460@NH2	68920	2.8881	3424
ANP@O2B	ARG_460@HH22	ARG_460@NH2	42588	2.8834	1.4271
ANP@N1	TYR_376@HH	TYR_376@OH	41146	2.8714	1.7291
TYR_376@OH	ANP@H62	ANP@N6	35812	2.9078	1.4787
ANP@O2B	LYS_553@HZ1	LYS_553@NZ	35686	2.7558	7.7985
ANP@O3'	ARG_460@HE	ARG_460@NE	35311	2.8872	1.2037
ANP@N3B	ARG_460@HH12	ARG_460@NH1	33325	2.8801	3.0579
ANP@N7	SER_300@H	SER_300@N	32915	2.9366	1.2460
ANP@O2A	LYS_553@HZ3	LYS_553@NZ	30469	2.7668	11.4373
ANP@O2B	LYS_553@HZ3	LYS_553@NZ	26326	2.7672	6.1195
ANP@O2'	ARG_460@H	ARG_460@N	26049	2.8969	1.6758
ANP@O2G	ARG_128@HH22	ARG_128@NH2	24728	2.8145	3.7735
ANP@O2A	LYS_553@HZ1	LYS_553@NZ	24328	2.7665	8.5033
ANP@O4'	ARG_460@HH11	ARG_460@NH1	24159	2.8953	1.8373
ANP@O1G	ARG_128@HH22	ARG_128@NH2	23932	2.8115	4.0027
ANP@O3G	ARG_128@HH12	ARG_128@NH1	22082	2.8275	3.1416
ANP@O1G	ARG_128@HH12	ARG_128@NH1	22014	2.8239	3.3492
ANP@O1B	LYS_553@HZ1	LYS_553@NZ	21976	2.7923	3.0612
ANP@O3G	ARG_128@HH22	ARG_128@NH2	21184	2.8173	3.5508
ANP@O2B	LYS_553@HZ2	LYS_553@NZ	20972	2.7645	6.1864
ANP@O2G	ARG_128@HH12	ARG_128@NH1	20749	2.8278	3.0167
ANP@O1B	LYS_553@HZ3	LYS_553@NZ	20565	2.7928	3.1306

ANP@O2A	LYS_553@HZ2	LYS_553@NZ	20080	2.7659	7.8193
TYR_376@OH	ANP@H61	ANP@N6	19516	2.9112	1.3267
ANP@O3A	LYS_553@HZ3	LYS_553@NZ	16348	2.8075	3.1426
ANP@O1B	LYS_462@HZ1	LYS_462@NZ	15740	2.8246	3.6301
ANP@O3A	LYS_553@HZ1	LYS_553@NZ	14202	2.8075	2.7098
ANP@O1B	LYS_462@HZ3	LYS_462@NZ	13732	2.8210	3.7694
ANP@O1B	LYS_553@HZ2	LYS_553@NZ	13017	2.7875	2.8048
ANP@O3A	LYS_462@HZ1	LYS_462@NZ	12982	2.8348	2.1352
ANP@O1B	LYS_462@HZ2	LYS_462@NZ	12826	2.8191	3.9392
ANP@O5'	SER_300@HG	SER_300@OG	12642	2.7847	2.3634
ANP@O5'	LYS_553@HZ3	LYS_553@NZ	12088	2.8514	1.5468
ANP@O3A	LYS_462@HZ2	LYS_462@NZ	11676	2.8343	2.1882
ANP@O3A	LYS_462@HZ3	LYS_462@NZ	11503	2.8340	2.1869
ANP@O5'	LYS_553@HZ1	LYS_553@NZ	11422	2.8510	1.5262
ANP@O5'	LYS_553@HZ2	LYS_553@NZ	11205	2.8512	1.4765
ANP@N3B	ARG_460@HH22	ARG_460@NH2	8622	2.9072	1.7429
ANP@O3A	LYS_553@HZ2	LYS_553@NZ	7878	2.8190	2.4603
ANP@N3B	LYS_462@HZ1	LYS_462@NZ	6824	2.8796	1.4572
ANP@N6	TYR_376@HH	TYR_376@OH	6752	2.8627	1.2802
ANP@O2A	HIE_221@HE2	HIE_221@NE2	5976	2.8420	2.6992
ANP@N6	SER_300@H	SER_300@N	5910	2.9234	1.4753
ANP@O2G	ARG_555@HE	ARG_555@NE	5841	2.8347	5.8062
ANP@O1G	ARG_555@HH21	ARG_555@NH2	5752	2.8272	3.6267
ANP@O2A	ARG_556@HH12	ARG_556@NH1	5619	2.8001	3.4096
ANP@N3B	LYS_462@HZ3	LYS_462@NZ	5613	2.8770	1.4385
ANP@N3B	LYS_462@HZ2	LYS_462@NZ	5232	2.8732	1.4012
ANP@O2G	ARG_555@HH12	ARG_555@NH1	5044	2.7966	3.9010
ANP@O5'	ARG_460@HH11	ARG_460@NH1	4607	2.8653	1.7726
ANP@O1G	ARG_555@HH12	ARG_555@NH1	4484	2.8011	3.7460
ANP@O2G	ARG_460@HH22	ARG_460@NH2	4156	2.8118	4.1685
ANP@O3G	ARG_555@HH12	ARG_555@NH1	4066	2.8046	3.1766
ANP@O3G	ARG_555@HH21	ARG_555@NH2	3954	2.8266	3.5367
ANP@O1A	LYS_462@HZ3	LYS_462@NZ	3797	2.7709	3.7153
ANP@O1G	ARG_555@HE	ARG_555@NE	3681	2.8382	4.7743
ANP@O2G	ARG_555@HH21	ARG_555@NH2	3675	2.8341	3.0297
ANP@O1A	LYS_462@HZ2	LYS_462@NZ	3549	2.7710	3.0411
ANP@O1G	LYS_462@HZ1	LYS_462@NZ	3528	2.7950	2.9400
ANP@O1A	LYS_462@HZ1	LYS_462@NZ	3511	2.7728	3.5075
ANP@O1G	LYS_462@HZ2	LYS_462@NZ	3505	2.7967	2.7171
ANP@O3G	ARG_555@HE	ARG_555@NE	3483	2.8386	4.6132

GLU_301@O	ANP@H61	ANP@N6	3414	2.8948	1.3146
ANP@O1G	LYS_462@HZ3	LYS_462@NZ	3345	2.7978	2.7713
ANP@O2G	LYS_462@HZ3	LYS_462@NZ	3142	2.8017	2.8668
ANP@O2G	ARG_555@HH22	ARG_555@NH2	3023	2.7933	3.9107
ANP@O3G	LYS_462@HZ2	LYS_462@NZ	2798	2.8057	2.7539
ANP@O2G	ARG_556@H	ARG_556@N	2591	2.8494	2.8255
ANP@O2G	LYS_462@HZ2	LYS_462@NZ	2556	2.8041	2.5714
ANP@O2G	LYS_462@HZ1	LYS_462@NZ	2506	2.8009	2.6745
ANP@O3G	LYS_462@HZ1	LYS_462@NZ	2455	2.8058	2.8218
ANP@O3G	LYS_462@HZ3	LYS_462@NZ	2441	2.8034	2.6533
GLU_301@O	ANP@H62	ANP@N6	2254	2.8858	1.3097
ANP@O1G	ARG_555@HH22	ARG_555@NH2	2039	2.8088	3.4618
ANP@O1G	LYS_553@HZ2	LYS_553@NZ	1984	2.8039	2.3932
ANP@O2'	ARG_460@HH11	ARG_460@NH1	1926	2.8933	1.7446
ANP@O3G	ARG_555@HH22	ARG_555@NH2	1921	2.8102	3.4613
ANP@O3G	LYS_553@HZ2	LYS_553@NZ	1879	2.7981	2.3458
ANP@O2B	ARG_555@HH21	ARG_555@NH2	1776	2.8234	2.2887
ANP@O3G	ARG_555@HH11	ARG_555@NH1	1774	2.8120	4.3374
ANP@O2G	ARG_555@HH11	ARG_555@NH1	1707	2.8132	3.3869
ANP@O1G	LYS_553@HZ3	LYS_553@NZ	1688	2.8108	2.1074
ANP@O3G	LYS_553@HZ3	LYS_553@NZ	1618	2.8068	2.0691
ANP@O1G	LYS_553@HZ1	LYS_553@NZ	1569	2.8097	1.9467
ANP@O3G	ARG_128@HH21	ARG_128@NH2	1559	2.8061	5.1623
ANP@O1G	ARG_555@HH11	ARG_555@NH1	1557	2.8193	3.0832
ANP@O2G	SER_551@HG	SER_551@OG	1556	2.7121	7.0727
ANP@O2G	ARG_128@HH21	ARG_128@NH2	1538	2.8070	4.3324
ANP@O3G	LYS_553@HZ1	LYS_553@NZ	1533	2.7969	2.1292
ANP@O1A	ARG_556@HH22	ARG_556@NH2	1528	2.7950	6.5579
ANP@O2G	LYS_553@HZ2	LYS_553@NZ	1526	2.8045	1.9268
ANP@O1A	HIE_221@HE2	HIE_221@NE2	1504	2.8517	1.7448
ANP@O1A	SER_300@HG	SER_300@OG	1475	2.6842	4.4428
ANP@O2G	LYS_553@HZ1	LYS_553@NZ	1459	2.8075	1.8777
ANP@O1G	ARG_460@HH22	ARG_460@NH2	1420	2.8216	1.9137
ANP@O2A	ARG_556@HH21	ARG_556@NH2	1418	2.8174	5.3712
ANP@O1G	ARG_460@HH12	ARG_460@NH1	1373	2.8279	2.2619
ANP@O4'	LYS_553@HZ3	LYS_553@NZ	1311	2.8540	1.2618
ANP@O2G	LYS_553@HZ3	LYS_553@NZ	1283	2.8005	1.8621
ANP@O4'	LYS_553@HZ2	LYS_553@NZ	1192	2.8617	1.2040
ANP@O3G	ALA_557@H	ALA_557@N	1032	2.8938	1.6433
ANP@O4'	SER_300@HG	SER_300@OG	999	2.8543	1.5440

ANP@O4'	LYS_553@HZ1	LYS_553@NZ	911	2.8540	1.2831
ANP@O1A	ARG_556@HH12	ARG_556@NH1	903	2.8744	1.3579
ANP@O1G	SER_551@HG	SER_551@OG	900	2.7213	6.5217
ANP@O1G	ARG_128@HH21	ARG_128@NH2	858	2.8133	3.4458
ANP@O1A	ARG_460@HH12	ARG_460@NH1	810	2.7851	2.4471
ANP@O2B	ARG_128@HH22	ARG_128@NH2	735	2.7765	7.5000
THR_176@O	ANP@H3B	ANP@N3B	727	2.9301	1.0786
ANP@O1B	ARG_128@HH12	ARG_128@NH1	664	2.8165	5.5333
ANP@O2A	ARG_460@HH12	ARG_460@NH1	611	2.8016	1.2520
ANP@O2A	ARG_556@HE	ARG_556@NE	605	2.8359	3.6890
ANP@O3G	SER_551@HG	SER_551@OG	583	2.7145	6.6250
ANP@O1A	ARG_460@HH22	ARG_460@NH2	488	2.7805	3.8425
ANP@N3B	LYS_553@HZ3	LYS_553@NZ	481	2.8849	2.1378
ANP@O2A	ARG_556@HH22	ARG_556@NH2	466	2.8435	2.0619
ANP@O2G	ARG_460@HH12	ARG_460@NH1	439	2.8501	1.7352
ANP@O1B	ARG_128@HH22	ARG_128@NH2	438	2.7970	5.2143
ANP@N3B	LYS_553@HZ1	LYS_553@NZ	388	2.8938	1.5397
ANP@O3G	ARG_128@HE	ARG_128@NE	377	2.8834	1.9534
ANP@N3B	LYS_553@HZ2	LYS_553@NZ	368	2.8937	2.0220
ANP@O3G	ARG_460@HH12	ARG_460@NH1	305	2.8411	1.5803
ANP@O2G	ARG_128@HE	ARG_128@NE	285	2.8814	1.8038
ANP@N3	ARG_302@HH11	ARG_302@NH1	242	2.9356	1.2040
ASP_463@OD2	ANP@HO2'	ANP@O2'	230	2.7321	6.0526
GLY_330@O	ANP@HO2'	ANP@O2'	221	2.7525	5.6667
ANP@O1G	ARG_128@HE	ARG_128@NE	204	2.8777	1.8545
ANP@O2G	ALA_557@H	ALA_557@N	174	2.8939	1.6571
ANP@O2B	ARG_128@HH12	ARG_128@NH1	170	2.8465	1.8889
ANP@O1A	ARG_555@HH12	ARG_555@NH1	166	2.7974	3.7727
ANP@O4'	ARG_460@HH21	ARG_460@NH2	150	2.9077	1.2397
ANP@O2A	SER_300@HG	SER_300@OG	141	2.7341	1.6023
ANP@O3G	ARG_556@H	ARG_556@N	133	2.8767	1.1982
ANP@O2G	ARG_556@HH11	ARG_556@NH1	117	2.8464	1.8281
ANP@O1A	ARG_555@HH22	ARG_555@NH2	111	2.8056	3.2647
ANP@O5'	ARG_460@HH12	ARG_460@NH1	81	2.8463	1.0125
ANP@O3G	TYR_220@HH	TYR_220@OH	76	2.7210	3.8000
SER_300@N	ANP@H62	ANP@N6	65	2.9548	1.0000
ANP@O2B	LYS_462@HZ2	LYS_462@NZ	50	2.8414	1.1628
ANP@O1G	ALA_557@H	ALA_557@N	50	2.9114	1.4286
ANP@O3G	ARG_460@HH22	ARG_460@NH2	49	2.8326	1.5806
ANP@O3A	ARG_460@HH11	ARG_460@NH1	44	2.8243	2.7500

ANP@O1G	TYR_220@HH	TYR_220@OH	41	2.7634	3.1538
SER_300@N	ANP@H61	ANP@N6	34	2.9502	1.0000
ANP@O2B	LYS_462@HZ3	LYS_462@NZ	33	2.8395	1.1379
ANP@O2'	ARG_556@HH21	ARG_556@NH2	24	2.8867	1.1429
ANP@O1G	ARG_460@HH21	ARG_460@NH2	22	2.8481	2.0000
ANP@O1G	THR_177@HG1	THR_177@OG1	21	2.7825	2.1000
VAL_554@O	ANP@H3B	ANP@N3B	21	2.9376	1.1667
ANP@O1G	ARG_556@H	ARG_556@N	20	2.8391	1.1111
ANP@O2'	ARG_556@HH12	ARG_556@NH1	19	2.8832	1.4615
ANP@O2B	LYS_462@HZ1	LYS_462@NZ	18	2.7689	1.1250
ANP@O3'	ARG_460@HH11	ARG_460@NH1	17	2.8656	1.0000
ANP@N7	GLY_330@H	GLY_330@N	15	2.9615	1.0000
ANP@O2G	TYR_220@HH	TYR_220@OH	13	2.8184	1.6250
ANP@N1	SER_300@H	SER_300@N	12	2.9096	1.0909
ANP@O3G	HIE_221@HE2	HIE_221@NE2	11	2.8578	1.3750
ANP@N7	SER_300@HG	SER_300@OG	11	2.8639	1.8333
GLY_330@O	ANP@H62	ANP@N6	11	2.9112	2.2000
ANP@O2G	ARG_460@HH11	ARG_460@NH1	10	2.7464	1.6667
ANP@O1A	ARG_460@HH11	ARG_460@NH1	10	2.8249	1.0000
ANP@O2A	ARG_460@HH11	ARG_460@NH1	10	2.8304	1.1111
ANP@O2'	TYR_329@HH	TYR_329@OH	10	2.9048	1.0000
ANP@O1G	ARG_128@HH11	ARG_128@NH1	9	2.7905	3.0000
ANP@N6	GLY_330@H	GLY_330@N	9	2.9483	1.0000
ASP_475@OD1	ANP@HO2'	ANP@O2'	6	2.8056	2.0000
ANP@O2A	ARG_555@HH12	ARG_555@NH1	6	2.8851	1.5000
ANP@O1A	ARG_556@HH21	ARG_556@NH2	5	2.8669	1.0000
ANP@O2B	ARG_555@HH12	ARG_555@NH1	5	2.9104	1.0000
TYR_329@OH	ANP@HO2'	ANP@O2'	5	2.9382	1.0000
ANP@N7	GLU_301@H	GLU_301@N	5	2.9522	1.0000
ARG_460@NH1	ANP@H3B	ANP@N3B	5	2.9674	1.0000
ANP@O2A	ARG_460@HH22	ARG_460@NH2	4	2.7784	2.0000
ANP@O1B	ARG_460@HH11	ARG_460@NH1	4	2.8454	1.0000
ANP@O1B	ARG_555@HH21	ARG_555@NH2	4	2.8706	1.0000
CYS_298@O	ANP@H61	ANP@N6	4	2.9428	1.0000
ANP@O2A	ARG_556@HH11	ARG_556@NH1	3	2.8412	1.0000
ANP@O5'	HIE_221@HE2	HIE_221@NE2	3	2.8590	1.5000
TYR_329@N	ANP@H61	ANP@N6	3	2.9739	1.0000
ANP@O2'	ARG_460@HE	ARG_460@NE	2	2.8356	2.0000
ANP@O1G	ARG_460@HH11	ARG_460@NH1	2	2.8656	2.0000
CYS_298@O	ANP@H62	ANP@N6	2	2.9093	1.0000

ANP@O3'	ARG_460@H	ARG_460@N	2	2.9332	1.0000
THR_177@OG1	ANP@H3B	ANP@N3B	2	2.9536	1.0000
GLY_330@O	ANP@H61	ANP@N6	2	2.9586	1.0000
ANP@O2G	HIE_221@HE2	HIE_221@NE2	1	2.6686	1.0000
ANP@O1G	THR_549@HG1	THR_549@OG1	1	2.6995	1.0000
ASP_463@OD1	ANP@HO2'	ANP@O2'	1	2.7118	1.0000
ANP@O3G	ARG_128@HH11	ARG_128@NH1	1	2.8575	1.0000
ILE_457@O	ANP@H62	ANP@N6	1	2.9001	1.0000
ASP_475@OD2	ANP@HO2'	ANP@O2'	1	2.9028	1.0000
TYR_329@N	ANP@H62	ANP@N6	1	2.9278	1.0000
ARG_555@NH2	ANP@H3B	ANP@N3B	1	2.9847	1.0000
ANP@O2'	LYS_462@HZ2	LYS_462@NZ	1	2.9862	1.0000
ANP@N6	VAL_303@H	VAL_303@N	1	2.9895	1.0000
ANP@O5'	ARG_460@HH22	ARG_460@NH2	1	2.9992	1.0000

Table S7: Number of Contacts between FadD23 and PLM within a 3 Å radius for 300ns.

#Set	**lifetime**	**lifetime$_{max}$**	**lifetime$_{avg}$**	**lifetime$_{frames}$**	**lifetime$_{name}$**
25	2105	121	5.7240	12049	VAL_336@O-PLM@O-H31
19	263	124	7.9696	2096	ASP_222@OD1-PLM@O-H31

Table S8: Number of Contacts between FadD23 and Simeprevir within a 3 Å radius over a 600ns trajectory.

#Set	**lifetime**	**lifetime$_{max}$**	**lifetime$_{avg}$**	**lifetime$_{frames}$**	**lifetime$_{name}$**
51	3270	115	4.9450	16170	LIG@O5-ARG_460@NH2-HH22
25	12492	162	6.5520	81847	LIG@O6-THR_176@OG1-HG1
28	260	309	6.7500	1755	LIG@O2-THR_177@OG1-HG1

Table S9. Number of contacts between FadD23 and ANP within a 3 Å radius over a 600 ns trajectory.

#Set	**lifetime**	**lifetime$_{max}$**	**lifetime$_{avg}$**	**lifetime$_{frames}$**	**lifetime$_{name}$**
75	29843	104	1.4271	42588	ANP@O2B-ARG_460@NH2-HH22
79	51340	106	1.3424	68920	ANP@O3A-ARG_460@NH2-HH22
176	233	107	6.5579	1528	ANP@O1A-ARG_556@NH2-HH22
138	24312	162	2.9508	71741	ANP@O1A-LYS_553@NZ-HZ3
116	24584	167	3.0607	75244	ANP@O1A-LYS_553@NZ-HZ1

61	40215	169	2.9587	118983	ANP@O1B-ARG_460@NH1-HH12
125	3390	170	6.1864	20972	ANP@O2B-LYS_553@NZ-HZ2
139	2664	173	11.4373	30469	ANP@O2A-LYS_553@NZ-HZ3
117	2861	224	8.5033	24328	ANP@O2A-LYS_553@NZ-HZ1
66	17215	249	4.1297	71092	ANP@O3A-ARG_460@NH1-HH12
128	2568	282	7.8193	20080	ANP@O2A-LYS_553@NZ-HZ2
136	4302	345	6.1195	26326	ANP@O2B-LYS_553@NZ-HZ3
114	4576	355	7.7985	35686	ANP@O2B-LYS_553@NZ-HZ1
188	14670	508	10.7436	157608	ASP_446@OD1-ANP@O2'-HO2'
74	36225	719	14.5797	528150	ANP@O1B-ARG_460@NH2-HH22
62	15857	994	28.4274	450773	ANP@O2B-ARG_460@NH1-HH12
189	19030	1131	18.8919	359512	ASP_446@OD2-ANP@O2'-HO2'

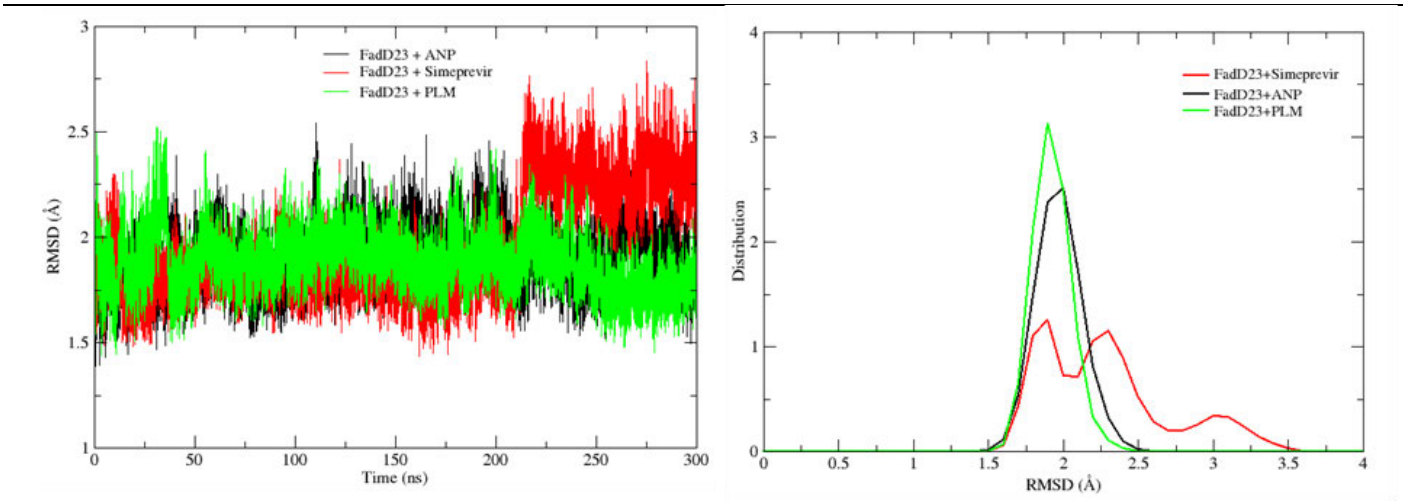

Figure S5: RMSD of ANP (black), Simeprevir (red), and PLM (green) over 300 ns trajectory.

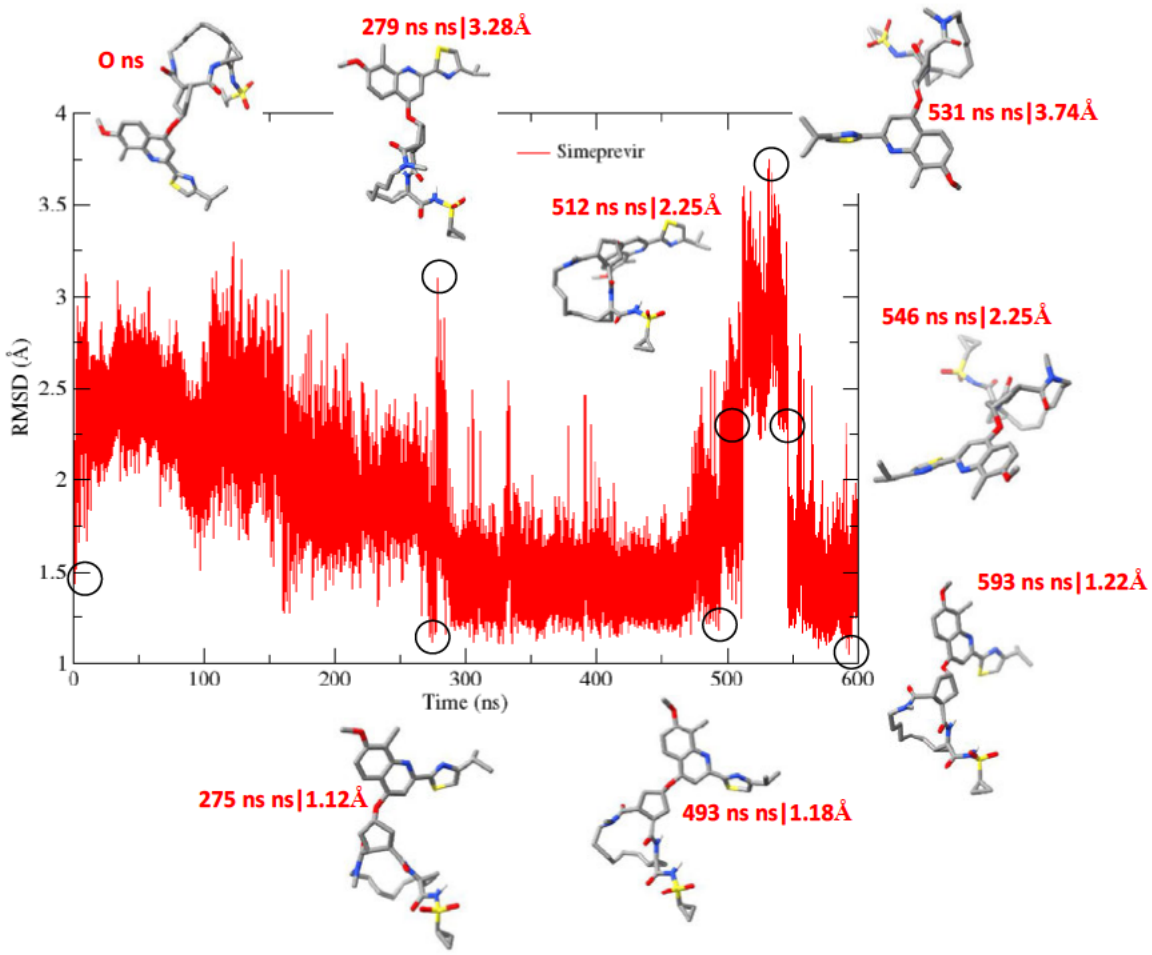

S6: Snapshots of Simeprevir conformational changes within FadD23 binding site during 600ns.

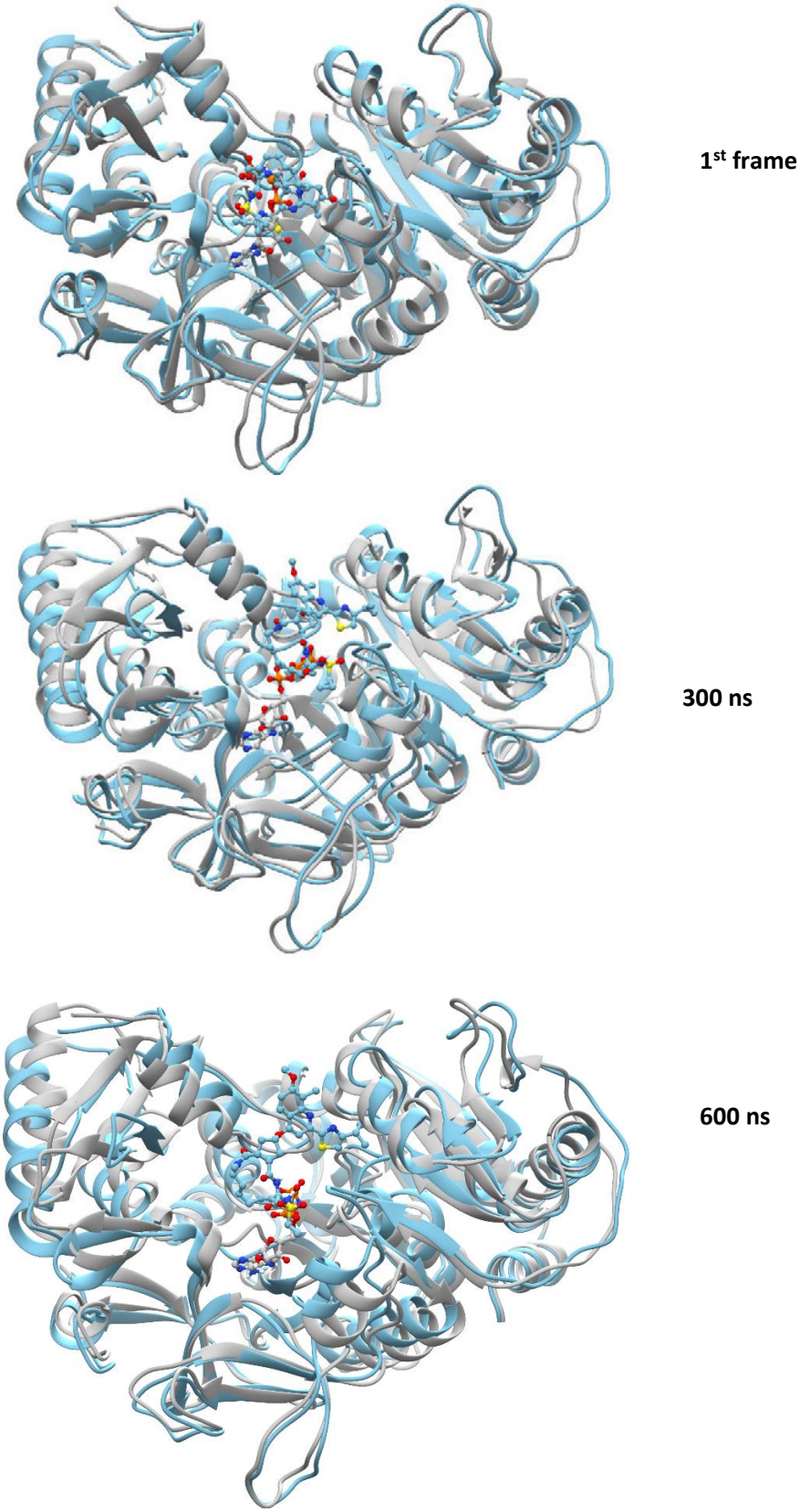

Figure S7: Superimposed structures of FadD23+ANP and FadD23+Simeprevir complexes taken 0 ns, 300 ns, and 600 ns of a trajectory.